Pd-oxide equilibration: a new experimental method for the direct determination of the activities of oxide components in melts and minerals

Thesis by

Laurinda Ann Chamberlin

In Partial Fulfillment of the Requirements

for the Degree of Doctor of Philosophy

Division of Geological and Planetary Sciences

California Institute of Technology

Pasadena, California

1994

(Submitted September 2, 1993)

Acknowledgements

I would like to express my thanks to several people who contributed to the work presented in this thesis. Dr. P. Carpenter and Dr. J.T. Armstrong provided invaluable assistance with electron microprobe analyses of Pd alloys. Dr. I. Hutcheon performed ion microprobe analyses of several Pd alloys. Dr. G. Mattioli donated synthetic $MgAl_2O_4$ spinel for this study and provided expertise on spinel. R. Millard, Dr. R. Peterson, Dr. R. Sack, and Dr. M. Carpenter shared results in advance of publication that led to great improvements in interpreting my thermodynamic data. J. Paque loaned 1 mm spinels grown from synthetic CAI melts for analysis of trace elements in spinel. Dr. H. Keppler aided in the review of the literature on the bonding properties of Pd alloys, and Mo Li assisted the discussion of the solid-state physics of Pd.

I particularly wish to thank my advisor, Dr. Edward M. Stolper, for sharing his wisdom and enthusiasm for science and for guiding me while allowing me to preserve a sense of independence. Thanks are also due in large measure to Dr. John R. Beckett, whose scientific acuity, encyclopedic knowledge of the literature, and unparagoned attention to detail were invaluable to me in the pursuit of this work.

This study was supported by NASA grant NAG 9-105. I would also like to acknowledge the support of NASA GSRP Fellowship NGT-50672.

Abstract

A new technique, Pd-oxide equilibration, has been developed for the experimental determination of the activities of oxide components in melts and minerals using the equilibrium between Pd alloy, oxygen, and the oxide component in the sample of interest. Due to the extraordinary stability of dilute alloys of Pd with Mg, Al, and Si, these metals dissolve into Pd in equilibrium with oxide-based materials in amounts easily measured with the electron microprobe at f_{O_2}'s that can be achieved with conventional gas-mixing techniques. Activity-composition relations for Pd-Mg, -Al, and -Si alloys were determined by equilibrating Pd at fixed f_{O_2} and T with periclase, corundum, and cristobalite ($a_{oxide} \equiv 1$). Because Mg, Al, and Si have constant activity coefficients in Pd at low concentrations, the activity of the oxide of each metal is a simple function of the ratio of the concentration of the metal in Pd in equilibrium with the sample to that in Pd in equilibrium with the pure oxide. Therefore, if Pd plus a melt or mineral and Pd plus pure oxide standards are equilibrated simultaneously at fixed T and f_{O_2}, the precision of the analytical technique is the major limitation on the determination of oxide activities. With Pd-oxide equilibration, all measurements of thermodynamic properties reflect equilibration at the temperature of interest, so no phase, ordering, or structural changes upon quenching influence the results. In addition, the method can be precise, since the only measurements involved in the determination of activities are the concentrations of various metals in the Pd, and there is no need for accurate knowledge of T or f_{O_2}.

The technique of Pd-oxide equilibration was used to determine activities of MgO and Al_2O_3 and ΔG_f°'s in stoichiometric $MgAl_2O_4$ spinel at 1150 to 1400°C. The results are in good agreement with those of JANAF (1985) but are distinct at the 1σ level from the ΔG_f°'s of Helgeson et al. (1978), Holland and Powell (1990), Berman (1988), and Hallstedt (1992), and at the 2σ level from Robie et al. (1978). This implies a larger residual entropy upon quenching than is accounted for by most compilations of thermodynamic data. These differences were accounted for by applying Landau theory corrections to the calorimetric heat contents (Bonnickson, 1955) using neutron diffraction measurements of the equilibrium amount of disorder in spinel as a function of temperature (Peterson et al., 1991). The corrected heat contents and measured ΔG_f°'s have been used to produce a new, self-consistent C_p function that can account for all experimental data. The results imply that nonconfigurational entropy contributions are important in spinel.

Pd-oxide equilibration was also used to measure the activities of MgO, Al_2O_3, and SiO_2 in melts in the five-component system $CaO\text{-}MgO\text{-}Al_2O_3\text{-}SiO_2\text{-}TiO_2$ (CMAST). Five bulk compositions were studied, including synthetic analogs of Type B, Type C, and forsterite-bearing Ca-Al-rich inclusions (CAIs) and one synthetic analog of an average Group 2 plagioclase-olivine inclusion (POI) from carbonaceous chondrites. Correlated variations between activity coefficient and liquid composition are observed in the melts, which may give insight into the relationships between thermodynamics and structure. The measured activities agree to within 10-35% of those calculated using Berman's (1983) model and are therefore generally consistent with

known phase equilibrium data in CMAS. Measured activities indicate that liquids of CAI and POI composition would be out of equilibrium with a solar gas and should volatilize Mg, SiO, and lesser Ca if they melt in such a gas.

The technique of Pd-oxide equilibration was also used to measure the activities of MgO and Al_2O_3 in spinel solid solutions in the $MgAl_2O_4$–$Al_{8/3}O_4$ compositional system at 1400°C. Eight compositions were studied, ranging from stoichiometric $MgAl_2O_4$ to corundum-saturated spinel. Activities of $MgAl_2O_4$ and γ-$Al_{8/3}O_4$ were calculated from the experimental values of a_{MgO} and $a_{Al_2O_3}$ using the free energy expressions of Chamberlin et al. (1993b) and Navrotsky et al. (1986). The $MgAl_2O_4$ activities are approximately Raoultian, whereas the γ-$Al_{8/3}O_4$ activities show a strong positive deviation from ideality. A plausible model for spinel solid solution at 1400°C based on Landau theory (Carpenter et al., 1993a,b) is set forth, with an assumed cation and vacancy distribution. The similarity between the free energies of mixing calculated from the activities and the enthalpies of mixing measured by Navrotsky et al. (1986) imply that entropies of mixing are virtually zero and that the solid solution is affected by significant short-range order. The ΔG_f° of spinel increases with increasing alumina content, indicating that excess alumina does not increase the condensation temperature of spinel in the solar nebula. However, the high P_{Al} in the solar nebula and the fact that ΔG_f° remains relatively constant at low alumina contents imply that the first spinel condensates would be somewhat aluminous.

Finally, Pd-oxide equilibration was used to measure the activities of MgO and SiO_2 in forsterite and protoenstatite. Four compositions were studied: nominally pure

forsterite, forsterite in equilibrium with protoenstatite, and forsterites that crystallized from liquids of two different bulk compositions in the system CMAST (POI and FOB). Measured oxide activities and ΔG_f°'s vary systematically with Ca content. The ΔG_f°'s are consistent with the literature values of Robie et al. (1978), Berman (1988), JANAF (1985), and Gillet et al. (1991) in this temperature range except in FOB, where they are lower. The free energy of formation (ΔG_f°) of protoenstatite from the oxides determined from the MgO and SiO_2 activities agrees with that of Berman (1988) to 1 kJ/mole. Low levels of Ca dissolved in forsterite may increase the number of point defects in the lattice and thereby decrease the mechanical strength of the mineral. The Pd-oxide equilibration technique, with its potential for directly and precisely determining oxide activities in melts and mineral solutions and free energies of formation of minerals, could be of considerable value in refining the existing thermodynamic data base.

Preface

The first chapter of this thesis is a revised version of a paper accepted to *Contributions to Mineralogy and Petrology*. Chapter 2 is a revised version of a manuscript soon to be submitted to *American Mineralogist*. Chapter 3 will be submitted as a paper to *Geochimica et Cosmochimica Acta*.

Table of Contents

Introduction

The thermodynamic properties of silicate melts are imperfectly understood, in part because of the difficulty of obtaining direct thermodynamic data on the liquid phase. Important insights into the properties of glasses and melts have been provided by calorimetric measurements, including solution calorimetry (Weill et al., 1980), transposed-temperature drop calorimetry (Navrotsky et al., 1989), and scanning calorimetry (Lange et al., 1991), but the development of widely applicable thermodynamic models for silicate melts based on calorimetric measurements is hindered by the limitations of calorimetric data. For example, it is difficult to relate measured properties of glasses to those of melts, to determine accurate derivatives in composition space of heat capacities and heats of solution, and to derive accurate entropy models for the complex liquid phase. One approach to resolving these problems has been to choose a specific functional form for the compositional dependence of the Gibbs free energy of the liquid phase and to calibrate the thermodynamic model using phase equilibrium and calorimetric data (Berman, 1983; Ghiorso et al., 1983). However, such models are subject to systematic errors, as they depend upon the validity of the particular functional form chosen to describe the free energy and the accuracy of the data with which they are calibrated. Moreover, the application of these models is limited in composition space, so that a model calibrated for complex natural systems is often inaccurate in simple subsystems.

Similar difficulties occur with mineral solid solutions and end-member minerals

that exhibit temperature-dependent disorder or structural changes on quenching. For solid solutions, one must again be able to determine the compositional dependence of heat capacities and heats of solution and to derive accurate entropy models when nonconfigurational contributions become important (for example, short-range ordering). Ordering changes can be energetically significant and difficult to quantify because of the complexities of determining site occupancies; the problem is acute for phases such as spinel, where site occupancies are only partially preserved on quenching because of slow reordering at low temperature. Instabilities of minerals at low temperatures or displacive phase changes to lower-symmetry structures may also interfere with efforts to measure thermodynamic properties of high-temperature minerals through calorimetric measurements.

In order to construct meaningful thermodynamic models for either melts or minerals, it is desirable to include direct measurements of activities to give direct information on the dependence of free energy on composition. In this work, an experimental technique is introduced that can provide precise, accurate data on activities in silicate liquids, minerals, and mineral solutions. The method, Pd-oxide equilibration, provides activities of oxide components through equilibration of the substance of interest with Pd metal at fixed T and f_{O_2}. It is related to techniques developed by the steel industry for the study of silicate slags in equilibrium with metallic iron (Fulton and Chipman, 1954; Langenberg et al., 1958; Langenberg and Chipman, 1959; Abraham et al., 1960; Rein and Chipman, 1963, 1965; Sharma and Richardson, 1965) but is more precise due to the extraordinary properties of Pd and the advance of modern

analytical techniques. It is also similar to more recent efforts to study the activities of transition metal oxides in melts by equilibration with an alloy containing the corresponding transition metal (Dudson and Fraser, 1980; Grove, 1981; Sahoo and Reddy, 1984; Tsukihashi et al., 1984; Ozturk and Fruehan, 1987; Grimsey, 1988; Snyder and Carmichael, 1992), but such methods have neither the precision of Pd-oxide equilibration nor its ability to measure the activities of the less easily reduced oxides such as MgO, Al_2O_3, and SiO_2.

With Pd-oxide equilibration, all measurements of thermodynamic properties reflect equilibration at the temperature of interest, so no phase, ordering, or structural changes upon quenching influence the results. In addition, the method can be precise, since the only measurements involved in the determination of activities are the concentrations of various metals in the Pd, and there is no need for accurate knowledge of T or f_{O_2}. In this work, the Pd-oxide equilibration technique is introduced and then applied to the determination of oxide activities in minerals, multicomponent silicate melts, and mineral solutions. The measured activities are used to determine free energies of formation for minerals, to explore the link between thermodynamic properties and structure for silicate melts, and to model the behavior of mineral solutions.

Chapter 1. Pd-oxide equilibration

This chapter discusses the technique of Pd-oxide equilibration in detail, including the theory behind the method, the experimental procedures used to calibrate it, the approach to analyzing for trace elements, and the consequences of the solution behavior of dilute Pd alloys for the precision of the technique. The description of the basics of the technique is followed by a theoretical explanation of the bonding behavior of Pd, an overview of the likely sources of error in using the technique, an exploration of the limitations of the technique, and a comparison of Pd-oxide equilibration with calorimetry.

Background

When a melt or mineral is equilibrated with vapor and a metal such as Fe, Pt, or Pd at a given f_{O_2}, a portion of each oxide component in the melt or mineral reduces and dissolves into the metal, creating an alloy. Taking as an example the component Al_2O_3 in the sample of interest, whether it be a melt or a mineral, the equilibrium between metal and sample is governed by the reaction:

$$2\ Al_{(metal)} + 3/2\ O_{2(gas)} = Al_2O_{3(sample)}\ . \qquad (1)$$

At fixed pressure, the equilibrium constant for this reaction is given by:

$$K(T) = \frac{a_{Al_2O_3}^{sample}}{(a_{Al}^{metal})^2 * f_{O_2}^{3/2}}\ , \qquad (2)$$

where T is the temperature in Kelvin, $a_{Al_2O_3}^{sample}$ is the activity of alumina in the sample

relative to a pure oxide such as corundum, a_{Al}^{metal} is the activity of Al in the alloy relative to pure Al metal, and f_{O_2} is the oxygen fugacity. If the activity of Al in the metal alloy is known as a function of its concentration (the measurable quantity), then $a_{Al_2O_3}^{sample}$ can be determined from Eqn. (2), because the f_{O_2} can be fixed experimentally and values of K(T) are tabulated in the literature (Robie et al., 1978; JANAF, 1985).

The problem is then to determine the activity of the solute in the alloy as a function of its concentration. At any T and f_{O_2}, the activity of Al in a metal can be determined through Eqn. (2) by equilibrating the metal with a substance of known Al_2O_3 activity, such as corundum ($a_{Al_2O_3}^{corundum} \equiv 1$). The activity-composition relationship of Al in the alloy can be obtained from a series of such experiments at constant T but different f_{O_2}'s through the relation:

$$a_{Al}^{metal} = \left[\frac{1}{K(T) * f_{O_2}^{3/2}} \right]^{1/2} = X_{Al}^{metal} * \gamma_{Al}^{metal} , \qquad (3)$$

where γ_{Al}^{metal} is the activity coefficient of Al in the metal and X_{Al}^{metal} is its mole fraction. Similar expressions can be written for the equilibration of a metal with periclase, cristobalite, or any other oxide of interest.

Establishing this kind of procedure for measuring oxide activities presents two main difficulties. The first is finding a metal that dissolves measurable concentrations of the solute metals at an f_{O_2} that is experimentally feasible. This is a problem because metal-oxide equilibrium curves for many oxides of interest, such as MgO, Al_2O_3, and SiO_2, lie at extremely low f_{O_2}'s, beyond the routine capabilities of one-

atmosphere gas-mixing techniques (Sato, 1971). The other difficulty is that even if the activity of a solute such as Al in the metal is known as a function of its concentration, an equation such as (2) is not in reality a precise vehicle for activity determinations because of the effects of propagating errors in T and f_{O_2} measurements. For example, a temperature uncertainty as small as ± 3° and an error in $\log_{10} f_{O_2}$ of ± 0.05 leads to errors of tens of percent in activities determined from an equation such as (2).

Both of these difficulties have been solved through the choice of Pd as the metal solvent in the experiments. Significant solubilities of Mg, Al, and Si in Pd in equilibrium with their oxides occur at f_{O_2}'s even 10 to 20 orders of magnitude above their respective metal-oxide equilibrium curves, so measurements of solute concentrations in Pd equilibrated with oxide-based materials at an f_{O_2} near the iron-wüstite (IW) oxygen buffer are feasible with the electron microprobe. This fact allowed the design of a series of experiments to explore the activity-composition relationships of these Pd alloys. The resulting discovery of the existence of a substantial region of Henrian behavior in dilute Pd alloys permitted the removal of the temperature and f_{O_2} contributions to the error in the activities and the resulting establishment of Pd-oxide equilibration as an experimentally simple and precise method for the determination of the thermodynamic properties of melts and minerals.

Experimental procedure

Sample preparation

Samples for Pd + pure oxide runs to determine activity coefficients in Pd-rich alloys were prepared by pressing analytical-grade MgO, Al_2O_3, or SiO_2 (JMC Puratronic) around 3-4 mm lengths of 99.997% pure 0.25 mm-diameter Pd wire (Alfa Products) (Fig. 1a). The MgO starting material was determined to be periclase by x-ray diffraction (XRD). The Al_2O_3 was initially partly amorphous (XRD) and was allowed to crystallize during the runs. XRD analysis of samples run at 1200°C for 48 hours and at 1400°C for 24 hours confirmed the presence of corundum. The initially amorphous SiO_2 remained amorphous during the 1200°C runs, but converted to cristobalite during the 1400°C runs, as demonstrated by XRD. The Pd + MgO and Pd + Al_2O_3 pellets were placed in open capsules made from ¼-inch diameter crushable magnesia or alumina rods (Ozark Technical Ceramics), which were drilled out to form open capsules (Fig. 1b). The Pd + SiO_2 pellets were placed in open capsules made from 6 mm O.D. silica glass tubes that were sealed at one end using a torch. The samples were suspended from Mo or Ir hanging wire and placed in a 1-atmosphere gas-mixing furnace.

Experimental methods

Experiments were conducted in a 1-atmosphere home-built furnace with $MoSi_2$ heating elements. Temperature was controlled to within 1-2°C by a Eurotherm 812 Controller/Programmer and measured by a Type S thermocouple calibrated at the melting point of gold. Stated temperatures are estimated to be accurate to ± 3°C. Oxygen fugacity was set using mixtures of H_2 and CO_2 and measured by an yttria-doped zir-

Figure 1. Illustration of experimental procedure for Pd + pure oxide experiments. (a) Pure Pd wire is pressed into a pellet of pure oxide powder. (b) Pd + oxide pellet is placed into an open capsule made of the same oxide as the pellet. (c) The run product is mounted in epoxy and polished for analysis by electron microprobe.

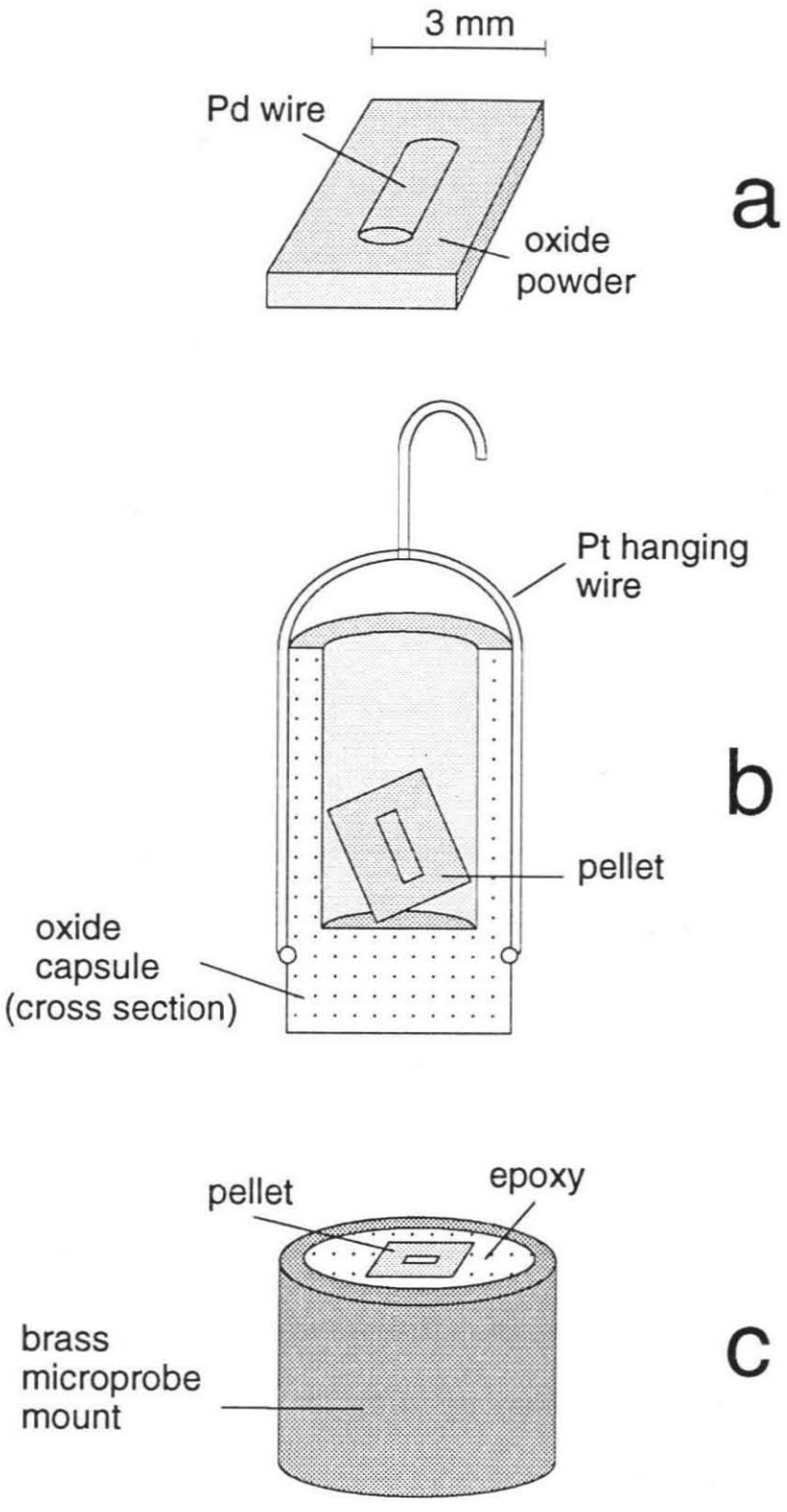
3 mm
Pd wire
oxide
powder
a
Pt hanging
wire
pellet
oxide
capsule
(cross section)
b
pellet
epoxy
brass
microprobe
mount
c

conia solid electrolyte oxygen sensor (Ceramic Oxide Fabricators Pty. Ltd., Australia). The sensor was calibrated to ± 1 mV at IW at 1200 and 1400°C by measuring changes in the resistance of high-purity iron wire as f_{O_2} was varied. Variation of the emf during experiments was usually 1 mV or less.

Experiments were performed at 1200 and 1400°C at oxygen fugacities ranging from half an order of magnitude above IW to about three orders of magnitude below. Run durations were 24 hours at 1400°C and 48 hours at 1200°C, which proved to be sufficient to homogenize the Pd alloys. Reversals were performed in all three alloy types by initially equilibrating Pd with oxide at a low f_{O_2}, then raising the f_{O_2} to the value of the final equilibration (see Tables 1-3). Demonstration of reversibility was not attempted in the Pd-Si system at 1400°C because of the limited amount of stable solid solution at this temperature. Experiments were terminated by drop-quenching the samples into a beaker of deionized water. The pellets were removed from their containers, mounted in epoxy, and rough-polished to expose a length-wise cross section through the Pd wire (Fig. 1c). The Pd was then fine-polished with diamond paste using an automatic polisher.

Electron microprobe measurement of trace elements

Because Mg, Al, and Si were expected to dissolve into Pd in only trace amounts in the f_{O_2} region of the experiments, special care was taken to obtain precise and accurate analyses of the Pd alloys produced in each experiment. Although the electron microprobe is a sufficiently sensitive instrument to detect these metals in amounts as

small as 20 ppm (J.T. Armstrong, pers. comm.), analysis of trace constituents is particularly vulnerable to errors in the estimation of the background at the peak positions and to interferences from peaks of other elements. Errors from these sources are magnified in the case of low concentrations because they comprise a far greater percentage of the signal than they do in the case of any major element.

Several measures were taken in order to solve background and interference problems for Mg, Al, and Si. The intensity of the Pd background under each of the solute peaks was estimated by measuring at one background position on each side of the peak and using linear interpolation to estimate the value underneath the peak. Because the interpolation is linear, the background positions were chosen as symmetrically as was feasible about the peak in order to obtain as closely as possible the true background directly at the peak position. This estimate of the background under the peak was nevertheless slightly in error, as the background is not precisely linear but actually has a slight curvature. Fitting the background to a polynomial expression does not lead to greater accuracy, as the influence of a number of second-order Pd lines in the vicinity of the Mg, Al, and Si peaks prevents a polynomial fit from being a better approximation than a linear one. Interference problems arise from the overlap of the Al Kα peak at 90.81 mm and the Pd Lβ 1 2nd-order peak at 90.02 mm and the Mg Kα peak at 107.56 mm and the Pd LL 2nd-order peak at 107.68 mm. There are fortunately no such overlaps at the Si Kα peak at 77.38 mm. To correct for curvature in the background and for interferences from the second-order peaks of Pd, a Puratronic Pd wire (JM Specialty Products, Lot #Z0293, 99.997% purity) was analyzed as a sample and

subtracted as a background correction from each regular analysis. These corrections are valid, since analysis by emission arc spectroscopy demonstrates that the Puratronic wire has less than 1 ppm each of Mg and Al and only 3 ppm Si, amounts undetectable by the electron probe. The emission spectroscopy does reflect a bulk analysis, but no inhomogeneity was evident within the Puratronic Pd wire itself upon repeated analysis, so the assumption of lot homogeneity was made.

Analysis of the Pd alloys was performed with a JEOL 733 Superprobe at an accelerating potential of 15 keV, a takeoff angle of 40°, and a beam current of 100 nA. Pure Mg, Al, Si, and Pd metal served as standards, and ZAF correction procedures were used to determine concentrations (Armstrong, 1988). A three-point transverse profile was analyzed across each Pd wire to determine heterogeneity. Every point in this profile was analyzed for at least 120 s, and all analysis points were at least 20 μm away from the edge of the wire to avoid secondary fluorescence from the surrounding oxide. For the trace constituents Mg, Al, and Si, the k-ratio for each analysis point was determined by averaging the k-ratios measured by two to three spectrometers per point. The error in this average k-ratio was assumed to be equal to its standard deviation over all analysis points. This standard deviation based on heterogeneity was similar in magnitude to the standard deviation of the mean based on counting statistics from the 6 to 9 independent analyses per wire. Corrections to the Mg, Al, and Si concentrations due to structure in the Pd background near the Mg, Al and Si peaks were determined by analyzing the Puratronic Pd standard wire (JM Specialty Products). Previously-analyzed binary Pd-Mg, Pd-Al, and Pd-Si alloys were

reanalyzed during each microprobe session as a check on reproducibility of analysis; based on the results of four sessions, the reproducibility with respect to mole fractions was found to be within 3% for Mg at X_{Mg} = 0.00720, 1% for Al at X_{Al} = 0.01090, and 2% for Si at X_{Si} = 0.00320. The Pd alloys acquired 100-200 ppm of Pt during the runs from volatilization of the Pt sample holders and the external electrode of the oxygen sensor; this Pt appears to have no effect on the activities determined in the experiments, as concentrations were highly variable within Pd sample wires and between runs and had no discernible effect on the reproducibility of the results.

Solution behavior of Mg, Al, and Si in Pd

Experimental run conditions and analyses of Pd alloys in equilibrium with periclase, corundum, and silica at 1200 and 1400°C are given in Tables 1-3. The experiments reveal that Mg, Al, and Si dissolve into Pd in amounts ranging up to thousands of ppm by weight at oxygen fugacities near IW. This is a vital point, as it means that electron microprobe-measurable amounts of Mg, Al, and Si can be driven into Pd at f_{O_2}'s easily achieved and controlled through conventional 1-atmosphere gas-mixing techniques. In addition, the concentrations are reversible. Another key result of the Pd-pure oxide equilibration experiments is the demonstration of Henrian behavior for Mg, Al, and Si in Pd. Plots of the activities of Mg, Al, and Si calculated using Eqn. (3) and thermodynamic data of Robie et al. (1978) versus their mole fractions in Pd at 1200 and 1400°C show that the activity of each of these components is directly proportional to its concentration, indicating that the activity coefficients are constant at

Table 1. Experimental data for Pd-periclase equilibration.

Table 1. Experimental data for Pd-periclase equilibration[a]			
T (°C)	$\log_{10} f_{O_2}$	a^{b}_{Mg}	X^{c}_{Mg}
1203	-11.88	1.82×10^{-10} (0.23)	0.00076 (5)
1202[d]	-13.46	1.09×10^{-9} (0.13)	-------
	-12.96	6.06×10^{-10} (0.75)	0.00202 (10)
1203	-12.98	6.37×10^{-10} (0.80)	0.00213 (38)
1197	-14.54	3.14×10^{-9} (0.34)	0.00804 (60)
1201	-14.72	4.45×10^{-9} (0.53)	0.01118 (20)
1202	-14.99	6.32×10^{-9} (0.78)	0.01441 (76)
1399	-9.69	4.45×10^{-9} (0.43)	0.00175 (3)
1402	-9.99	6.96×10^{-9} (0.71)	0.00261 (3)
1399[d]	-11.50	3.68×10^{-8} (0.36)	-------
	-10.60	1.30×10^{-8} (0.15)	0.00467 (26)
1402	-10.62	1.43×10^{-8} (0.15)	0.00481 (6)
1402	-10.98	2.17×10^{-8} (0.22)	0.00733 (5)
1401	-11.12	2.48×10^{-8} (0.25)	0.00836 (16)

a. Numbers in parentheses indicate 1σ errors in the last digits based on heterogeneity. Temperatures are estimated to be accurate to ± 3°C and f_{O_2}'s to ± 0.05 log units.

b. Activities calculated from ΔG°_{f} for MgO of Robie et al. (1978). 1σ errors refer to pre-exponential factors and are based on propagation of T, f_{O_2} errors.

c. Mole fraction of Mg in Pd alloy.

d. Reversal. First line refers to conditions of initial equilibration, second to conditions of final equilibration.

Table 2. Experimental data for Pd-corundum equilibration.

Table 2. Experimental data for Pd-corundum equilibration[a]			
T (°C)	$\log_{10} f_{O_2}$	a_{Al}^{b}	X_{Al}^{c}
1200	-12.78	1.06×10^{-12} (0.18)	0.00207 (10)
1202[d]	-13.46	3.76×10^{-12} (0.72)	-------
	-12.96	1.57×10^{-12} (0.30)	0.00335 (1)
1202	-13.11	2.03×10^{-12} (0.39)	0.00364 (36)
1202	-13.45	3.67×10^{-12} (0.70)	0.00599 (18)
1203	-13.96	9.26×10^{-12} (1.90)	0.01571 (144)
1400	-9.69	1.82×10^{-11} (0.25)	0.00193 (3)
1401	-9.71	1.95×10^{-11} (0.28)	0.00195 (6)
1401[d]	-10.51	8.06×10^{-11} (1.20)	-------
	-10.18	4.39×10^{-11} (0.63)	0.00427 (11)
1401	-10.18	4.39×10^{-11} (0.63)	0.00438 (1)
1400	-10.18	4.28×10^{-11} (0.59)	0.00448 (6)
1406	-10.66	1.22×10^{-10} (0.23)	0.01130 (9)
1401	-11.12	2.22×10^{-10} (0.32)	0.01902 (5)
1406	-11.12	2.67×10^{-10} (0.50)	0.02393 (11)

a. Numbers in parentheses indicate 1σ errors in the last digits based on heterogeneity. Temperatures are estimated to be accurate to ± 3°C and f_{O_2}'s to ± 0.05 log units.

b. Activities calculated from ΔG_f° for Al_2O_3 of Robie et al. (1978). 1σ errors refer to pre-exponential factors and are based on propagation of T, f_{O_2} errors.

c. Mole fraction of Al in Pd alloy.

d. Reversal. First line refers to conditions of initial equilibration, second to conditions of final equilibration.

Table 3. Experimental data for Pd-silica equilibration.

Table 3. Experimental data for Pd-silica[a] equilibration[b]			
T (°C)	$\log_{10} f_{O_2}$	a_{Si}^{c}	X_{Si}^{d}
1199	-11.51	3.58×10^{-12} (0.67)	0.00020 (3)
1200	-11.88	8.44×10^{-12} (1.6)	0.00036 (3)
1199	-11.90	8.56×10^{-12} (1.6)	0.00034 (2)
1198	-12.24	1.78×10^{-11} (0.32)	0.00096 (7)
1197	-12.63	4.17×10^{-11} (0.73)	0.00196 (4)
1200	-12.77	6.63×10^{-11} (1.3)	0.00328 (4)
1199	-12.77	5.44×10^{-11} (1.0)	0.00249 (12)
1199	-12.79	6.74×10^{-11} (1.3)	0.00335 (20)
1199[e]	-13.04	1.17×10^{-10} (0.22)	-------
	-12.79	6.74×10^{-11} (1.3)	0.00364 (19)
1196	-12.83	6.35×10^{-11} (1.1)	0.00317 (3)
1201	-12.86	8.52×10^{-11} (1.7)	0.00353 (4)
1202	-12.86	9.06×10^{-11} (1.8)	0.00447 (3)
1198	-12.89	7.71×10^{-11} (1.4)	0.00365 (4)
1196	-12.92	7.49×10^{-11} (1.3)	0.00393 (4)
1199	-12.98	1.05×10^{-10} (0.20)	0.00510 (9)
1200	-13.05	1.29×10^{-10} (0.25)	0.00578 (4)
1401	-9.00	5.83×10^{-11} (1.0)	0.00057 (5)
1401	-9.01	5.99×10^{-11} (1.0)	0.00066 (4)
1402	-9.21	9.84×10^{-11} (1.7)	0.00098 (6)
1401	-9.30	1.17×10^{-10} (0.20)	0.00084 (6)
1401	-9.39	1.45×10^{-10} (0.25)	0.00136 (7)
1405	-9.55	2.43×10^{-10} (0.45)	0.00261 (5)
1401	-9.59	2.27×10^{-10} (0.39)	0.00212 (3)
1400	-9.64	2.47×10^{-10} (0.42)	0.00214 (6)
1401	-9.66	2.68×10^{-10} (0.46)	0.00207 (9)
1401	-9.68	2.82×10^{-10} (0.48)	0.00247 (3)
1400	-9.69	2.80×10^{-10} (0.47)	0.00257 (4)
1401	-9.69	2.91×10^{-10} (0.50)	0.00257 (16)
1402	-9.70	3.06×10^{-10} (0.54)	0.00264 (9)

Table 3 (continued).

a. Standard state is silica glass at T=1200°C, cristobalite at T=1400°C.
b. Numbers in parentheses indicate 1σ errors in the last digits based on heterogeneity. Temperatures are believed to be accurate to ± 3°C and f_{O_2}'s to ± 0.05 log units.
c. Activities calculated from ΔG_f° for silica glass and cristobalite of Robie et al. (1978). 1σ errors refer to pre-exponential factors and are based on propagation of T, f_{O_2} errors.
d. Mole fraction of Si in Pd alloy.
e. Reversal. First line refers to conditions of initial equilibration, second to conditions of final equilibration.

each temperature in all three systems over the composition ranges studied (Figs. 2a-f).

Constancy of the activity coefficient for each solute in Pd is important, as it allows oxide activities to be determined to high precision. If an experiment is performed in which Pd plus a sample is equilibrated at the same time as Pd plus an oxide standard, then sample and standard are at the same T, and one can write (for the case of Al_2O_3, cf. Eqn. 2):

$$K(T) = \frac{a_{Al_2O_3}^{sample}}{(\gamma_{Al}^{Pd,sample} * X_{Al}^{Pd,sample})^2 * f_{O_2}^{3/2}} = \frac{1}{(\gamma_{Al}^{Pd,corundum} * X_{Al}^{Pd,corundum})^2 * f_{O_2}^{3/2}}, \quad (4)$$

where $X_{Al}^{Pd,sample}$ is the mole fraction of Al in Pd in equilibrium with the melt or mineral, $X_{Al}^{Pd,corundum}$ is the mole fraction of Al in Pd in equilibrium with the pure oxide standard corundum, and $a_{Al_2O_3}^{corundum} \equiv 1$. The sample and standard are also at the same oxygen fugacity, so the f_{O_2} cancels on both sides of the equation, leaving only γ_{Al}^{Pd} and the mole fraction of Al in Pd to be determined for sample and standard. If one performs the experiment at an f_{O_2} such that $X_{Al}^{Pd,sample}$ and $X_{Al}^{Pd,corundum}$ both fall within the region of Henrian behavior, then γ_{Al}^{Pd} is a constant and also cancels on both sides of Eqn. (4). One then obtains:

$$a_{Al_2O_3}^{sample} = \left[\frac{X_{Al}^{Pd,sample}}{X_{Al}^{Pd,corundum}} \right]^2, \quad (5a)$$

and similarly for MgO:

$$a_{MgO}^{sample} = \frac{X_{Mg}^{Pd,sample}}{X_{Mg}^{Pd,periclase}}, \quad (5b)$$

Figure 2. Activity versus mole fraction for Pd alloys in equilibrium with pure oxides, showing Henrian behavior: periclase at (a) 1200 and (b) 1400°C; corundum at (c) 1200°C and (d) 1400°C; silica glass at (e) 1200°C and cristobalite at (f) 1400°C. Errors are 1σ based on heterogeneity of Pd alloys for X_i and propagation of T and f_{O_2} measurement errors for a_i. Best-fit lines are forced through the origin. R is the linear correlation coefficient.

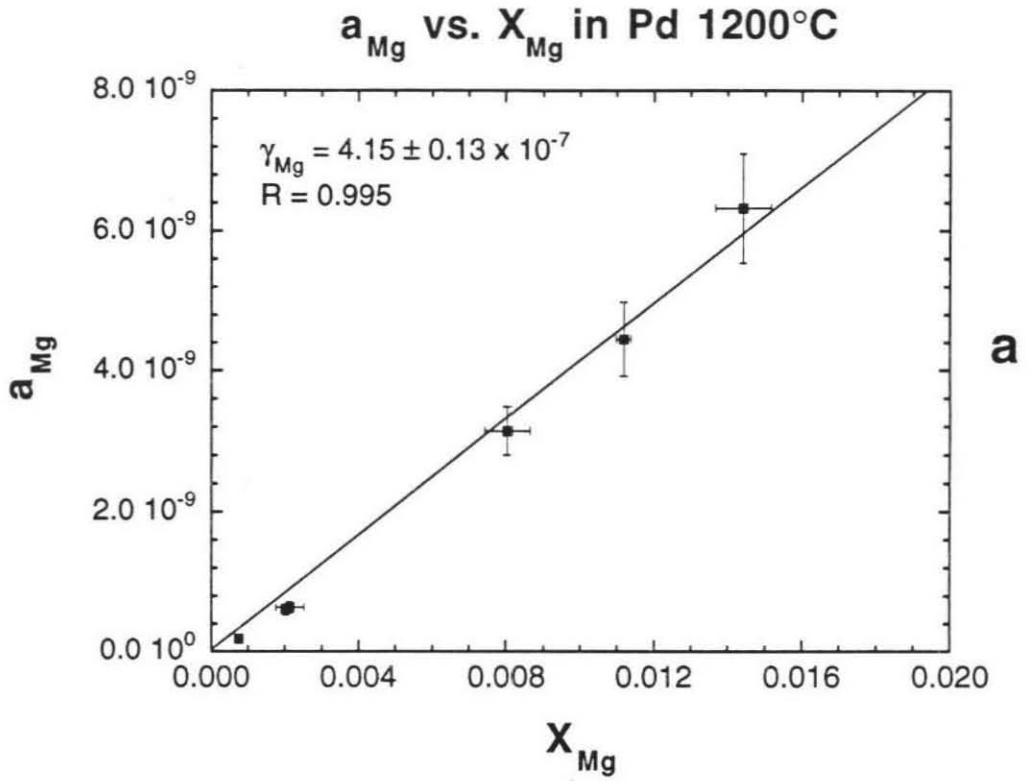
a_Mg vs. X_Mg in Pd 1200°C
γ_Mg = 4.15 ± 0.13 x 10^-7
R = 0.995
8.0 10^-9
6.0 10^-9
4.0 10^-9
2.0 10^-9
0.0 10^0
a_Mg
0.000
0.004
0.008
0.012
0.016
0.020
X_Mg
a

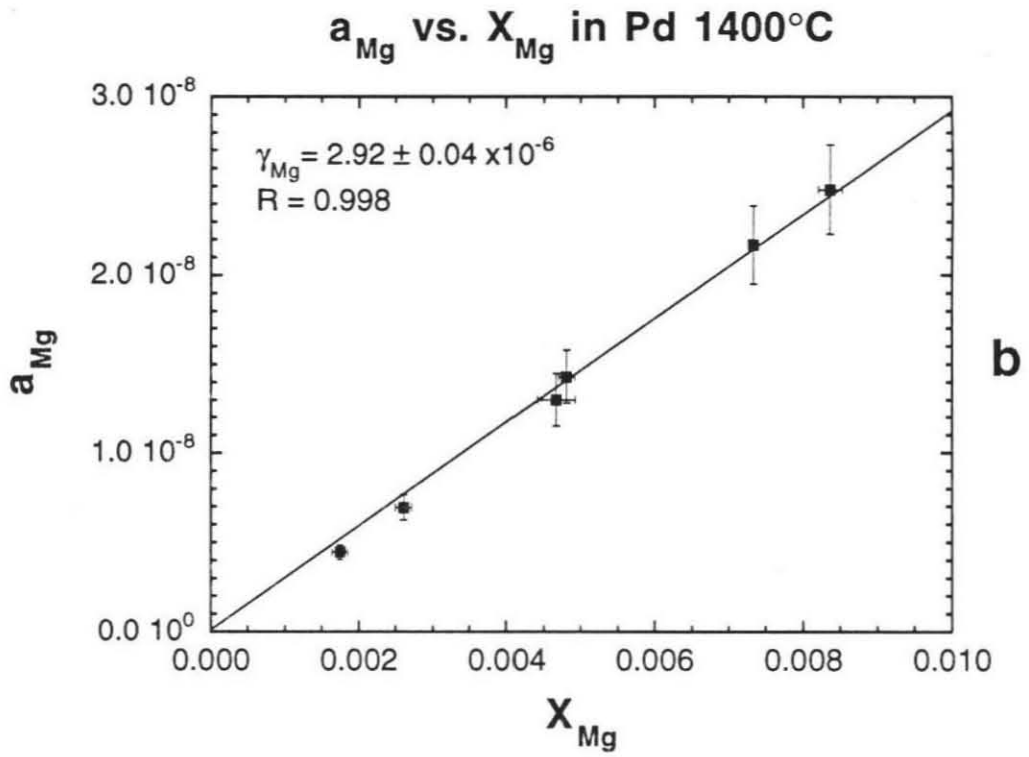
a_Mg vs. X_Mg in Pd 1400°C
γ_Mg = 2.92 ± 0.04 x10^-6
R = 0.998
3.0 10^-8
2.0 10^-8
1.0 10^-8
0.0 10^0
a_Mg
0.000
0.002
0.004
0.006
0.008
0.010
X_Mg
b

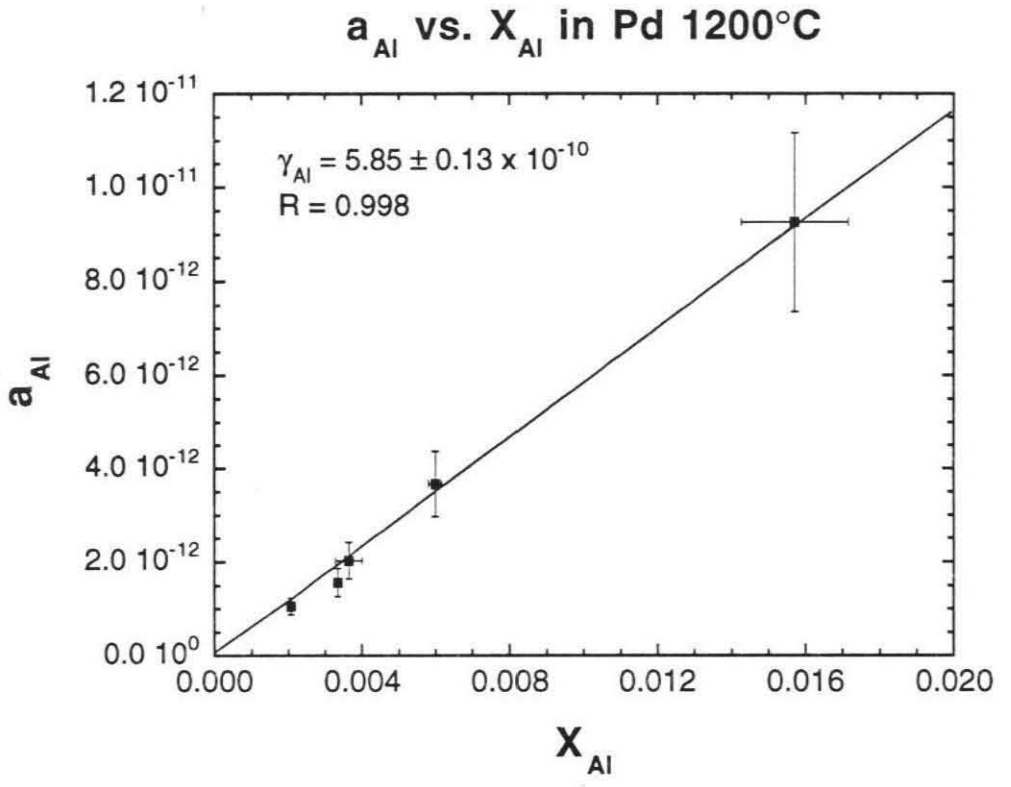
a_Al vs. X_Al in Pd 1200°C
γ_Al = 5.85 ± 0.13 x 10^-10
R = 0.998
a_Al
X_Al
1.2 10^-11
1.0 10^-11
8.0 10^-12
6.0 10^-12
4.0 10^-12
2.0 10^-12
0.0 10^0
0.000
0.004
0.008
0.012
0.016
0.020

c

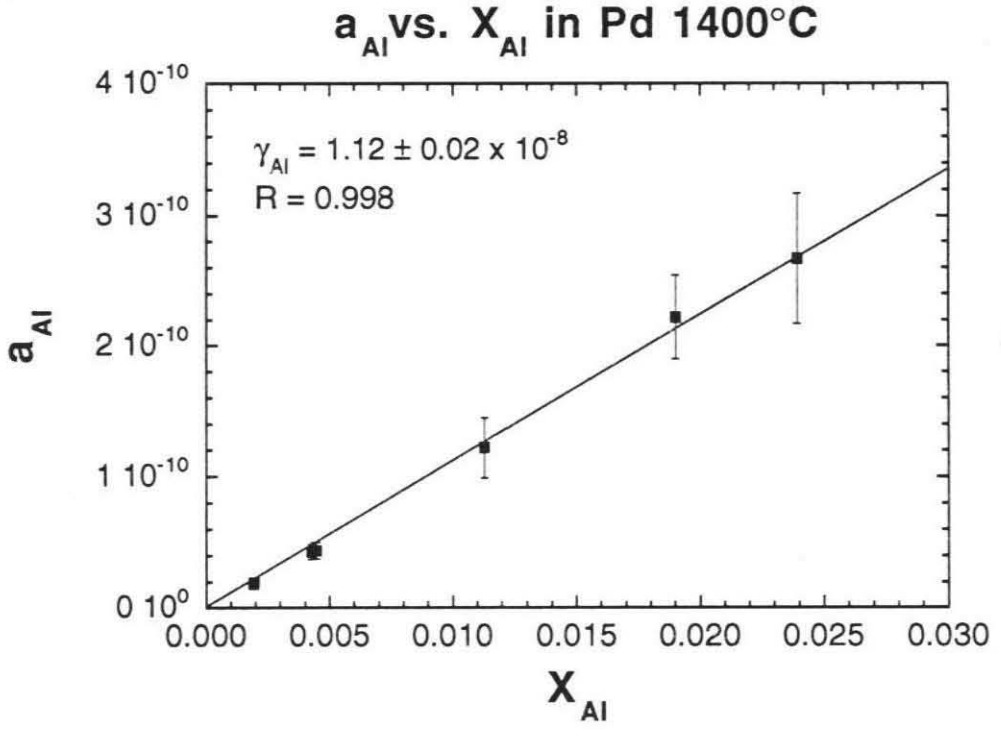
a_Al vs. X_Al in Pd 1400°C
γ_Al = 1.12 ± 0.02 x 10^-8
R = 0.998
a_Al
X_Al
4 10^-10
3 10^-10
2 10^-10
1 10^-10
0 10^0
0.000
0.005
0.010
0.015
0.020
0.025
0.030

d

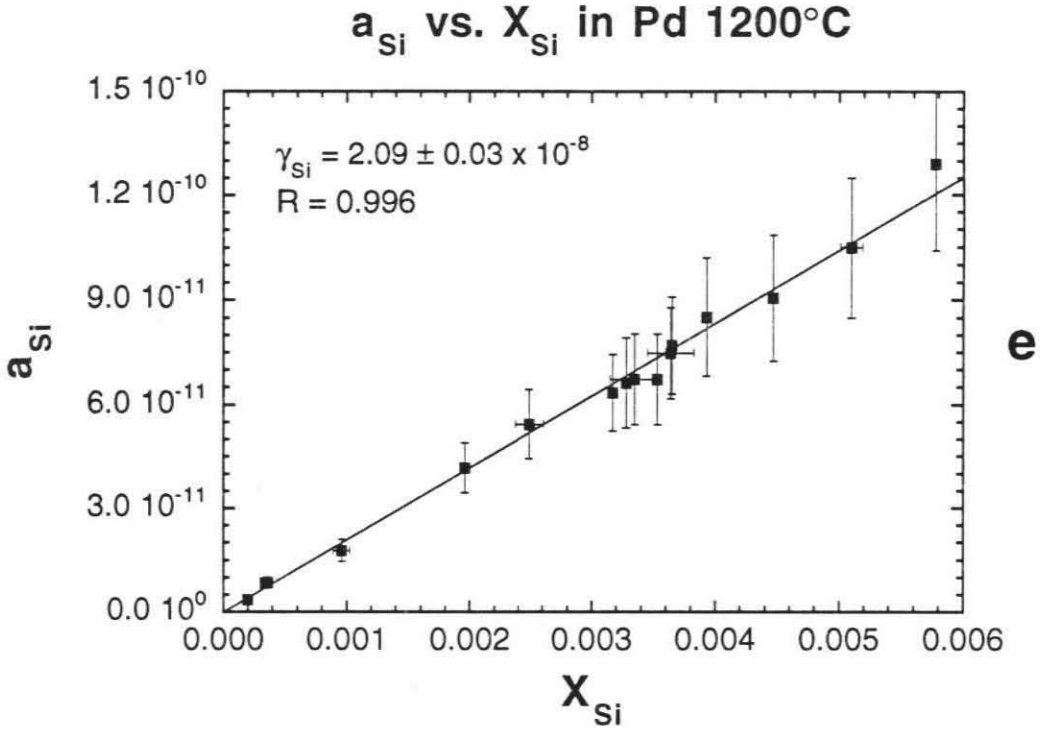
a_Si vs. X_Si in Pd 1200°C
γ_Si = 2.09 ± 0.03 x 10^-8
R = 0.996
a_Si
X_Si
1.5 10^-10
1.2 10^-10
9.0 10^-11
6.0 10^-11
3.0 10^-11
0.0 10^0
0.000
0.001
0.002
0.003
0.004
0.005
0.006

e

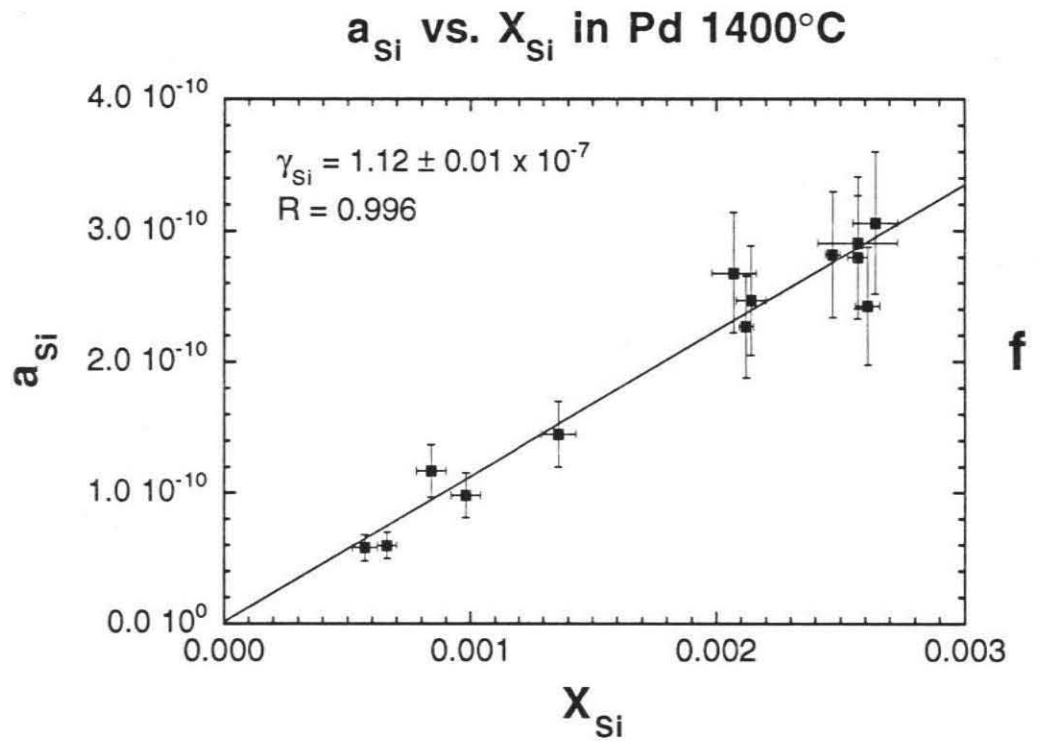
a_Si vs. X_Si in Pd 1400°C
γ_Si = 1.12 ± 0.01 x 10^-7
R = 0.996
a_Si
X_Si
4.0 10^-10
3.0 10^-10
2.0 10^-10
1.0 10^-10
0.0 10^0
0.000
0.001
0.002
0.003

f

and SiO_2:

$$a_{SiO_2}^{sample} = \frac{X_{Si}^{Pd,sample}}{X_{Si}^{Pd,silica}} \quad . \tag{5c}$$

Using this technique, errors associated with uncertainties in T, f_{O_2}, and γ_i^{Pd} are eliminated, and the problem is reduced to optimizing the precision of analysis of the Pd alloys. It has been demonstrated that quantities of Mg, Al, and Si that can be measured to within a few percent precision with the electron microprobe can be driven into Pd within the region of constant γ_i^{Pd}. Therefore, if Pd plus sample is run at the same time as Pd plus pure oxide to ensure that sample and standard equilibrate at the same T and f_{O_2}, and the resulting alloys are kept within the region of Henrian behavior, a_{oxide}^{sample} can also be determined to a precision of a few percent.

Solid-state physics of Pd

The capacity of Pd in equilibrium with MgO, Al_2O_3, or SiO_2 to dissolve measurable amounts of Mg, Al, or Si at f_{O_2}'s 10 to 20 orders of magnitude above their metal-oxide equilibrium curves requires explanation. Several other metals (Pt, Rh, Ni, Au, Fe, and Mo) were tested for this behavior by equilibrating them with SiO_2 at a variety of f_{O_2}'s, but they exhibited this ability only at oxygen fugacities significantly more reducing than required for Pd alloy formation. The extreme bonding properties of Pd have been noted previously and have inspired a small body of work on the subject in the physical chemistry literature. Pd has been found to alloy with H, B, Cd, Nb, Zr, Al, Th, U, Zn, In, and Gd in a highly nonideal way (Brodowsky and

Husemann, 1966; Brodowsky and Schaller, 1969; Brodowsky et al., 1980; Cima and Brewer, 1980; Kleykamp and Kang, 1991; Schaller, 1976, 1978, 1979; Schaller and Brodowsky, 1978a,b; Schaller et al., 1972). These alloys are characterized by extremely negative partial molar excess free energies of mixing, $\Delta\overline{G}_i^E$, for the solutes at low concentration (as low as -410 kJ/mole for Th at 800°C and -570 kJ/mole for U at 1200°C; Schaller, 1979; Kleykamp and Kang, 1991). These very negative $\Delta\overline{G}_i^E$'s correspond to extremely low activity coefficients for the solutes (on the order of 10^{-20} for Th at 800°C and U at 1200°C; compare 10^{-6} to 10^{-10} for Mg, Al, and Si at 1200-1400°C) and lead to high concentrations at low activities.

The anomalous bonding behavior of Pd can be tied to the electronic configuration of the metal. In its metallic state, Pd has a hybrid *4d-5s* band with vacancies (Frölich, 1936; Ziman, 1969). The extraordinary stability of the alloys is apparently due to the transfer of *s-p* valence electrons from the solute atoms to the electron gas of the alloy, filling these vacancies and lowering the total energy of the system. This is not the full explanation, however, as vacancies occur also in the *s-d* bands of other metals, and although some of them, such as Pt, Rh, Fe, and Ni, show alloying behavior similar to that of Pd, none exhibits it to the same degree. The difference may be related to the fact that Pd is the only element in the periodic table with a d^{10} atomic ground state, its electronic configuration being $4d^{10}$. The vacancies that are produced through bonding in pure Pd to form the metallic ground state may be more energetically unfavorable in Pd than in metals formed by elements that do not have a d^{10} atomic state, leading to a more negative free energy of mixing for Pd than for other metals

when alloys are formed with nontransition elements. The remarkable stability of Pd-Th and Pd-U alloys can be traced to the electronic structure of the solutes; the *f*-metals have very tightly-bound *f* orbitals but large, loosely-bound *s-p* orbitals and therefore readily donate electrons to the Pd solvent (Mo Li, pers. comm.).

Sources of experimental error

Factors beyond the uncertainties in the analysis of the Pd alloys may contribute inaccuracy to the determinations of oxide activities by Pd-oxide equilibration.

(1) One source of error could be T and f_{O_2} gradients in the furnace that prevent the sample and standards from truly equilibrating at the same T and f_{O_2}. The likely maximum gradient between sample and standard is 1°C in the furnace used for the experiments, which it is estimated would influence activity by only ~7%. Actual gradients are apparently much less, however, as no variation in alloy composition with lateral position was observed when multiple samples of the same oxide were run simultaneously in the furnace. This is therefore discounted as a significant source of error.

(2) Another potential source of error is the claim that the activity coefficients are constant in the dilute concentration range. The uncertainties in a_i in Fig. 2 are large due to uncertainties in f_{O_2} and T measurement. Given the errors, one cannot rule out in detail deviations from Henry's law based on the data shown in Fig. 2. However, the data are consistent with Henrian behavior, as the residuals are virtually identical for linear versus quadratic fits. Using a quadratic instead of a linear fit would change calculated activities of oxide components by only about 5 to 10%.

(3) Other potential sources of error are the corrections to the Mg, Al, and Si contents in Pd to account for structure in the Pd background. The corrections are well characterized, however, as they are based on multiple analyses of a Pd standard in each microprobe session. Moreover, if the corrections are not made, the corresponding activity vs. composition plots for the Pd alloys coexisting with pure oxides fall on linear arrays that do not pass through the origin; this suggests that the background corrections are appropriate.

(4) A more serious source of error could lie in interactions between Mg, Al, and Si in a Pd alloy equilibrated with a mineral or melt sample. The activity coefficients of Mg, Al, and Si in Pd and their Henrian behavior have been established in binary alloys, but equilibration of Pd with a mineral or melt creates a ternary or higher alloy. It is possible that the presence of multiple solutes in the alloy raises the total concentration of solutes to the point where the individual solutes begin to interact and Henry's law is no longer obeyed. To test for this possibility, experiments were performed in oxide-saturated multicomponent systems, where one should measure an activity of one for the saturating oxide in spite of the presence of more than one solute dissolved in the Pd. These experiments were performed on a cristobalite-saturated melt in the system CaO-MgO-Al_2O_3-SiO_2[1] and on periclase- and corundum-saturated spinels in the system MgO-Al_2O_3 (Tables 5, 16; see also Chamberlin et al., 1993b,d). In each case, the activity of the saturating oxide was determined to be equal within error to one. This is

[1] CaO 19.57, MgO 1.84, Al_2O_3 9.80, SiO_2 68.79 wt%; T = 1401°C, $\log_{10}f_{O_2}$ = -9.694, $X_{Si}^{Pd,melt}$ = 0.00267(5), $X_{Si}^{Pd,cristobalite}$ = 0.00266(5), a_{SiO_2} = 1.00 ± 0.03; symbols as in Table 4.

a good indication that interactions are negligible, although one cannot prove that the concentrations of all the solutes are unaffected.

(5) A final important source of error could be depletion of a thin layer of a mineral next to the Pd in one or more of its oxide components due to solution of Mg, Al, and Si in the Pd in nonstoichiometric proportions. If the mineral does not diffusively rehomogenize on the time scale of the experiment, the measured activities will not reflect those of the bulk mineral. This type of disequilibrium can be checked for by post-run microanalysis of the mineral to verify stoichiometry, by comparing ΔG_f°'s of the mineral by itself and in a melt (providing the composition of the mineral remains the same in the melt) since diffusion rates are faster and rehomogenization is less of a problem in a melt, and by conducting reversal experiments. Based on all three of these criteria, this was not a significant problem in the majority of the spinel experiments reported here (see Chapter 2), but anomalous results at 1150°C suggest that it could become important at lower temperatures.

Limitations of the technique

The application of Pd-oxide equilibration to the precise determination of oxide activities using solid Pd is of course limited to temperatures lower than the melting point of Pd at 1552°C. Although liquid Pd can dissolve large amounts of solute at experimentally-achievable f_{O_2}'s, it has not been demonstrated that the liquid exhibits Henrian behavior, the experiments being confined to temperatures of 1400°C and below. If the ability to use the technique with good precision is limited to the solid

state, the difficulty with the low melting point of Pd may be overcome through the use of another metal. A preliminary experiment equilibrating Rh with SiO_2 shows that Rh dissolves Si in amounts comparable to Pd at an f_{O_2} about an order of magnitude lower, so Rh, with its melting point of 1966 ± 3°C, may be an acceptable substitute at higher temperatures. There is also likely a lower practical temperature limit to the usefulness of this technique, because of the greater difficulty at low temperature in achieving diffusive rehomogenization of minerals after the initial thin-layer depletion next to the Pd.

In addition, measurement of SiO_2 activities presents a difficult problem at high temperatures (~1400°C), because the region of solid solution in Pd-Si alloys, already small (Moffatt, 1982), shrinks with increasing temperature due to melting. In the case of MgO and Al_2O_3, when a particularly low activity is encountered, precision of measurement can be raised by lowering the f_{O_2} of the experiment and thereby boosting the Mg and Al concentrations in the Pd wire in equilibrium with the sample. This works because Mg and Al have a wide range of solid solution with Pd (Nayeb-Hashemi and Clark, 1985; McAlister, 1986). However, because of the limited solid solution in the Pd-Si system, if the experimental f_{O_2} is lowered too much, the Pd alloy in equilibrium with the silica standard will melt and the resulting liquid alloy will fall at several atom % Si, probably outside the region of Henrian behavior. Because of this, determinations of SiO_2 activities below about 0.2 at high temperature will be imprecise, unless the Si concentrations can be measured using a method of greater sensitivity than the electron microprobe, such as the ion microprobe, or by the use of Rh, with its higher

melting point.

Finally, there are cases where the activity of a particular oxide component cannot be determined to high precision. For example, so far the measurement of CaO activities through the use of the electron microprobe has not been established. At even the most reducing conditions feasible with an yttria-zirconia O_2 sensor ($\log_{10}f_{O_2} \sim -11$ at 1400°C), no detectable Ca was found in Pd equilibrated with CaO. Ca was detectable by ion microprobe analysis but was inhomogeneously distributed (I. Hutcheon, pers. comm.). The uneven distribution may reflect quench exsolution of an initially homogeneous Pd-Ca alloy stable at high temperature: although undetectable with the electron microprobe, such "hot spots" are occasionally observed in Pd-Mg, -Al, and -Si alloys using the ion microprobe and may be related to variable quench rates.

Comparison with calorimetry

Calorimetry has been the most frequently used method for determining the thermodynamic properties of geologically-relevant materials. Calorimetry is highly successful in many cases, but determining activities from calorimetric enthalpies of mixing requires combining the enthalpy data with a mixing model that provides entropies (thereby increasing uncertainty) and differentiation of these results with respect to composition. In contrast, Pd-oxide equilibration directly provides activities of oxides in multicomponent liquids without the need for additional data manipulation. Moreover, these activities have low, well-defined experimental errors that provide tight constraints on solution models for melts.

For minerals, Pd-oxide equilibration provides a useful complement to calorimetry, the latter of which can be used to obtain precise ΔH_f° or C_p but does not directly yield ΔG_f° or activity, the most crucial thermodynamic properties from a petrological standpoint. Pd-oxide equilibration yields precise ΔG_f° but less precise ΔH_f° or C_p, and currently operates over a smaller temperature range. Used together, calorimetric ΔH_f° and ΔG_f° from Pd-oxide equilibration give tight constraints on the value of ΔS_f°, which can be used to test various entropy models for mineral systems. A significant feature of Pd-oxide equilibration is that measured thermodynamic properties reflect equilibration at high temperature, so no structural or ordering changes in the mineral on quenching affect the results. Experimental activities and free energies therefore reflect those of the mineral in its equilibrium state at a particular temperature, a fact not necessarily true in drop calorimetric experiments. The technique therefore offers an excellent method for checking and correcting calorimetric results over the temperature range 1100 to 1400°C when irregularities are suspected in the data.

Summary

Pd-oxide equilibration is a new experimental technique for the determination of the activities of oxide components in melts and minerals. It takes advantage of the equilibrium between Pd alloy, oxygen, and an oxide component in a melt or mineral. Due to the unusual stability of dilute Pd alloys, Pd metal in equilibrium with a melt or mineral dissolves electron probe-measurable amounts of Mg, Al, and Si at oxygen fugacities within a few orders of magnitude of the IW buffer, making this method

feasible with routine gas-mixing techniques. Because Mg, Al, and Si in Pd exhibit Henrian behavior in the dilute region, the activity of each of their oxides in the melt or mineral is a simple function of the ratio of the concentration of the metal in Pd in equilibrium with the melt or mineral to that in Pd in equilibrium with the pure oxide. The ability to analyze for Mg, Al, and Si in the alloy is the major limitation on precision, because the effects of uncertainties in T, f_{O_2}, and γ_i in the Pd are eliminated. This makes it possible to determine oxide activities in melts and free energies of formation of minerals to a precision of a few percent. This technique, with its potential for directly and precisely determining oxide activities in melts and free energies of formation of minerals, could be of considerable value in refining the existing thermodynamic data base.

Chapter 2. The thermodynamics of $MgAl_2O_4$ spinel

In this chapter, Pd-oxide equilibration is applied to the determination of oxide activities in stoichiometric $MgAl_2O_4$ spinel. The effect of cation disorder on the thermodynamics of $MgAl_2O_4$ spinel is described, with an emphasis on the usefulness of the technique of Pd-oxide equilibration for obtaining equilibrium thermodynamic properties of spinel. This is followed by an account of the experimental procedure used for measuring activities and free energies of formation and the measured values. The results are combined with calorimetric data and direct measurements of cation disorder to derive thermodynamic properties as a function of temperature for spinel with equilibrium disorder. Finally, the expected effect of the corrected free energies on phase equilibria involving spinel is discussed.

The ordering problem in spinel

Spinels are constituents of many igneous and metamorphic rocks due to their wide stability in pressure, temperature, and composition space. They occur in rocks as varied as lherzolite, gabbro, basalt, acid granulite, granite, and contact-metamorphosed limestone and argillite. Also, nearly pure end-member $MgAl_2O_4$ spinel is a common phase in Ca-Al-rich inclusions (CAIs) in meteorites (MacPherson et al., 1988) and is likely to have been one of the first high-temperature mineral condensates in the primitive solar nebula (Grossman, 1972). Partly because of their widespread occurrence, spinels are important petrogenetic indicators and have been used in the calibration of a

variety of widely-used mineral geothermometers and geobarometers (Buddington and Lindsley, 1964; Sack, 1980; Mattioli et al., 1989, Sack and Ghiorso, 1991). However, our understanding of spinel equilibria is complicated by an incomplete knowledge of the thermodynamic properties of the various end-members.

Deficiencies in the current data base are illustrated by the case of $MgAl_2O_4$, the end-member spinel that gives its name to the mineral group. Calorimetric measurements of heat capacity and heat content (King, 1955; Bonnickson, 1955) have given appreciable insight into the thermodynamics of $MgAl_2O_4$, but these measurements are insufficient because they do not account for the variable amount of cation disorder present in the mineral. The cation configuration of spinel varies with increasing temperature from a "normal" distribution, $Mg^{2+}(Al_2^{3+})O_4$, with Al^{3+} restricted to octahedral sites, towards an "inverse" distribution, $Al^{3+}(Mg^{2+}Al^{3+})O_4$, with Al^{3+} substituting into tetrahedral sites (Navrotsky and Kleppa, 1967). Due to kinetic factors, if spinel is equilibrated at high temperature and then quenched rapidly to below 900-1000°C, it fails to reorder to the equilibrium state appropriate to the quench temperature but instead retains a residual amount of the disorder present at high temperature (Wood et al., 1986; Millard et al., 1992). This residual disorder greatly complicates interpretation of heat capacity and drop calorimetric heat content measurements on $MgAl_2O_4$. Because synthetic spinels are never perfectly normal, heat capacities measured at low temperature ($T < 300$°C) on synthetic spinel (King, 1955) actually apply to spinel with nonequilibrium disorder. Likewise, heat contents measured on samples quenched from high temperature to below ~1000°C are lower than the equilibrium values because a

disordering contribution is lost (Navrotsky and Kleppa, 1967). Moreover, because spinel can reorder somewhat between 700 and 1000°C, calorimetric data obtained below 1000°C are strongly influenced by the thermal history of the starting material.

Researchers have employed a number of methods to extract the equilibrium thermodynamic properties of spinel. For example, Helgeson et al. (1978), Berman (1988), and Holland and Powell (1990) combined phase equilibrium data with calorimetric constraints to produce internally consistent sets of thermodynamic data intended to incorporate the equilibrium disorder in the spinel without explicitly quantifying it. However, the accuracy of these models for spinel depends on the quality of the phase equilibrium and calorimetric data employed and on the validity of the models used to describe the free energies of individual phases in each equilibrium. An alternative is to estimate the enthalpy and entropy of disordering and recalculate the free energy of formation to equilibrium values (JANAF, 1985), but this procedure is vulnerable to errors in estimating the cation distribution in the spinel and in the model adopted to calculate the entropy. Overall, these various sources yield derived free energies of formation of $MgAl_2O_4$ spinel from the oxides, ΔG_f°, ranging over more than 10 kJ/mole. This is a significant discrepancy, since ΔG_f° is only about 30 to 40 kJ/mole. Pd-oxide equilibration, however, can be used to determine the actual equilibrium thermodynamic properties of spinel, as the data reflect equilibration at high temperature and are therefore independent of ordering changes that occur upon quenching.

Experimental procedure

Sample preparation

Powdered stoichiometric $MgAl_2O_4$ spinel for these experiments was provided by Dr. Glen S. Mattioli of the University of Puerto Rico, Mayaguez. Details of the spinel synthesis are given in Mattioli et al. (1987). The spinel was analyzed by X-ray diffraction (XRD), and the lattice parameter, a_0 = 8.0855(11) Å , is consistent with pure stoichiometric spinel (a_0 = 8.0844(3), Navrotsky et al., 1986). In addition, periclase-saturated spinels were synthesized by grinding mixtures of reagent-grade MgO and Al_2O_3 (JMC Puratronic) for 5 hours under ethanol in an agate mortar and sintering for 48 hours in air at 1400°C. XRD analysis of the sintered material confirmed the presence of periclase and spinel. Samples were prepared by pressing the powdered spinel into pellets around 3-4 mm lengths of 0.25 mm diameter 99.997% pure Pd wire (Alfa Products). No binder was used because of the tendency of organic binders to leave a carbon residue in the sample at low f_{O_2}. The pellets were placed in ¼-inch diameter Pd foil buckets. Experiments were also conducted on spinel-saturated synthetic melts in the system CaO-MgO-Al_2O_3-SiO_2-TiO_2. Details of the synthesis are given in Chapter 3 and Chamberlin et al. (1993c). The melts are analogs of melilite-rich Type B Ca-Al-rich inclusions (CAIs) in meteorites; bulk composition and variation of liquid composition with temperature are described in Chapter 3, Stolper (1982), and Chamberlin et al. (1993c). Glassy powdered starting material was pressed into pellets around 3-4 mm lengths of pure Pd wire and melted onto Pd wire loops with a small H_2/O_2 torch. The pure oxide standards were prepared by pressing analytical-grade MgO and Al_2O_3 (JMC Puratronic) around 3-4 mm lengths of pure Pd wire.

Before pressing, the initially amorphous Al_2O_3 was converted to corundum (confirmed by XRD) by heating for about 6 hours at 1500°C in a Pt crucible. The MgO starting material was found by XRD to be crystalline periclase. The Pd + periclase or Pd + corundum pellets were placed in open capsules made from ¼-inch diameter crushable magnesia or alumina rods (Ozark Technical Ceramics) that were drilled out to form open capsules.

Experimental methods

Experiments were conducted in a 1-atmosphere home-built furnace with $MoSi_2$ heating elements. Temperature was controlled to within 1-2°C by a Eurotherm 812 Controller/Programmer and measured by a Type S thermocouple calibrated at the melting point of gold. Stated temperatures are estimated to be accurate to ± 3°C. Oxygen fugacity was set using mixtures of H_2 and CO_2 and measured by an yttria-doped zirconia solid electrolyte oxygen sensor (Ceramic Oxide Fabricators Pty. Ltd., Australia). The sensor was calibrated at the iron-wüstite buffer at 1200 and 1400°C by measuring changes in the resistance of pure iron wire. Drift of the emf of the sensor during a run was typically 1 mV or less.

The samples and standards were suspended from Ir hanging wire and placed adjacent to each other in a 1-atmosphere gas-mixing furnace. Runs were done in the temperature range from 1150 to 1400°C at 50°C intervals. The oxygen fugacity was typically an order of magnitude or two below iron-wüstite. Experiments at T > 1250°C were run for 1 to 3 days, while those at lower temperatures were equilibrated for 10

days. The results on stoichiometric spinel were reversed at 1200 and 1350°C by approaching equilibrium from the high concentration side through first equilibrating the Pd wires with the spinel, periclase, and corundum at f_{O_2}'s half an order of magnitude lower than those of the final equilibrations. Reversals on the CAI experiments were performed similarly. Runs were terminated by drop-quenching into deionized water. The pellets were removed from their containers, mounted in epoxy, and rough-polished to expose a length-wise cross section through the Pd wire. The Pd was then fine-polished with diamond paste using an automatic polisher.

Analytical techniques

The Pd wires were analyzed as described in Chapter 1. Post-run analyses were performed on the nominally stoichiometric and the CAI spinels to determine their Mg:Al ratios. These analyses were performed on the JEOL 733 Superprobe at 15 keV, a 40° takeoff angle, a 30 s counting time, and a 1 nA beam current to restrict the sampling volume to about 1 μm. Concentrations were determined through ZAF correction procedures (Armstrong, 1988). Analysis points on the stoichiometric spinel ranged from within 5 μm of the Pd to 1 mm or more away. Standardization was done on a stoichiometric Union Carbide $MgAl_2O_4$ laser crystal. Because the overvoltages for Mg and Al are virtually identical, signal loss due to the porosity of the powdered spinel pellets and trapped bubbles or cracks inside the CAI glasses is the same for both elements, and Mg:Al ratios can be determined to better than 1%. CAI spinels were also analyzed for trace Ca, Ti, and Si. In order to minimize the signal from the surrounding

glass, 1 mm diameter crystals grown from an identical bulk composition in cooling-rate experiments (Stolper and Paque, 1986: runs 47, 50, 59, 61, and 79) were used. Standardization was done on spinel, anorthite, and rutile, and analyses were performed at 15 keV, 40°, 100 s, and 30 nA.

Activities and free energies

Experimental run conditions and analysis of Pd alloys are given in Table 4. Post-run analysis of selected pure and CAI spinels, including reversal experiments, show that in the main they are stoichiometric to within a mole percent. Analysis of a pellet from a failed experiment run at 1150°C shows a slight depletion in MgO (Mg:Al ranges down to 0.486). CaO, SiO_2, and TiO_2 contents of the 1 mm CAI spinels from the earlier cooling rate experiments of Stolper and Paque (1986) were determined to be about 150, 250, and 400 ppm respectively. Table 5 shows the derived activities of MgO and Al_2O_3 relative to periclase and corundum for spinel and the ΔG_f°'s calculated from them using the equilibrium:

$$MgO_{(periclase)} + Al_2O_{3(corundum)} = MgAl_2O_{4(spinel)}\ , \qquad (1)$$

and the relation:

$$\Delta G_f^\circ = -\,RT\ \ln \frac{1}{a_{MgO}^{spinel}\ a_{Al_2O_3}^{spinel}}\ , \qquad (2)$$

where $a_{MgAl_2O_4}^{spinel} \equiv 1$ for pure end-member spinel with an equilibrium state of order. Table 5 includes the activities and ΔG_f°'s determined for stoichiometric and periclase-saturated spinel, and for the spinels crystallized from melts of bulk Type B CAI com-

Table 4. Experimental data for $MgAl_2O_4$[a].

Table 4. Experimental data for $MgAl_2O_4$[a]						
T (°C)	$\log_{10}f_{O_2}$	time (hrs.)	$X_{Mg}^{Pd,spinel}$	$X_{Mg}^{Pd,periclase}$	$X_{Al}^{Pd,spinel}$	$X_{Al}^{Pd,corundum}$
1154	-13.63	260	0.00090 (16)	0.00140 (14)	0.00066 (6)	0.00191 (2)
1200	-12.44	240	0.00091 (4)	0.00097 (3)	0.00029 (7)	0.00113 (7)
1201	-12.98	264	0.00142 (7)	0.00179 (7)	0.00071 (1)	0.00271 (6)
1201[c]	-13.49	144	-------	-------	-------	-------
	-12.91	192	0.00156 (9)	0.00171 (17)	0.00067 (6)	0.00267 (7)
1251	-11.79	45	0.00094 (8)	0.00136 (9)	0.00049 (4)	0.00178 (10)
1250[d]	-11.58	144	0.00094 (4)	-------	0.00026 (3)	0.00118 (3)
1300[e]	-11.32	89	0.00202 (11)	0.00201 (11)	0.00068 (1)	0.00291 (4)
1299[f]	-12.04	42	0.00083 (10)	0.00462 (16)	0.00440 (10)	0.00947 (16)
1300[f]	-11.32	64	0.00045 (10)	0.00218 (10)	0.00139 (2)	0.00299 (1)
1302[f]	-11.42	70	0.00059 (5)	0.00229 (9)	0.00158 (2)	0.00357 (5)
1300[c,f]	-12.29	48	-------	-------	-------	-------
	-12.09	48	0.00078 (6)	0.00478 (9)	0.00416 (4)	0.00950 (9)
1301[c,e]	-11.90	72	-------	-------	-------	-------
	-11.73	72	0.00056 (8)	0.00335 (9)	0.00260 (4)	0.00602 (1)
1305	-11.19	68	0.00148 (8)	0.00197 (9)	0.00070 (7)	0.00248 (1)
1350[f]	-10.71	48	0.00062 (11)	0.00263 (13)	0.00180 (3)	0.00378 (6)
1350[f]	-11.37	43	0.00116 (13)	0.00646 (17)	0.00640 (7)	0.01398 (38)
1351[f]	-10.65	48	0.00051 (11)	0.00236 (7)	0.00136 (15)	0.00305 (3)
1351[c]	-11.02	48	-------	-------	-------	-------
	-10.61	48	0.00206 (12)	0.00206 (12)	0.00070 (7)	0.00283 (9)
1352[c,f]	-11.60	24	-------	-------	-------	-------
	-11.35	48	0.00097 (7)	0.00501 (12)	0.00431 (4)	0.00929 (9)
1352	-10.66	43	0.00221 (3)	0.00235 (4)	0.00085 (3)	0.00343 (8)
1356[d]	-10.33	23	0.00151 (4)	-------	0.00046 (3)	0.00213 (20)
1397[e]	-10.20	66	0.00287 (13)	0.00267 (6)	0.00107 (5)	0.00424 (7)
1400	-10.17	44	0.00186 (7)	0.00294 (9)	0.00131 (4)	0.00438 (7)
1400	-10.17	38	0.00261 (5)	0.00281 (5)	0.00120 (8)	0.00459 (5)
1401[f]	-10.16	39	0.00067 (7)	0.00291 (5)	0.00214 (10)	0.00441 (1)
1401[f]	-10.66	42	0.00111 (6)	0.00515 (4)	0.00482 (4)	0.01024 (15)
1402[f]	-10.18	41	0.00086 (5)	0.00360 (10)	0.00248 (1)	0.00516 (8)
1399[c,f]	-11.50	24	-------	-------	-------	-------
	-10.60	24	0.00085 (9)	0.00467 (26)	0.00372 (9)	0.00801 (4)
1400[d]	-9.65	45	0.00153 (4)	-------	0.00044 (1)	0.00198 (9)

a. Numbers in parentheses indicate 1σ errors in the last digits based on heterogeneity. Temperatures are estimated to be accurate to ± 3°C and f_{O_2}'s to ± 0.05 log units.

Table 4 (continued).

b. $X_i^{Pd,\,j}$ defined as mole fraction of solute i dissolved in Pd alloy in equilibrium with phase j.
c. Reversal. First line refers to conditions of initial equilibration, second to conditions of final equilibration.
d. Periclase-saturated spinel, a_{MgO} assumed to be one.
e. Periclase-saturated spinel.
f. Spinel-saturated bulk Type B CAI melt.

Table 5. Derived data for $MgAl_2O_4$[a].

Table 5. Derived data for $MgAl_2O_4$[a]			
T (°C)	a_{MgO}	$a_{Al_2O_3}$	ΔG_f° (J)
1154	0.643 (0.131)	0.119 (0.022)	-30495 (3264)
1200	0.938 (0.057)	0.066 (0.035)	-34073 (6538)
1201	0.793 (0.032)	0.069 (0.004)	-35609 (866)
1201[b]	0.912 (0.104)	0.063 (0.011)	-35011 (2557)
1251	0.691 (0.072)	0.076 (0.016)	-37337 (2977)
1250[c]	1.00	0.050 (0.012)	-37985 (3028)
1300[d]	1.00 (0.074)	0.055 (0.002)	-37933 (1081)
1299[e]	0.180 (0.022)	0.216 (0.012)	-42203 (1757)
1300[e]	0.206 (0.047)	0.216 (0.006)	-40705 (3007)
1302[e]	0.258 (0.024)	0.196 (0.007)	-39082 (1307)
1300[b,e]	0.163 (0.013)	0.192 (0.005)	-45445 (1101)
1301[b,e]	0.167 (0.024)	0.187 (0.006)	-45364 (1929)
1305	0.751 (0.053)	0.080 (0.015)	-36895 (2630)
1350[e]	0.236 (0.043)	0.227 (0.009)	-39494 (2517)
1350[e]	0.180 (0.021)	0.210 (0.012)	-44200 (1755)
1351[e]	0.216 (0.047)	0.196 (0.044)	-42697 (4222)
1351[b]	1.00 (0.082)	0.061 (0.013)	-37765 (3084)
1352[b,e]	0.194 (0.014)	0.215 (0.006)	-42614 (1048)
1352	0.940 (0.020)	0.061 (0.005)	-38624 (1146)
1356[c]	1.00	0.047 (0.010)	-41321 (2900)
1397[d]	1.07 (0.030)	0.064 (0.006)	-37229 (1303)
1400	0.633 (0.031)	0.089 (0.006)	-40011 (1161)
1400	0.929 (0.024)	0.068 (0.009)	-38418 (1876)
1401[e]	0.230 (0.024)	0.235 (0.021)	-40612 (1914)
1401[e]	0.216 (0.012)	0.230 (0.007)	-41785 (885)
1402[e]	0.239 (0.015)	0.224 (0.007)	-40769 (977)
1399[b,e]	0.182 (0.020)	0.216 (0.010)	-44734 (1659)
1400[c]	1.00	0.050 (0.005)	-41633 (1396)

a. Numbers in parentheses indicate 1σ errors from propagation of analytical errors based on heterogeneity.
b. Reversal.
c. Periclase-saturated spinel, a_{MgO} assumed to be one.
d. Periclase-saturated spinel.
e. Spinel-saturated CAI melt.

position. The ΔG_f°'s determined in the periclase-saturated spinel are within 1σ error of those determined for the stoichiometric mineral, as expected given the minimal MgO solid solution implied by the $MgO\text{-}Al_2O_3$ phase diagram below 1500°C (Roy et al., 1953; Alper et al., 1962; Lejus, 1964; Colin, 1968). The ΔG_f°'s of $MgAl_2O_4$ determined from the CAI spinels are typically up to 4 or 5 kJ/mole more negative but still within 2σ error of those for stoichiometric $MgAl_2O_4$. The deviation may be due to the presence of the impurities in the CAI spinels. The offset of the 1154°C point (Fig. 3) from the trend of the others suggests that diffusive rehomogenization of the spinel during experiments may become a problem at $T < 1200$°C. However, a close approach to equilibrium in the pure spinel runs at $T \geq 1200$°C is demonstrated by the other analyses and by the reversal experiments, which reproduce the ΔG_f°'s within 1σ error. The reversals on the CAI spinels reproduce the ΔG_f°'s of the pure spinels within 2σ error.

The experimentally determined values of ΔG_f° of spinel are shown in Fig. 3 with values from six compilations of thermodynamic data for minerals (Robie et al., 1978; Helgeson et al., 1978; Berman, 1988; JANAF, 1985; Holland and Powell, 1990; Hallstedt, 1992). The experimental data are in good agreement with JANAF (1985) but are for the most part distinct at the 1σ level from the other compilations and at the 2σ level from the calorimetric values (Robie et al., 1978). The variation of the experimental free energies in this study with temperature implies an entropy of formation on the order of 11-13 J/moleK in this temperature range (see Eqn. 11), a value comparable to that in JANAF (1985) (12-13 J/moleK) and less than Hallstedt (1992) (~16

Figure 3. Free energy of formation of spinel from the oxides (ΔG_f°) versus temperature (K), showing experimental data (1σ errors from propagation of analytical errors based on heterogeneity) and literature values: 1. Robie et al. (1978); 2. Helgeson et al. (1978); 3. Holland and Powell (1990); 4. Berman (1988); 5. this study, Eqn. (11); 6. JANAF (1985); 7. Hallstedt (1992).

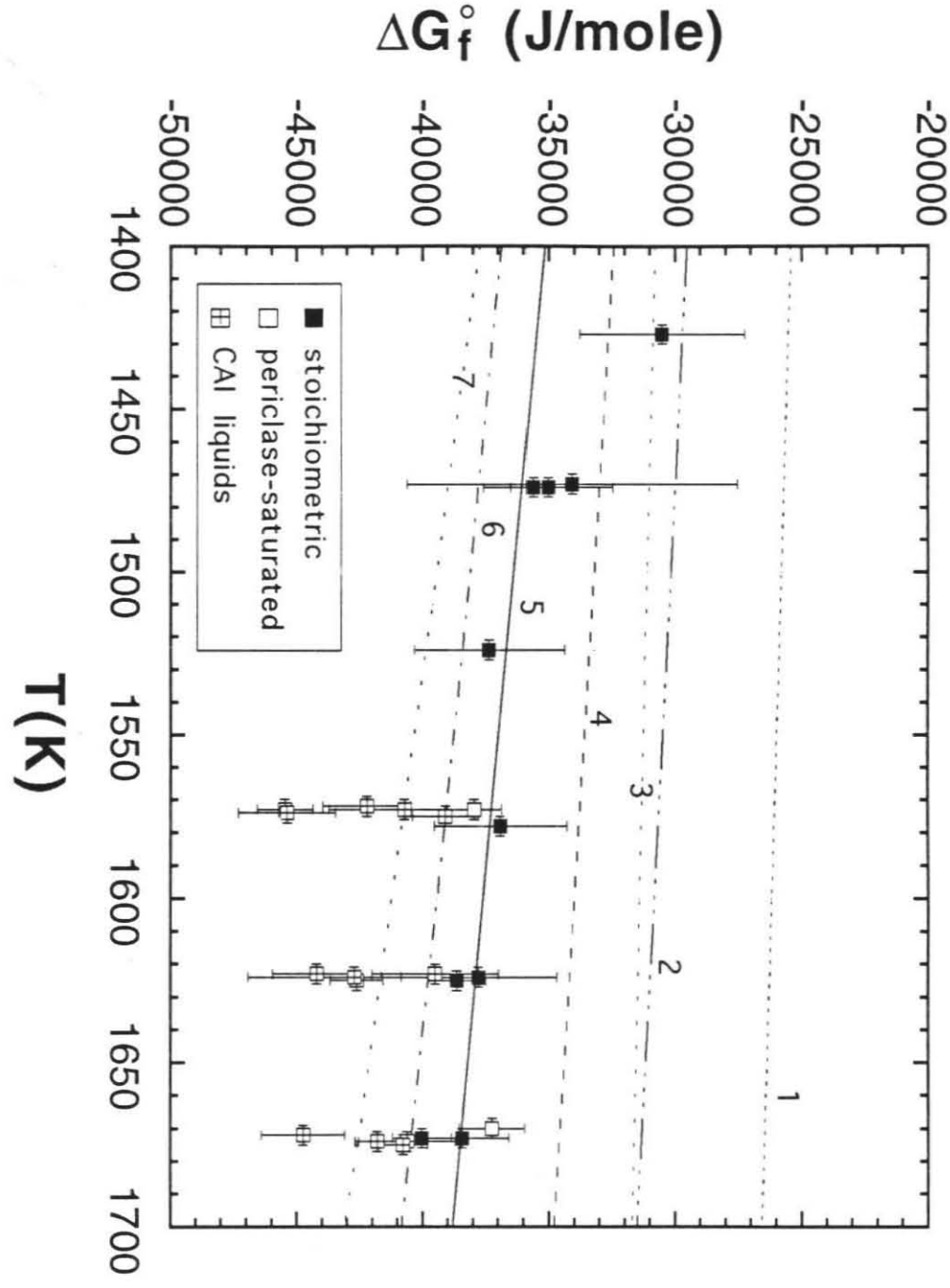
ΔG°f of spinel from the oxides vs. T
ΔG°f (J/mole)
-20000
-25000
-30000
-35000
-40000
-45000
-50000
1400
1450
1500
1550
1600
1650
1700
T(K)
stoichiometric
periclase-saturated
CAI liquids
1
2
3
4
5
6
7

J/moleK) but substantially larger than those of the four other data sets (2.5 to 8 J/moleK).

Activities

Table 5 reveals that the activity of MgO in spinel varies from about 0.2 in the CAI spinels to 1 in the MgO-saturated spinels, although all the spinels appear to have the same Mg:Al ratios and the ΔG_f°'s calculated from Eqn. (5) agree within 2σ. This behavior is explicable in terms of the shape of the free energy curve for spinel. Fig. 4 shows a schematic molar Gibbs free energy ($\bar{G}$) versus composition diagram at constant P and T for the system MgO-Al_2O_3. For spinel of any particular Mg:Al ratio, the tangent line to the spinel curve at that composition has a slope of $\mu_{Al_2O_3}^{spinel} - \mu_{MgO}^{spinel}$ and intercepts at $X_{MgO} = 1$ and $X_{Al_2O_3} = 1$ of μ_{MgO}^{spinel} and $\mu_{Al_2O_3}^{spinel}$. The activity of MgO in the spinel relative to a periclase standard state, a_{MgO}^{spinel}, is equal to $\exp[(\mu_{MgO}^\circ - \mu_{MgO}^{spinel})/RT]$, where μ_{MgO}° is the free energy per mole or chemical potential of pure periclase. Likewise, the activity of Al_2O_3 in the spinel relative to a corundum standard state, $a_{Al_2O_3}^{spinel}$, is equal to $\exp[(\mu_{Al_2O_3}^\circ - \mu_{Al_2O_3}^{spinel})/RT]$, where $\mu_{Al_2O_3}^\circ$ is the chemical potential of pure corundum. For stoichiometric spinel, ΔG_f° is the difference between the free energy of a simple mechanical mixture of the oxides, $(\mu_{MgO}^\circ + \mu_{Al_2O_3}^\circ)/2$, and the free energy of spinel (Mg:Al = 0.5). If the Mg:Al ratio of the spinel is changed slightly from the stoichiometric value, ΔG_f° changes very little, but if, as assumed in the construction, the spinel free energy curve is strongly concave upward

Figure 4. Schematic representation of molar free energy ($\overline{G}$) versus composition for the system MgO-Al_2O_3. The $\overline{G}$ curves of periclase and corundum are placed arbitrarily for ease of depiction. Intercepts of tangent lines with vertical axes give the chemical potentials μ of MgO and Al_2O_3; the dashed line between μ°_{MgO} and $\mu^{\circ}_{Al_2O_3}$ is for a mechanical mixture of pure MgO and Al_2O_3, and the solid line is for stoichiometric spinel. The length of the dashed arrow gives ΔG°_f, the free energy of formation of stoichiometric spinel from the oxides.

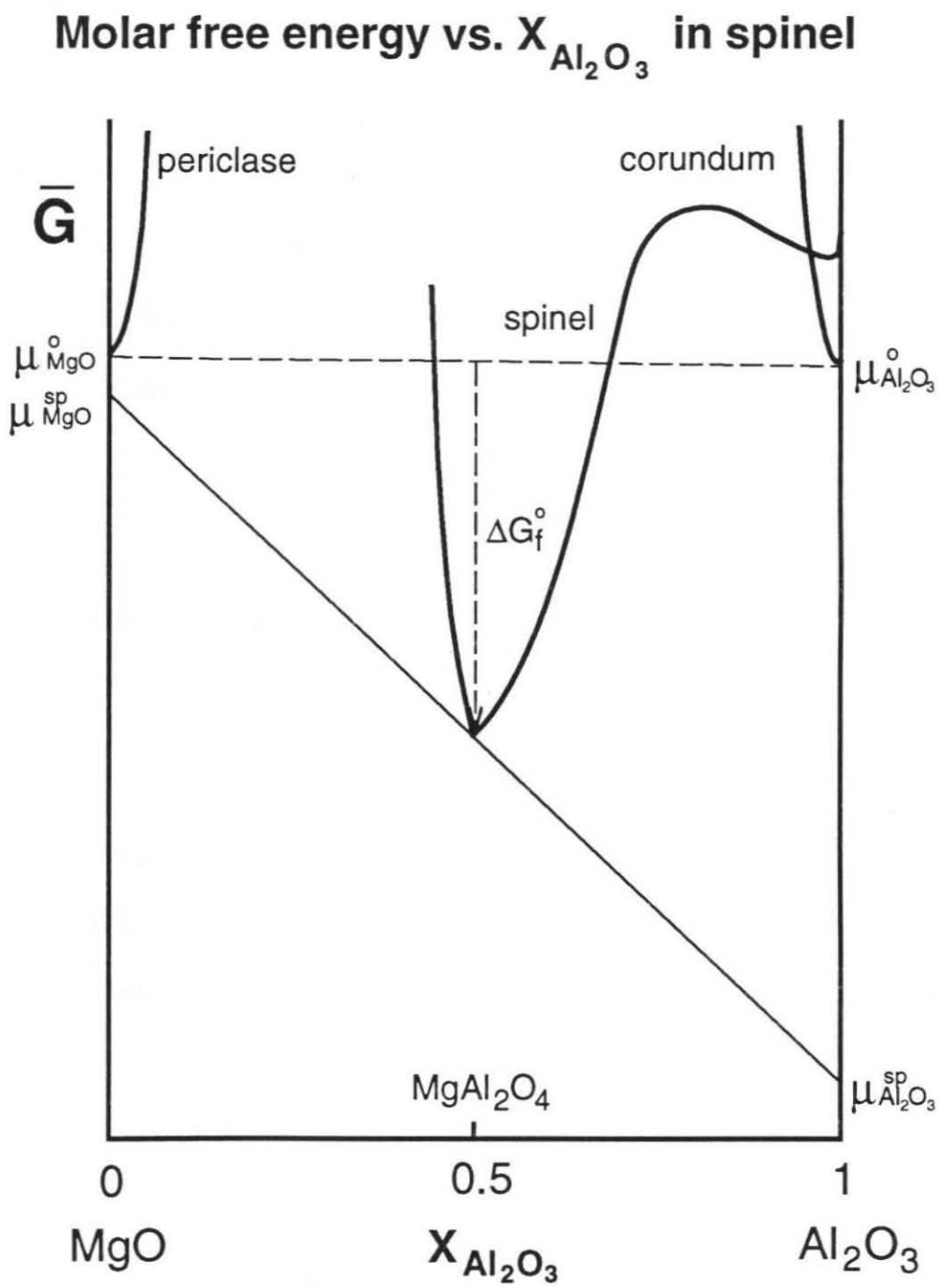
Molar free energy vs. $X_{Al_2O_3}$ in spinel
periclase
corundum
$\overline{G}$
spinel
μ^{o}_{MgO}
μ^{sp}_{MgO}
$\mu^{o}_{Al_2O_3}$
ΔG^{o}_{f}
$MgAl_2O_4$
$\mu^{sp}_{Al_2O_3}$
0
0.5
1
MgO
$X_{Al_2O_3}$
Al_2O_3

near stoichiometric spinel, the tangent to the free energy curve at the new Mg:Al ratio differs considerably from that of stoichiometric spinel. Thus in spinel, and probably in any mineral that displays little deviation from stoichiometry, oxide activities may vary widely with only minimal changes in the free energy of formation from the oxides.

The sharpness of the spinel $\overline{G}$ curve is further supported by consideration of the Gibbs-Duhem equation, which requires that variations in a_{MgO} be coupled with variations in $a_{Al_2O_3}$ in the binary system $MgO\text{-}Al_2O_3$. Specifically, for spinel,

$$\frac{d\mu_{MgO}^{spinel}}{d\mu_{Al_2O_3}^{spinel}} = \frac{d \ln a_{MgO}^{spinel}}{d \ln a_{Al_2O_3}^{spinel}} = - \frac{X_{Al_2O_3}^{spinel}}{X_{MgO}^{spinel}} . \quad (3)$$

For stoichiometric $MgAl_2O_4$,

$$\frac{d \ln a_{MgO}^{spinel}}{d \ln a_{Al_2O_3}^{spinel}} = -1 . \quad (4)$$

A plot of ln a_{MgO} versus ln $a_{Al_2O_3}$ in stoichiometric, periclase-saturated, and CAI spinels at 1400°C is shown in Fig. 5. A best-fit line with a slope of -1.0 as required by the Gibbs-Duhem equation is shown for comparison and fits the data well. This and the similar values of ΔG_f° for all of the spinels in the study indicates that, as illustrated schematically in Fig. 5, the free energy curve (or surface, given the minor element contents of the CAI spinels) is indeed very strongly curved in the vicinity of stoichiometric $MgAl_2O_4$. The fact that a_{MgO} in nominally stoichiometric $MgAl_2O_4$ is generally close to one, indicating near saturation with periclase, and that ΔG_f°'s of periclase-saturated spinels agree with those of the stoichiometric spinels also support a

Figure 5. Ln a_{MgO} versus ln $a_{Al_2O_3}$ for spinel at 1400°C (1σ error bars), fit to a line of slope -1.0. Symbols as in Fig. 3. R is the linear correlation coefficient.

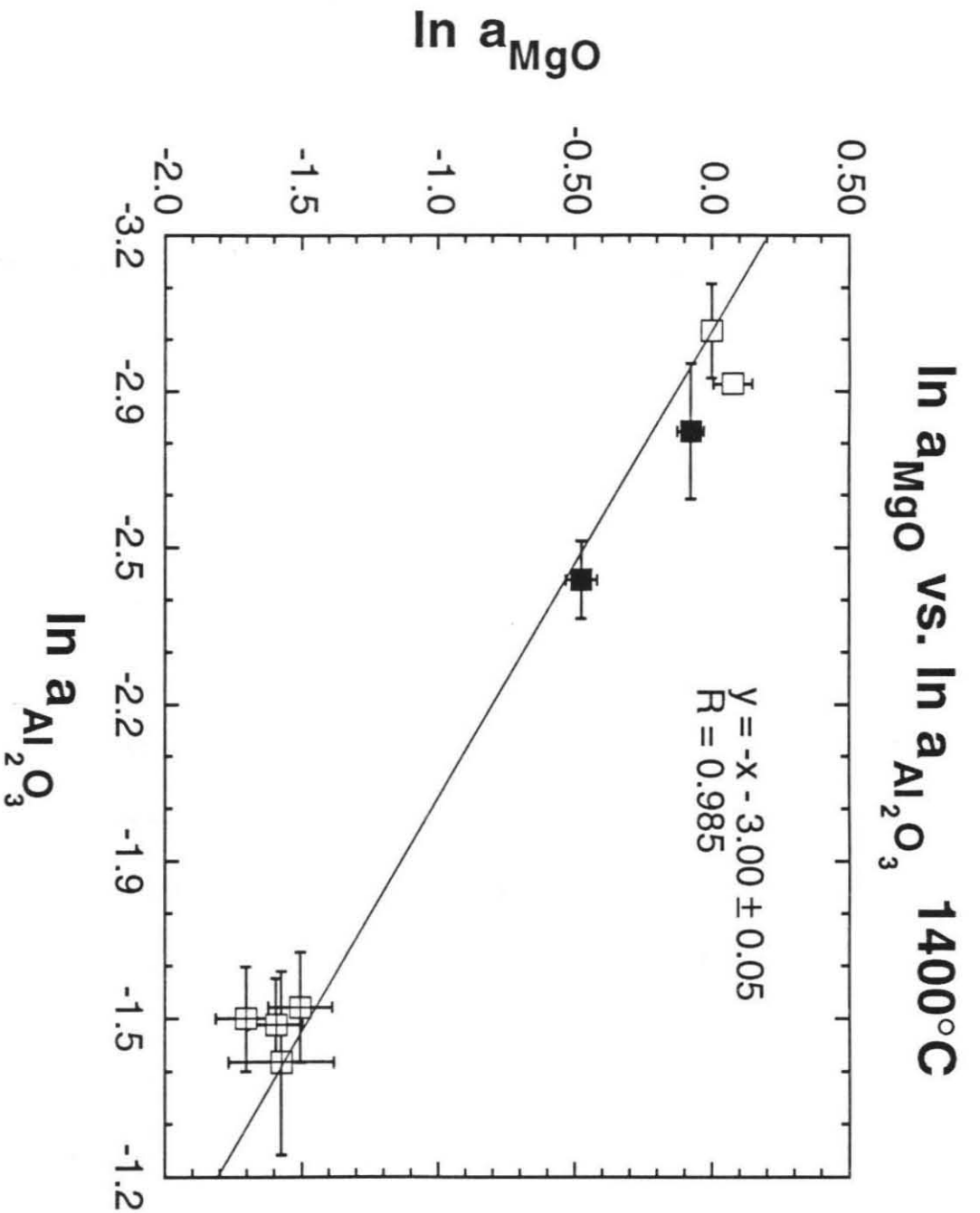
ln a_{MgO} vs. ln $a_{Al_2O_3}$ 1400°C
ln a_{MgO}
ln $a_{Al_2O_3}$
y = -x - 3.00 ± 0.05
R = 0.985
0.50
0.0
-0.50
-1.0
-1.5
-2.0
-3.2
-2.9
-2.5
-2.2
-1.9
-1.5
-1.2

sharp free energy curve very near pure $MgAl_2O_4$.

The idea that the free energy surface is strongly curved near stoichiometric spinel is also consistent with the MgO-Al_2O_3 phase diagram (Roy et al., 1953; Alper et al., 1962; Lejus, 1964; Colin, 1968), which shows that spinel exhibits very little solid solution towards MgO at temperatures below 1500°C, although there is significant alumina solid solution, requiring a more gentle curvature in the direction of alumina-rich spinels. Above 1500°C, there is some uncertainty as to whether the amount of MgO solid solution increases (Lejus, 1964; Shirasuka and Yamaguchi, 1974). If it does, the μ-X curve at higher temperatures must have a more rounded shape in the vicinity of $MgAl_2O_4$, and activities would vary less dramatically with deviations from stoichiometry.

The extreme changes in the activities of MgO and Al_2O_3 between the binary and CAI spinels may reflect the solution of tiny amounts of CaO, SiO_2 and TiO_2 in the CAI spinel. Because of the very strong curvature of the free energy surface, the addition of these impurities may cause a radical change in the position of the tangent plane to the surface, resulting in strong changes in the activities. The presence of these trace components may also decrease the short-range order that is believed to play a significant role in the energetics of spinel (Carpenter, 1993b; see also **A corrected thermodynamic expression for $MgAl_2O_4$**), which may have a bearing on the small apparent lowering in ΔG_f° between the stoichiometric and CAI spinels. If the solution of minor components can have such a dramatic influence on the activities of the major components in spinel, this effect may be important in any nominally pure mineral in a

multicomponent system.

Free energies of formation

There are several reasons for the differences between the experimental values of ΔG_f° in this study and those of the other workers shown in Fig. 3. Values given by Robie et al. (1978) were derived from the calorimetric work of Bonnickson (1955) and King (1955) with no correction for the amount of Mg-Al disorder in the spinel. Such calculations lead to entropies at high temperature that are lower than the true equilibrium values, and because ΔS_f° of spinel from periclase and corundum is positive, to ΔG_f°'s that are too high. If the effect of ordering on enthalpy were negligible, the addition of 8.2 J/moleK of residual disorder to the entropy of Robie et al. (1978) would bring their ΔG_f°'s into agreement with the data of this study. However, a somewhat greater amount of residual disorder would be needed if there is an ordering effect on enthalpy. The thermodynamic data bases of Helgeson et al. (1978), Berman (1988), and Holland and Powell (1990) were all obtained by computer optimization of phase equilibrium and calorimetric data. Values of ΔG_f° for spinel are based mostly on experiments in which the spinel obtained an equilibrium amount of disorder at high temperature, and it is evident in Fig. 3 that their values agree more closely with those in this study than do the Robie et al. (1978) values. The discrepancies between their results and those in this study can probably be attributed to uncertainties in the phase equilibrium and calorimetric data used to constrain the fits. In particular, many of the equilibria used in these studies to derive the thermodynamic properties of spinel also

involve pyrope and aluminous enstatite, two phases whose thermodynamic properties are poorly known (Tequi et al., 1991).

The agreement of the data in this study with values given by JANAF (1985) is surprising and probably fortuitous. The JANAF compilation relies on the heat capacity equation of Landa and Naumova (1979) and includes a zero-point entropy correction of 8.2 J/moleK based on a disorder estimate of 15% from Navrotsky and Kleppa (1967). NMR and neutron-diffraction studies (Wood et al., 1986; Peterson et al., 1991; Millard et al., 1992) indicate that the residual disorder of spinels quenched from high temperature is actually variable and greater than 15% (up to $x = 0.39 \pm 0.04$ at 900°C, $x = 0.35 \pm 0.02$, or $x = 0.29 \pm 0.03$ at 1000°C, respectively, where x is the fraction of tetrahedral sites occupied by Al^{3+}), so the basis for the JANAF correction is almost certainly invalid. It appears that JANAF (1985), using questionable assumptions, have nevertheless obtained the correct values for ΔG_f°.

A corrected thermodynamic expression for $MgAl_2O_4$

The measured values of ΔG_f° of spinel in this study represent spinel with an equilibrium state of order, but as explained previously, the calorimetric heat contents and heat capacities do not. The heat contents, $H_T^\circ - H_{298}^\circ$, should be equal to the difference between the enthalpy of spinel with equilibrium order at temperature T and the enthalpy of spinel with equilibrium order at the reference temperature 298 K. Because of incomplete reordering during a drop calorimetric experiment, an enthalpy contribution is lost and the measured heat contents are underestimated. Given some

knowledge of the ordering state of spinel as a function of temperature and time, it should be possible to correct the calorimetric data to reflect equilibrium disorder. The corrected values for $H_T^\circ - H_{298}^\circ$ and the experimental values for ΔG_f° can then be simultaneously fit to the empirical form of Berman and Brown (1985) to derive a corrected thermodynamic expression for $MgAl_2O_4$ applicable over a wide temperature range.

The disordering reaction for Mg and Al on the tetrahedral and octahedral sites,

$$[Mg^{2+}]^{tet} + (Al^{3+})^{oct} = [Al^{3+}]^{tet} + (Mg^{2+})^{oct} , \quad (5)$$

is associated with an enthalpy of disordering, ΔH_D, given by:

$$\Delta H_D(T) = H_{x=x}^\circ(T) - H_{x=0}^\circ(T) , \quad (6)$$

where x is the fraction of tetrahedral sites occupied by Al^{3+} and $H_{x=x}^\circ(T)$ is the total enthalpy of spinel with disorder x at temperature T relative to the enthalpy of purely normal spinel, $H_{x=0}^\circ(T)$. Given an appropriate expression for enthalpy as a function of order, one can use Eqn. (6) to correct the calorimetric enthalpy measurements for the missing disordering contribution. Carpenter et al. (1993b) provide an expression for the free energy of ordering by fitting the in situ neutron diffraction measurements of Mg-Al order versus temperature by Peterson et al. (1991) and the enthalpy of ordering measurements of Navrotsky et al. (1986) to a Landau theory formulation. Landau theory has the advantage of being able to account for nonconfigurational entropy contributions such as short-range ordering, which Carpenter et al. (1993b) inferred may significantly lower the entropy of $MgAl_2O_4$ from purely configurational values.

The relationship between Mg-Al order and temperature given by Carpenter et al. (1993b) is:

$$1.908\ Q^5 + 0.0023\ (T - 395)\ Q - 1 = 0\ , \qquad (7)$$

where Q is an order parameter equal to -3/2 x + 1, defined such that Q = 0 for a completely random spinel. The free energy of ordering between completely disordered $MgAl_2O_4$ spinel and $MgAl_2O_4$ with equilibrium order is (J/mole):

$$G^{ord} = -8575 \pm 5048\ Q + 9.85 \pm 5.81\ (T - 395)Q^2 + 2727 \pm 1605\ Q^6\ . \qquad (8)$$

From this expression, noting that G = H − TS, the enthalpy of ordering is given by:

$$H^{ord} = -8575 \pm 5048\ Q - 3895 \pm 2293\ Q^2 + 2727 \pm 1605\ Q^6\ . \qquad (9)$$

The enthalpy of ordering is therefore temperature independent, and combining Eqns. (6) and (9), the enthalpy of disordering from x = 0 to x = x (or from Q = 1 to Q = -3/2 x + 1) is given by:

$$\Delta H_D = H^{ord}_{Q=-3/2x+1} - H^{ord}_{Q=1}\ . \qquad (10)$$

If the temperature at which reordering stopped in each calorimetric measurement is known, one can use Eqn. (7) to estimate the residual disorder quenched into the spinel and Eqn. (10) to correct the calorimetric heat contents of Bonnickson (1955) for the missing disordering contribution.

According to the NMR measurements of Wood et al. (1986) and Millard et al. (1992), all samples quenched rapidly from T > 1000°C retain a state of disorder appropriate to ~1000°C. Assuming that the disorder measured by Peterson et al.

(1991) at 1000°C, x = 0.35, is characteristic of all spinels quenched from T > 1000°C, a ΔH_D corresponding to x = 0.35 is added to the calorimetric heat contents at T > 1000°C (Fig. 6a). Because spinel can reorder to the equilibrium state upon annealing between 700 and 1000°C, the spinel in this temperature range probably reorders in the calorimeter to its equilibrium state before it is dropped. A ΔH_D appropriate to the equilibrium disorder for the temperature of the experiment is therefore added. Correction of heat contents below 700°C is more problematic. Bonnickson (1955) conducted heat content measurements between 421 and 1805 K. It is assumed that Bonnickson (1955) began his experiments at 1805 K and moved to progressively lower temperatures, and that because of repeated drops of the same sample, the synthetic spinel eventually gained a state of order appropriate to ~700°C. Due to slow kinetics, the spinel could not have reordered any further in the calorimeter during experiments at T < 700°C (Fischer, 1967), and therefore all of the low-temperature values were measured on spinel with the equilibrium degree of disorder appropriate to 700°C (x = 0.25). To correct the calorimetric values at T < 700°C, a ΔH_D is subtracted for ordering between x = equilibrium and x = 0.25 (ΔH_{D1}; Fig. 6b), and a ΔH_D is added for ordering between x = 0 and x = 0.25 (ΔH_{D2}; Fig. 6b), which amounts to adding the ΔH_D for ordering between x = 0 and x = equilibrium (Fig. 6b). Table 6 and Fig. 7 show the calorimetrically-measured heat contents and the corrected values. If it is assumed instead that Bonnickson began his experiments at 421 K and moved to progressively higher temperatures, then the low temperature experiments were performed on spinel with x = 0.35 (the value characteristic of the synthesis temperature of his starting mat-

Figure 6. Schematic representation of enthalpy of spinel versus temperature. (a) Above about 1273 K, spinel cools along the x_{eqm} curve, where it has the equilibrium amount of disorder at each temperature. When temperature drops below 1273 K, disorder is frozen in at x = 0.35, and spinel cools along the curve corresponding to x = 0.35. The actual heat content at 1273 K is equal to the measured heat content plus the disordering enthalpy ΔH_D between x = 0 and x = 0.35. (b) Spinel heated to 973 K < T < 1273 K in the calorimeter can anneal to x_{eqm}, but it cannot reorder below 973 K. Therefore, below 973 K, the disorder is frozen at x = 0.25, and spinel cools along the curve x = 0.25. The actual heat content at T < 973 K is equal to the measured heat content minus the disordering enthalpy ΔH_{D1} between x = eqm and x = 0.25 plus the disordering enthalpy ΔH_{D2} between x = 0 and x = 0.25.

a Corrections to enthalpy measurements, $T \geq 1273$ K

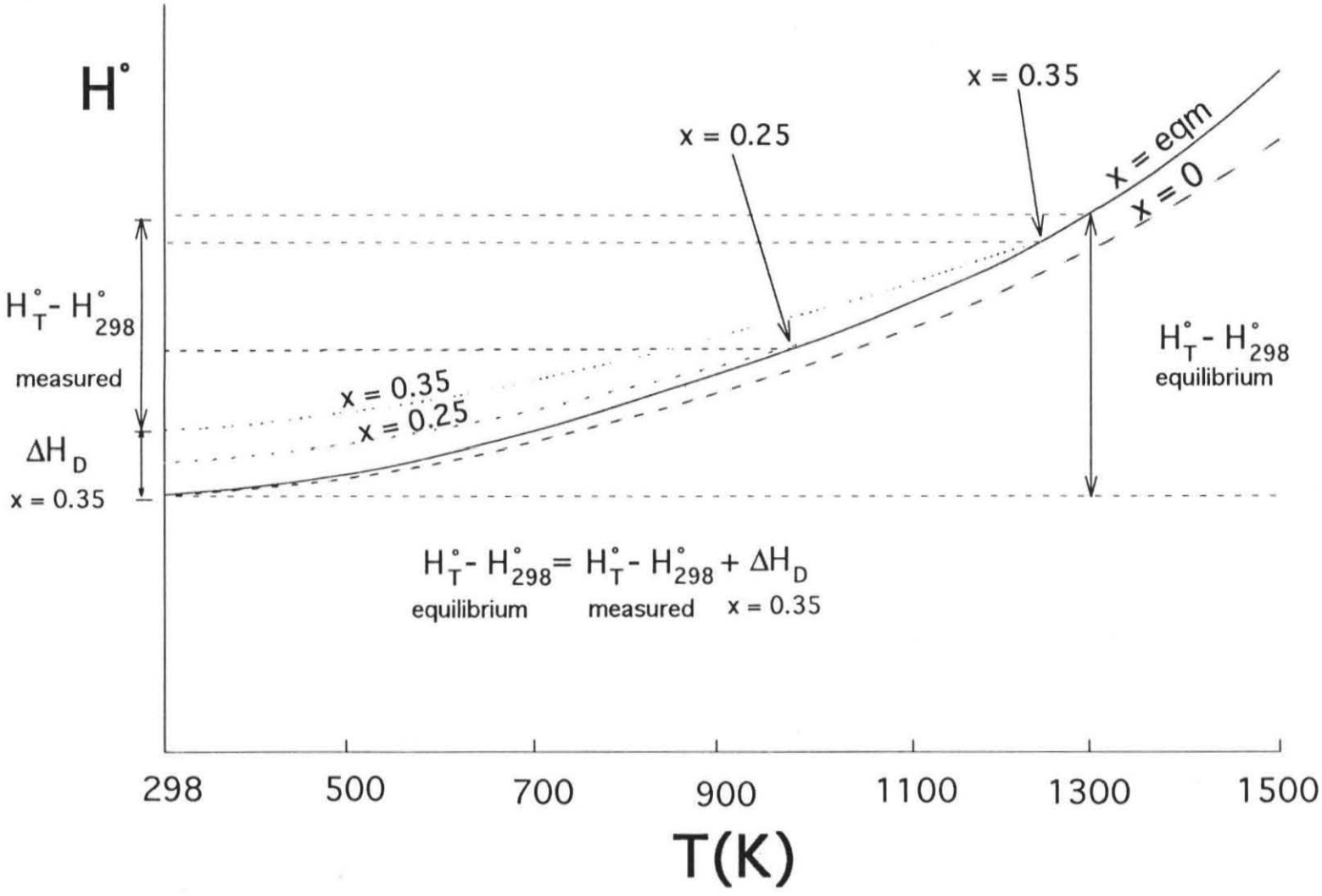

b Corrections to enthalpy measurements, $T \leq 1273$ K

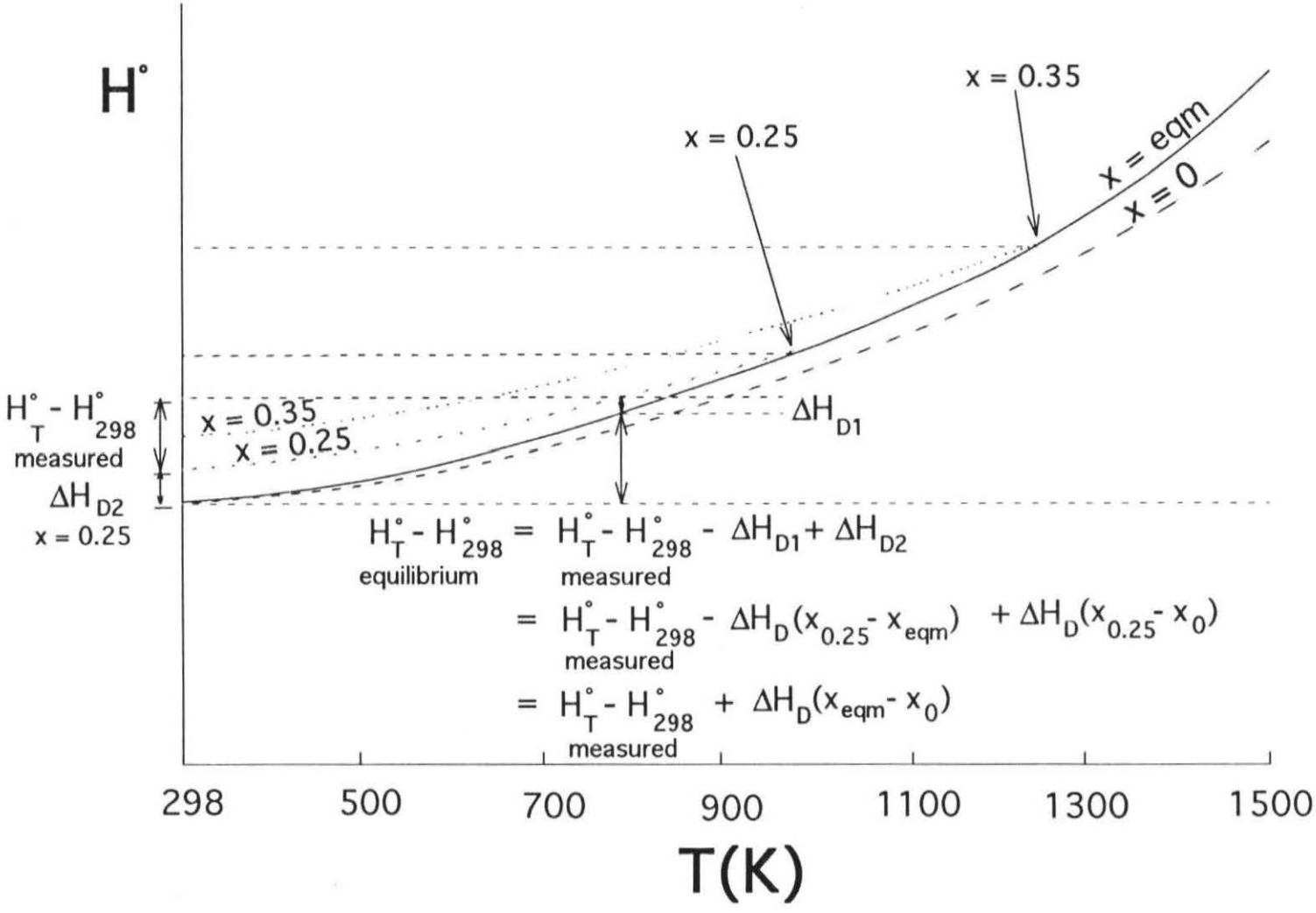

Table 6. Measured and corrected $H_T^\circ - H_{298}^\circ$ for spinel (J/mole).

Table 6. Measured and corrected $H^{\circ}_T - H^{\circ}_{298}$ for spinel (J/mole).					
T (K)	measured[a]	x[b]	ΔH^c_D	corrected[d]	fit (Eqn. 11)
298.15	0.0	0.0	0.0	0.0	0.0
421.0	16025	0.087	517	16542	16892
485.7	25397	0.10	709	26106	26585
584.5	40836	0.13	1058	41894	42149
767.4	70584	0.19	1930	72514	72757
814.4	78324	0.20	2153	80477	80914
909.0	94433	0.23	2729	97162	97623
1020.9	113930	0.27	3383	117313	117822
1109.9	130332	0.30	3924	134256	134177
1212.2	149327	0.34	4584	153911	153249
1325.5	170331	0.35	4822	175153	174672
1388.4	182548	0.35	4822	187370	186687
1508.2	205267	0.35	4822	210089	209785
1610.1	224221	0.35	4822	229043	229635
1695.0	241710	0.35	4822	246532	246301
1805.5	262295	0.35	4822	267117	268152

a. Bonnickson (1955).

b. Fraction of tetrahedral sites occupied by Al^{3+} based on Eqn. (7) (see text); experimental errors of Peterson et al. (1991) range from 0.01 to 0.02.

c. Disordering enthalpy (Eqn. 10).

d. Measured + ΔH_D.

Figure 7. Drop calorimetric measurements (Bonnickson, 1955), corrected values, and fit values (Eqn. 11) of heat contents of spinel versus T (K). Errors (1σ) are about the size of the points.

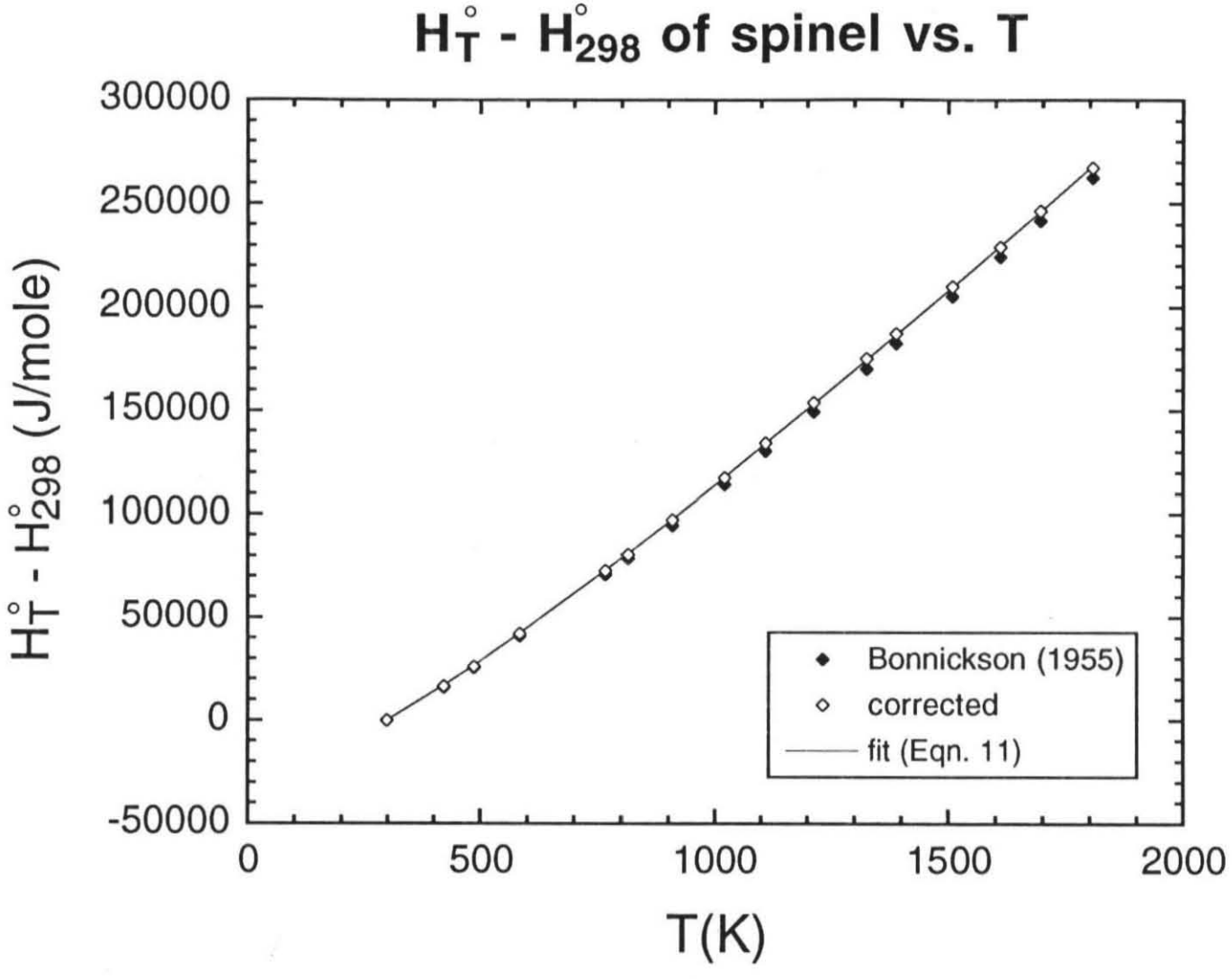
$H_T^\circ - H_{298}^\circ$ of spinel vs. T
$H_T^\circ - H_{298}^\circ$ (J/mole)
300000
250000
200000
150000
100000
50000
0
-50000
0
500
1000
1500
2000
T(K)
Bonnickson (1955)
corrected
fit (Eqn. 11)

erial, 1480-1500°C). The enthalpies at low temperature would then be over-corrected and would not join smoothly with the thermodynamically-required point at T = 298.15 K ($H^\circ_T - H^\circ_{298} = 0$).

In order to fit the ΔG°_f values, one must also determine corrected values for enthalpy of formation (ΔH°_f) and entropy at 298.15 K (S°_{298}). Solution calorimetric measurement of ΔH°_f from the oxides at 970 K gives $\Delta H^\circ_f(970) = -22510 \pm 783$ J/mole (Charlu et al., 1975). It is assumed that this value applies to spinel with equilibrium disorder, as the spinel was heated at 700°C for several hours before the enthalpy of solution measurement was made. One can also determine a value for S°_{298} given the Landau theory assumption that enthalpy of ordering is temperature-independent, which implies that heat capacity C_p is independent of state of order. King (1955) measured C_p at temperatures between 51 and 298.16 K, fit the values as a function of T, and integrated C_p/T to obtain $S^\circ_{298} = 80.58 \pm 0.42$ J/moleK, assuming zero entropy at 0 K. Although the spinel studied by King was synthesized at 1480-1500°C and thus probably had $x \sim 0.35$, the value of 80.58 J/moleK would be correct for a spinel with x = 0 at 298 K given the assumption that C_p is independent of x.

The corrected enthalpy values and the experimental ΔG°_f's were fit simultaneously using Mathematica (Wolfram Research, Inc.). To test the Landau theory assumption that C_p is order-independent, the value of S°_{298} was also fit. This gave ($\chi^2 = 5.8$):

$$C_p = 247.367 \pm 10.637 - 2075.74 \pm 295.43\ T^{-1/2} - 0.444501 \pm 0.0631316\ T^{-2} - 0.00113143 \pm 0.0001607\ T^{-3}, \quad (11)$$

$\Delta H_f^\circ(298)$ = -25441 ± 10878 J/mole (from the oxides), -2302.631 ± 11.473 kJ/mole (from the elements), and S_{298}° = 81.1 ± 2.75 J/moleK. The fit value for S_{298}° is identical within error to the calorimetric value of King (1955), implying that the assumption that C_p is independent of state of order is justified. The fit is rather sensitive to the value of S_{298}°, however. If S_{298}° is constrained to the value of King (1955), the fit is considerably worse, with predicted values of heat contents ranging from 2 kJ/mole lower to 4 kJ/mole higher than input values, and predicted ΔG_f°'s as much as 13 to 20 kJ/mole higher than measured values. It is nevertheless notable that the Landau theory approach (Eqn. 11) reproduces all the available experimental data within error, supporting the idea that nonconfigurational entropy plays a significant role in determining the energetics of spinel.

An alternative approach to modeling the thermodynamic properties of spinel is to correct and refit the calorimetric data using a regular solution model, which assumes entropy is purely configurational and therefore does not account for short-range order. Here:

$$\Delta H_D = \Delta H_D^{ideal} + \Delta H_D^{excess} = x\Delta H^{int} + \omega x(1-x) \ , \qquad (12)$$

where ΔH_D^{ideal} is the ideal and ΔH_D^{excess} the nonideal contribution to the enthalpy of Mg-Al disordering, ΔH^{int} is the temperature-independent enthalpy of interchanging one mole of Mg and Al on the octahedral and tetrahedral sites, and ω is a temperature-independent Margules parameter. Sack and Ghiorso (1991) fit the neutron diffraction data of Peterson et al. (1991) to obtain for the relationship between order and tempera-

ture:

$$-18.41 = RT \ln \frac{x^2}{(1-x)(2-x)} + 15.06(1-2x) , \qquad (13)$$

which in turn yields (c.f. O'Neill and Navrotsky, 1983):

$$\Delta H_D = 33.47x - 15.06x^2 . \qquad (14)$$

Eqn. (14) results in enthalpy corrections at high temperature about twice the size of those given by Eqn. (10) and hence in a larger corrected heat capacity dependence on temperature. This forces a downward adjustment of S°_{298} by ~6 J/moleK relative to King's (1955) calorimetrically-derived value in order to accommodate the available enthalpy and free energy data, well outside the errors in King's determination. This large adjustment in S°_{298} violates the requirement of Eqn. (14) that C_p be independent of state of order. Such a C_p dependence on order has been neither demonstrated nor quantified, and the Landau approach is preferred since it is able to more straightforwardly account for all experimental data.

Further observations on disorder

On the basis of their calorimetric data and NMR measurements of the Mg-Al disorder in spinel, Wood et al. (1986) postulated the existence of substantial short-range order in the spinel lattice. They noted that if calorimetrically-derived entropies of spinel (Bonnickson, 1955) are corrected by adding the configurational entropy term:

$$\Delta S_{conf} = -R\{x \ln x + (1-x) \ln(1-x) + x \ln(x/2) + (2-x) \ln[1-(x/2)]\} \qquad (15)$$

to correct for frozen-in disorder, then there is a substantial mismatch between the

calculated and observed pressure-temperature positions of the equilibrium between pyrope, forsterite, enstatite, and spinel at 18-30 kbar and 900-1600°C that indicates that the corrected entropies are too high. Although their conclusions are partly a consequence of overestimating the degree of disorder in spinel (Peterson et al., 1991; Millard et al., 1992), they are supported by the work of Carpenter et al. (1993), who inferred from applying Landau theory that the entropy of spinel was less than configurational, and by the success in this work in describing the known thermodynamic data on spinel with a Landau enthalpy of ordering expression. The failure of the regular solution model to describe the same data base without allowing C_p to vary with degree of order also suggests that nonconfigurational effects in the spinel lattice are important. HRTEM investigations have not yielded independent evidence of short-range order in spinel (Navrotsky et al., 1986), but it may exist at a scale not detectable by this method.

Fiske and Stebbins (1989) have suggested that a second type of disorder may be present in $MgAl_2O_4$ at high temperature. Their NMR work on natural single crystals shows that annealing at 800°C of samples quenched from high temperature causes the diminution and disappearance of certain satellite transition peaks, a process which they link either to changes in structure or to disordering on sites other than the octahedral and tetrahedral ones. The presence of a second type of disorder would certainly complicate efforts to correct to equilibrium disorder, as this disordering has not been characterized, and its effects cannot be included. Because of this, it is assumed in the treatment of the data that although this second type of disorder may be present, it is

either not an energetically significant process or it is adequately accounted for by the calorimetry or Landau corrections.

Effect on phase equilibrium calculations

One advantage of an internally consistent thermodynamic data base such as that of Berman (1988) is that free energies of reaction and hence phase equilibria can be calculated in a self-consistent fashion. Since the entire experimental phase equilibrium and calorimetric data set influences the results for each phase, it offers the opportunity to refine the thermodynamic properties of phases that are only poorly known. The experimental values for the free energy of spinel from this study provide a new constraint that can be used in the manner of Berman (1988) to further refine the heat capacity equations and standard state properties of poorly-understood phases. From Fig. 3, ΔG_f° of spinel as given by Berman (1988) is 4 to 5 kJ/mole too high. Since Berman's (1988) data base is constructed to match phase equilibria, there must be a compensating error in Berman's (1988) free energy of the reaction for pyrope + forsterite = spinel + 4 enstatite, in ΔG_f° of one or more of the other three components in the reaction. The probable candidates are pyrope and aluminous enstatite, whose properties are less well constrained than those of forsterite. In particular, there are no heat capacity or heat content measurements on pyrope above about 1070°C, due to its tendency to break down above this temperature at 1 bar (Téqui et al., 1991). This means that a heat capacity equation fit to the low-temperature data must be extrapolated to temperatures far above the region in which it is well constrained. This extrapolation can intro-

duce several kJ/mole error into ΔG_f°, as it is heavily dependent on the form of the C_p equation used (Téqui et al., 1991, Fig. 5).

Summary

The technique of Pd-oxide equilibration was applied to the determination of the activities of MgO and Al_2O_3 in stoichiometric $MgAl_2O_4$ spinel in the temperature region 1150 to 1400°C. This method is ideal for the study of spinel, since all concentrations of Mg and Al in Pd are established by equilibration at high temperature and therefore reflect the equilibrium amount of disorder in the spinel. The experimental activities were used to calculate the free energy of formation of spinel from the oxides. The results indicate more negative ΔG_f°'s than given in most compilations of thermodynamic data, likely due to inadequate corrections for the state of order of the spinels used in calorimetric experiments. Calorimetric heat contents were corrected to reflect equilibrium disorder using in situ neutron diffraction measurements of the equilibrium amount of disorder in $MgAl_2O_4$ (Peterson et al., 1991) and the Landau enthalpy of ordering (Carpenter et al., 1993). Fitting the corrected heat contents and experimental ΔG_f°'s to produce a new heat capacity equation and re-estimating enthalpy of formation and entropy at 298.15 K demonstrates that the Landau approach can explain all available thermodynamic data. In contrast, using a regular solution model results in an inadequate description of the data, suggesting that short-range ordering plays an important role in determining the energetics of spinel.

Chapter 3. The thermodynamic properties of CAI melts

In this chapter, the technique of Pd-oxide equilibration is applied to the measurement of the activities of oxide components in silicate melts relevant to the origin of Ca-Al-rich inclusions (CAIs) in carbonaceous chondrite meteorites. It begins with a brief description of CAIs and related inclusions and follows with an account of the experimental procedures used to determine activities of oxide components in silicate melts with bulk compositions similar to CAIs. The relationship between thermodynamics and melt structure is explored, the measured activities are compared with those predicted for the experimental compositions by the model of Berman (1983), and free energies of formation are calculated for the solid phases that crystallize from the melts. Finally, the measured activities are used to infer the conditions of formation of CAIs in the solar nebula.

Calcium-aluminum-rich inclusions

As described in Chapter 1, the role of silicate melts in terrestrial or meteoritic igneous processes has been difficult to evaluate in part because the thermodynamics of silicate melts are so poorly understood, a direct consequence of the paucity of direct thermodynamic data on the liquid phase. One area in which the poor understanding of silicate melts has had an impact is investigations into the role of melting in the evolution of CAIs. CAIs are mm- to cm-sized aggregates of highly refractory minerals that are found in carbonaceous chondrite meteorites (MacPherson et al., 1988). The phase

assemblage of CAIs typically consists of varying proportions of melilite solid solution, $MgAl_2O_4$ spinel, perovskite, hibonite, fassaite (titanian pyroxene) and lesser anorthite or forsterite, plus enclosed opaque assemblages (nuggets of metal plus sulfide and oxide). CAIs are classified into four basic kinds: Type A, consisting mostly of melilite with lesser pyroxene; Type B, dominated by pyroxene and melilite; Type C, which has abundant anorthite; and forsterite-bearing, characterized by the presence of forsterite. The composition fields for the four types of CAIs are shown projected from $MgAl_2O_4$ spinel onto the plane anorthite-gehlenite-forsterite in Fig. 8. A distinct but similar group of inclusions are the plagioclase-olivine inclusions, or POIs, which are intermediate between Type C CAIs and ferromagnesian chondrules (Sheng et al., 1991; Sheng, 1992). They are similar in mineralogy and texture to CAIs but are distinguished from them by a lack of melilite and opaque assemblages and by an abundance of olivine and aluminous enstatite. The composition field of POIs is also shown in Fig. 8. The similarities between CAIs and POIs suggest that they may be closely related, possibly formed and modified by the same processes.

Although CAIs have long been interpreted to contain primitive high-temperature material produced during the earliest stages of solid condensation of the solar nebula (Grossman, 1972; 1973), a number of lines of evidence suggest that many CAIs were at least partially molten at some point in their history. Perhaps the most direct evidence is that many CAIs exhibit rounded outlines and interlocking textures compatible with formation from a molten state (Blander and Fuchs, 1975), and a few actually contain glass (Marvin et al., 1970; Kurat, 1975; Ireland et al., 1991). In addition, major

Figure 8. Projection through $MgAl_2O_4$ spinel onto the plane anorthite-gehlenite-forsterite (Stolper, 1982), showing the bulk compositions (boxed) and their crystallization paths (dashed lines). Spinel-saturated liquidus is contoured in °C. Also shown are the composition fields of the four types of CAIs: Type A, Type B, Type C, and forsterite-bearing (MacPherson et al., 1988), and the composition field of POIs (Sheng et al, 1991). Sp = spinel, an = anorthite, cpx = clinopyroxene, me = melilite, fo = forsterite, mont = monticellite, hib = hibonite, cor = corundum.

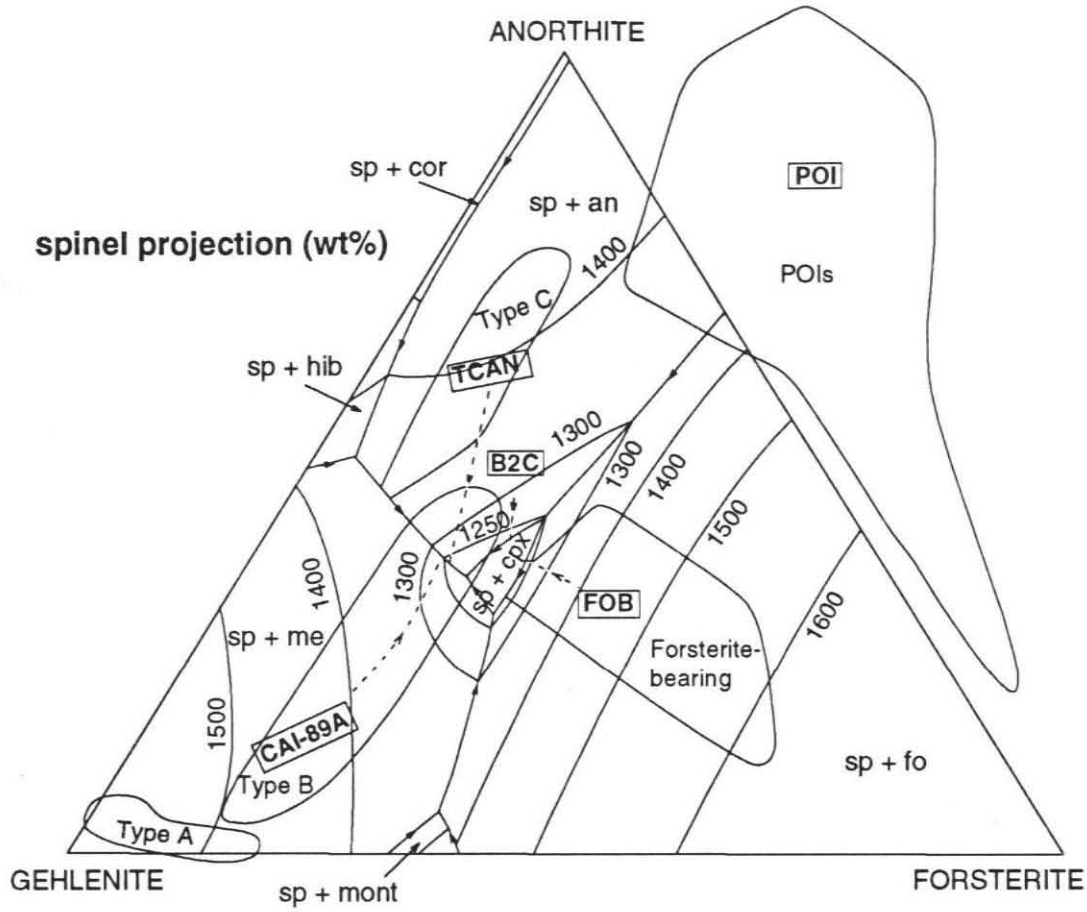
ANORTHITE
spinel projection (wt%)
sp + cor
sp + an
POI
POIs
1400
Type C
sp + hib
TCAI
1300
B2C
1300
1400
1250
1500
sp + cpx
1400
1300
FOB
sp + me
Forsterite-
bearing
1600
1500
CAI-89A
Type B
sp + fo
Type A
GEHLENITE
sp + mont
FORSTERITE

element zoning patterns in melilite in CAIs are also consistent with crystallization from a melt (MacPherson and Grossman, 1981; MacPherson et al., 1984). ^{26}Mg isotopic heterogeneity between anorthite and melilite also suggests multiple melting events (MacPherson and Davis, 1993).

Although the occurrence of melting at some stage in the development of CAIs seems very likely, it has not been established at what stage it took place. Some workers infer that the molten stage was the initial phase, pointing out that kinetic factors favor the metastable condensation of supercooled liquids over solids (Blander and Fuchs, 1975), and that Type Cs lie on the liquid condensation trend calculated by Wagner and Larimer (1978) (Wark, 1987). However, cooling-rate studies have shown that CAI textures are not compatible with substantial supercooling (Stolper and Paque, 1986), and in any case, liquid condensation appears to require nebular pressures of at least 1 atmosphere (Grossman and Clark, 1973), five orders of magnitude higher than likely for the protosolar nebula (Wood and Morfill, 1988). Other workers place the melting event after solid condensation, envisioning a period of melting resulting in vaporization of Mg and Si to produce a range of CAI compositions (Wark et al., 1987). This is compatible with the positive correlation between MgO and SiO_2 observed in Type B's (Beckett, 1986), but is seldom supported by clear isotopic evidence in favor of volatilization (MacPherson et al., 1988). The mechanism causing melting remains unclear because of probable overprinting by multiple events, but it most likely was similar to the process responsible for melting chondrules and was almost certainly a transient phenomenon (Wood and Morfill, 1988).

Previous workers have appealed to very simplified thermodynamic models (Wagner and Larimer, 1978) or indirect arguments to explore the role of silicate melts during condensation in the primitive solar nebula (Grossman and Clark, 1973). The question of the stability of silicate liquids in nebular environments can be quantitatively addressed with the technique of Pd-oxide equilibration, as it allows the activities of MgO, Al_2O_3, and SiO_2 to be measured directly in silicate melts and so is ideal for the study of melts relevant to CAI genesis.

Experimental procedure

Sample preparation

Five compositions were selected for study, corresponding to melilite-rich (CAI-89A) and anorthite-rich (B2C) Type B CAIs, an average Type C CAI (TCAN), a forsterite-bearing CAI (FOB), and an average Group 2 plagioclase-olivine inclusion (POI). Bulk compositions of the starting materials are given in Table 7 and shown projected from $MgAl_2O_4$ spinel onto the plane anorthite-gehlenite-forsterite in Fig. 8. Melt characteristics and synthesis conditions are as follows:

1.) CAI-89A: This composition represents an average coarse-grained Type B CAI (Wark, 1979). It was originally synthesized for the trace-element partitioning study of Beckett et al. (1990) and is virtually identical to the composition CAIB used in the studies of Stolper (1982) and Stolper and Paque (1986). Spinel is on the liquidus at 1550°C, followed by melilite (1400°C), anorthite (1260°C), and Ti-Al-rich pyroxene (1230°C). The starting material was prepared from powders of reagent-grade $CaCO_3$,

Table 7. Bulk compositions of silicate liquids (wt%).

Table 7. Bulk compositions of silicate liquids (wt%).[a]					
	CAI-89A	B2C	TCAN[b]	FOB[c]	POI
CaO	29.0	22.8	24.5	20.5	11.0
MgO	9.7	12.5	5.8	19.1	16.7
Al_2O_3	27.6	27.0	28.9	22.2	21.9
SiO_2	31.5	36.2	38.8	36.8	49.3
TiO_2	1.32	1.42	1.32	1.37	0.81
Total	99.1	99.9	99.4	99.9	99.7

a. Electron microprobe analyses: 15 keV, 10 nA, 20 μm beam, 30 s; standardized on anorthite, forsterite, and rutile. Averages of several analyses; variations are within 1 wt%.

b. Analyzed by J. Paque.

c. Nominal.

MgO, Al_2O_3, SiO_2, and TiO_2 (Alfa Products) that were dried overnight ($CaCO_3$ at 400°C, oxides at 1000°C) before weighing. The powders were mixed together in an automatic agate mortar under ethanol for 5 hours and then decarbonated at 1000°C. The resulting oxide mix was melted in air for 6 hours at ~1600°C, quenched to a glass, and powdered in an agate mortar.

2.) B2C: This composition represents the extreme anorthite-rich end of Type B2 CAIs as estimated by Grossman and Ganapathy (1976). Paque and Stolper (1984) studied the phase relations of B2C and determined that spinel is on the liquidus (~1540°C), followed by anorthite (~1290°C), and melilite plus Ti-pyroxene (~1245°C). Synthesis of glassy starting material was identical to that of CAI-89A.

3.) TCAN: This composition is modeled after an estimate of the average bulk composition of Type C inclusions studied by Wark (1987); it was synthesized and studied by Paque and Stolper (1984), who determined that the liquidus phase was anorthite (1403 ± 3°C), followed by spinel (1385 ± 5°C), melilite (1258 ± 7°C) and Ti-pyroxene (1229 ± 9°C). Spinel is resorbed as Ti-pyroxene crystallizes. Synthesis conditions were similar to those for CAI-89A and B2C except that TCAN was melted at 1500°C.

4.) FOB: This composition corresponds to a relatively Mg-poor representative of forsterite-bearing CAIs as defined by Wark et al. (1987). Because liquidus temperatures for these compositions are prohibitively high, 5 wt% spinel component was subtracted for ease of synthesis. According to the model of Berman (1983), spinel is on the liquidus at 1510°C, and in the experiments the melt is saturated with both forsterite and spinel at ~1400°C. It is likely that Ti-pyroxene joins the stable phase assemblage

between 1200 and 1250°C (Stolper, 1982). Synthesis conditions were similar to those for CAI-89A.

5.) POI: This is an average of the compositions defined as Group 2 POIs (Sheng et al., 1991; Sheng, 1992). Group 2 POIs are the most SiO_2-rich POIs and this also represents the most SiO_2-rich composition studied. It was chosen to extend the compositional range of the study toward more siliceous regions and to allow comparison of observations on CAIs to similar meteoritic inclusions. POI is estimated through the melt model of Berman (1983) to have forsterite on the liquidus at 1305°C, followed by spinel at 1270°C, and pyroxene at 1230°C. Synthesis of this starting material was similar to CAI-89A, except that it was melted overnight at ~1400°C.

Powdered glassy starting material of each bulk composition was pressed into pellets around 3-4 mm lengths of 99.997% pure 0.25 mm-diameter Pd wire (Alfa Products) and melted onto loops of 0.25 mm-diameter Pd wire using a small H_2/O_2 torch. Oxide standards were prepared by pressing analytical-grade MgO, Al_2O_3, or SiO_2 (JMC Puratronic) around 3-4 mm lengths of 0.25 mm-diameter Pd wire. Examination of starting materials by XRD revealed that the MgO was crystalline periclase, but the Al_2O_3 and SiO_2 were both amorphous. Accordingly, the Al_2O_3 and SiO_2 were first converted to corundum and cristobalite respectively by heating at ~1500°C for about 6 hours. The Pd + periclase or Pd + corundum pellets were placed in open capsules made from ¼-inch diameter crushable magnesia and alumina rods (Ozark Technical Ceramics) that were drilled out to form open capsules. The Pd + cristobalite pellets were placed in open capsules made from 6 mm O.D. silica glass tubes that were sealed

at one end using a torch.

Experimental methods

Experiments were conducted in a 1-atmosphere home-built furnace with $MoSi_2$ heating elements and H_2/CO_2 gas-mixing capabilities. Temperature was controlled to within 1-2°C by a Eurotherm 812 Controller/Programmer and measured by a Type S thermocouple calibrated at the melting point of gold. Stated temperatures are believed accurate to ± 3°C. Oxygen fugacity was set using mixtures of H_2 and CO_2 and measured by an yttria-doped zirconia solid electrolyte oxygen sensor (Ceramic Oxide Fabricators Pty. Ltd., Australia). The sensor was calibrated at the iron-wüstite buffer at 1200 and 1400°C by measuring changes in the resistance of pure iron wire. Drift of the emf of the sensor during a run was typically 1 mV or less.

The samples and standards were suspended from Ir hanging wire and placed adjacent to each other in the 1-atmosphere gas-mixing furnace. Experiments were done in the temperature range 1250 to 1400°C, where appreciable liquid is present (> 50%). The oxygen fugacity of the experiments was typically an order of magnitude or two below iron-wüstite. The experiments were conducted for 48 to 72 hours and terminated by drop-quenching into deionized water. Reversals were performed by first equilibrating the Pd wires with melt and standards at f_{O_2}'s lower than those of the final equilibrations so that the equilibrium concentrations were approached from the high concentration side. After quenching, the glass beads and oxide pellets were mounted in epoxy and rough-polished to expose a length-wise cross section through the Pd

wire. The Pd was then fine-polished with diamond paste using an automatic polisher.

Analytical techniques

The Pd alloys were analyzed as described in Chapter 1. Analyses of most of the glassy bulk compositions and of the glasses quenched from each experimental temperature were performed with the JEOL 733 Superprobe at an accelerating potential of 15 keV, a beam current of 10 nA, and a counting time of 30 s. The beam was defocussed to 20 μm to avoid Si loss in the glasses. Anorthite, forsterite, and rutile served as standards, and concentrations were determined through ZAF correction procedures (Armstrong, 1988). The bulk composition of TCAN was analyzed previously by J. Paque.

Activities in CAI melts

Experimental run conditions and analyses of Pd alloys in equilibrium with melt and oxide standards are given for each bulk composition in Table 8. Melt compositions at each temperature are given in Table 9. Derived activities of MgO, Al_2O_3, and SiO_2 are given in Table 10. Precision ranges from 1 to 25%, depending on the magnitude of the activity determined, with the greatest precision attained for activities above 0.4, where solute concentrations in the sample wire are at their highest. The lowest precision is for activities below 0.15, where solute concentrations are low and more difficult to measure. The average precision for this data set, where most activities are near 0.2, is 12%. The activity coefficients of MgO, Al_2O_3, and SiO_2 derived from the experiments are given in Table 11.

Table 8. Experimental data for silicate liquids.

Table 8. Experimental data for silicate liquids[a,b].

T (°C)	$\log_{10} f_{O_2}$	time (hrs.)	$X_{Mg}^{Pd,melt}$	$X_{Mg}^{Pd,periclase}$	$X_{Al}^{Pd,melt}$	$X_{Al}^{Pd,corundum}$	$X_{Si}^{Pd,melt}$	$X_{Si}^{Pd,cristobalite}$
CAI-89A								
1299	-12.04	42	0.00083 (10)	0.00462 (16)	0.00440 (10)	0.00947 (16)	-------	-------
1300	-11.32	64	0.00045 (10)	0.00218 (10)	0.00139 (2)	0.00299 (1)	-------	-------
1302	-11.42	70	0.00059 (5)	0.00229 (9)	0.00158 (2)	0.00357 (5)	-------	-------
1300[c]	-12.29	48	-------	-------	-------	-------	-------	-------
	-12.09	48	0.00078 (6)	0.00478 (9)	0.00416 (4)	0.00950 (9)	-------	-------
1301[c]	-11.90	72	-------	-------	-------	-------	-------	-------
	-11.73	72	0.00056 (8)	0.00335 (9)	0.00260 (4)	0.00602 (1)	-------	-------
1300	-11.24	46	-------	-------	-------	-------	0.00035 (3)	0.00315 (5)
1302	-11.16	48	-------	-------	-------	-------	0.00044 (5)	0.00353 (8)
1351	-10.65	48	0.00051 (11)	0.00236 (7)	0.00136 (15)	0.00305 (3)	-------	-------
1350	-10.71	48	0.00062 (11)	0.00263 (13)	0.00180 (3)	0.00378 (6)	-------	-------
1348	-10.25	45	-------	-------	-------	-------	0.00018 (3)	0.00193 (5)
1351	-10.42	35	-------	-------	-------	-------	0.00031 (4)	0.00279 (5)
1350	-11.37	43	0.00116 (13)	0.00646 (17)	0.00640 (7)	0.01398 (38)	-------	-------
1352[c]	-11.60	24	-------	-------	-------	-------	-------	-------
	-11.35	48	0.00097 (7)	0.00501 (12)	0.00431 (4)	0.00929 (9)	-------	-------
1401	-10.16	39	0.00067 (7)	0.00291 (5)	0.00214 (10)	0.00441 (1)	-------	-------
1402	-10.18	41	0.00086 (5)	0.00360 (10)	0.00248 (1)	0.00516 (8)	-------	-------
1401	-10.66	42	0.00111 (6)	0.00515 (4)	0.00482 (4)	0.01024 (15)	-------	-------
1399[c]	-11.50	24	-------	-------	-------	-------	-------	-------
	-10.60	24	0.00085 (8)	0.00467 (26)	0.00372 (9)	0.00801 (4)	-------	-------
1401	-9.67	43	-------	-------	-------	-------	0.00025 (5)	0.00272 (2)
B2C								
1251	-12.04	69	0.00049 (12)	0.00171 (5)	0.00112 (3)	0.00255 (10)	-------	-------
1252	-12.19	45	-------	-------	-------	-------	0.00135 (5)	0.00529 (5)
1302	-11.44	44	0.00052 (6)	0.00240 (10)	0.00176 (2)	0.00372 (10)	-------	-------
1299[c]	-11.58	72	-------	-------	-------	-------	-------	-------
	-11.41	48	0.00037 (8)	0.00227 (9)	0.00157 (4)	0.00335 (21)	-------	-------
1302	-11.16	48	-------	-------	-------	-------	0.00079 (5)	0.00353 (8)
1350	-10.67	36	0.00056 (6)	0.00258 (6)	0.00187 (5)	0.00376 (10)	-------	-------
1353	-10.41	43	-------	-------	-------	-------	0.00076 (16)	0.00288 (5)
1351	-10.43	48	-------	-------	-------	-------	0.00053 (8)	0.00276 (6)
1350[c]	-10.86	38	-------	-------	-------	-------	-------	-------
	-10.68	22	0.00046 (8)	0.00246 (9)	0.00153 (7)	0.00343 (10)	-------	-------
1400	-10.19	43	0.00070 (10)	0.00334 (12)	0.00236 (12)	0.00495 (10)	-------	-------
1401	-9.67	42	-------	-------	-------	-------	0.00056 (2)	0.00234 (4)
1400[c]	-10.41	22	-------	-------	-------	-------	-------	-------
	-10.19	24	0.00052 (8)	0.00292 (15)	0.00223 (8)	0.00412 (5)	-------	-------
TCAN								
1300	-11.41	65	0.00034 (6)	0.00235 (6)	0.00150 (4)	0.00311 (2)	-------	-------
1301	-11.22	61	-------	-------	-------	-------	0.00046 (4)	0.00336 (5)
1353	-10.75	17	0.00037 (5)	0.00261 (9)	0.00206 (10)	0.00360 (5)	-------	-------
1352	-10.41	36	-------	-------	-------	-------	0.00052 (5)	0.00259 (4)
1398	-10.42	42	0.00033 (7)	0.00411 (18)	0.00417 (6)	0.00682 (45)	-------	-------
1400	-9.66	37	-------	-------	-------	-------	0.00035 (5)	0.00192 (13)

Table 8. (Cont.)								
FOB								
1302	-11.72	60	0.00073 (8)	0.00343 (24)	0.00213 (7)	0.00556 (12)	-------	-------
1300	-11.25	67	-------	-------	-------	-------	0.00051 (6)	0.00328 (7)
1351	-11.31	45	0.00118 (8)	0.00488 (15)	0.00363 (6)	0.00947 (4)	-------	-------
1350	-10.38	45	-------	-------	-------	-------	0.00033 (8)	0.00205 (11)
1402	-10.30	45	0.00098 (8)	0.00364 (7)	0.00227 (3)	0.00614 (59)	-------	-------
1400	-9.68	39	-------	-------	-------	-------	0.00037 (6)	0.00250 (7)
POI								
1282	-11.32	85	0.00025 (10)	0.00153 (7)	0.00101 (1)	0.00180 (5)	-------	-------
1278	-11.35	36	-------	-------	-------	-------	0.00127 (11)	0.00210 (7)
1301	-11.44	60	0.00035 (5)	0.00250 (12)	0.00176 (7)	0.00348 (7)	-------	-------
1304	-10.97	64	-------	-------	-------	-------	0.00104 (4)	0.00188 (13)
1353	-10.70	46	0.00047 (6)	0.00267 (18)	0.00175 (4)	0.00359 (2)	-------	-------
1353	-10.06	43	-------	-------	-------	-------	0.00064 (6)	0.00112 (9)
1402	-9.64	43	0.00029 (4)	0.00197 (12)	0.00084 (9)	0.00193 (1)	-------	-------
1400	-9.54	44	-------	-------	-------	-------	0.00093 (6)	0.00179 (4)

a. Numbers in parentheses indicate 1σ errors in the last digits based on counting statistics. Temperatures are estimated to be accurate to $\pm$ 3°C and f_{O_2}'s to $\pm$ 0.05 log units.

b. $X_i^{Pd,\,j}$ defined as mole fraction of solute i dissolved in Pd alloy in equilibrium with phase j.

c. Reversal. First line refers to conditions of initial equilibration, second to conditions of final equilibration.

Table 9. Compositions of silicate liquids (wt%).

Table 9. Compositions of silicate liquids (wt%).[a]					
T(°C)	1250	1280	1300	1350	1400
CAI-89A					
CaO	-----	-----	30.8	31.9	31.2
MgO	-----	-----	8.0	7.8	7.9
Al_2O_3	-----	-----	21.1	21.6	23.9
SiO_2	-----	-----	38.1	36.5	34.8
TiO_2	-----	-----	1.71	1.63	1.44
Total	-----	-----	99.7	99.4	99.2
ϕ[b]	-----	-----	sp+me	sp+me	sp
B2C					
CaO	27.0	-----	25.4	24.6	24.5
MgO	11.4	-----	10.6	10.4	10.9
Al_2O_3	18.2	-----	20.7	21.5	22.9
SiO_2	42.2	-----	41.3	40.3	39.6
TiO_2	1.65	-----	1.50	1.49	1.51
Total	100.5	-----	99.5	98.3	99.4
ϕ	sp+an	-----	sp	sp	sp
TCAN					
CaO	-----	-----	28.4	26.4	24.7
MgO	-----	-----	7.1	6.6	5.9
Al_2O_3	-----	-----	22.6	25.8	29.0
SiO_2	-----	-----	40.0	39.1	38.7
TiO_2	-----	-----	1.93	1.60	1.26
Total	-----	-----	100.1	99.6	99.5
ϕ	-----	-----	sp+an	sp+an	an
FOB					
CaO	-----	-----	25.4	23.9	22.4
MgO	-----	-----	14.1	16.3	17.7
Al_2O_3	-----	-----	16.9	16.8	17.0
SiO_2	-----	-----	42.3	41.8	40.5
TiO_2	-----	-----	1.49	1.42	1.44
Total	-----	-----	100.2	100.2	99.0
ϕ	-----	-----	sp+fo	sp+fo	sp+fo
POI					
CaO	-----	10.5	11.3	11.0	11.1
MgO	-----	15.5	15.9	17.0	17.0
Al_2O_3	-----	20.6	21.8	21.7	21.6
SiO_2	-----	52.1	50.2	50.4	50.3
TiO_2	-----	1.05	0.74	0.75	0.75
Total	-----	99.7	100.0	100.9	100.8
ϕ	-----	fo	fo	none	none

a. Electron microprobe analyses: 15 keV, 10 nA,

Table 9 (continued).

20 μm beam, 30 s; standardized on anorthite, forsterite, and rutile. Averages of several analyses of two runs at each temperature. Variations at each temperature are within 1 wt%.

b. Other phases present. sp = $MgAl_2O_4$ spinel, me = melilite, an = anorthite, fo = forsterite.

Table 10. Experimental and modeled activities for liquids.

Table 10. Experimental and modeled activities for liquids.							
		experimental[a]			Berman (1983)[b]		
liquid	T (°C)	a_{MgO}	$a_{Al_2O_3}$	a_{SiO_2}	a_{MgO}	$a_{Al_2O_3}$	a_{SiO_2}
CAI-89A	1300	0.195 (0.039)	0.200 (0.012)	0.118 (0.009)	0.252	0.293	0.078
CAI-89A	1350	0.207 (0.025)	0.214 (0.013)	0.102 (0.013)	0.261	0.257	0.065
CAI-89A	1400	0.217 (0.025)	0.226 (0.008)	0.094 (0.018)	0.262	0.272	0.061
B2C	1251	0.287 (0.068)	0.193 (0.017)	0.244 (0.009)	0.253	0.269	0.128
B2C	1300	0.190 (0.038)	0.222 (0.002)	0.206 (0.015)	0.227	0.307	0.142
B2C	1350	0.201 (0.023)	0.223 (0.034)	0.218 (0.027)	0.218	0.294	0.144
B2C	1400	0.194 (0.016)	0.260 (0.047)	0.239 (0.019)	0.224	0.289	0.134
TCAN	1300	0.145 (0.025)	0.233 (0.011)	0.136 (0.012)	0.190	0.332	0.119
TCAN	1350	0.138 (0.020)	0.327 (0.033)	0.201 (0.018)	0.167	0.402	0.135
TCAN	1400	0.078 (0.017)	0.374 (0.050)	0.182 (0.028)	0.141	0.481	0.155
FOB	1300	0.213 (0.028)	0.147 (0.011)	0.156 (0.019)	0.277	0.213	0.132
FOB	1350	0.242 (0.007)	0.147 (0.005)	0.161 (0.040)	0.298	0.192	0.129
FOB	1400	0.269 (0.022)	0.137 (0.026)	0.148 (0.025)	0.316	0.182	0.123
POI	1280	0.163 (0.068)	0.315 (0.019)	0.605 (0.056)	0.137	0.279	0.569
POI	1300	0.140 (0.022)	0.256 (0.023)	0.553 (0.045)	0.150	0.335	0.487
POI	1350	0.175 (0.024)	0.238 (0.012)	0.571 (0.069)	0.156	0.277	0.468
POI	1400	0.147 (0.022)	0.189 (0.041)	0.520 (0.037)	0.156	0.237	0.455

a. Average of all determinations from data in Table 8. Where multiple runs at one T are present, 1σ standard deviation of all determinations is shown in parentheses. Otherwise, the 1σ experimental error based on heterogeneity is shown.

b. 1σ errors estimated to be about 10-30% based on comparison with measurements of Rein and Chipman (1963; 1965).

Table 11. Activity coefficients for liquids.

Table 11. Activity coefficients for liquids[a].				
liquid	T (°C)	γ_{MgO}	$\gamma_{Al_2O_3}$	γ_{SiO_2}
CAI-89A	1300	1.581 (0.316)	1.556 (0.093)	0.300 (0.023)
CAI-89A	1350	1.714 (0.207)	1.618 (0.098)	0.269 (0.034)
CAI-89A	1400	1.754 (0.203)	1.527 (0.062)	0.257 (0.046)
B2C	1251	1.690 (0.400)	1.801 (0.159)	0.579 (0.021)
B2C	1300	1.174 (0.235)	1.777 (0.016)	0.487 (0.035)
B2C	1350	1.244 (0.143)	1.689 (0.258)	0.519 (0.064)
B2C	1400	1.155 (0.095)	1.864 (0.337)	0.584 (0.136)
TCAN	1300	1.308 (0.226)	1.674 (0.079)	0.326 (0.029)
TCAN	1350	1.320 (0.191)	2.013 (0.203)	0.481 (0.043)
TCAN	1400	0.814 (0.177)	2.014 (0.269)	0.433 (0.067)
FOB	1300	1.029 (0.135)	1.501 (0.112)	0.375 (0.046)
FOB	1350	1.025 (0.030)	1.527 (0.052)	0.395 (0.098)
FOB	1400	1.039 (0.085)	1.393 (0.264)	0.373 (0.063)
POI	1280	0.703 (0.293)	2.576 (0.155)	1.154 (0.107)
POI	1300	0.587 (0.092)	1.982 (0.178)	1.095 (0.089)
POI	1350	0.698 (0.096)	1.877 (0.095)	1.142 (0.138)
POI	1400	0.584 (0.087)	1.497 (0.325)	1.0425 (0.074)

a. 1σ error bars from propagation of errors based on heterogeneity shown in parentheses.

Activity-composition relations

The thermodynamic properties of silicate melts are a reflection of the underlying structure. In order to understand the link between thermodynamics and melt structure, one must examine the dependence of the activity coefficients $\gamma_i = a_i/X_i$ on composition. Examination of γ_i instead of a_i allows one to consider the thermodynamic properties independently of the compositional contribution inherent in the activity parameter. The structure of silicate melts is determined by the interaction of species that tend to either form or break up networks of three-dimensional cation-oxygen bonds. The dominant network-forming species in the melts in this study is Si^{4+}, which forms tetrahedral units linked by sharing one or more bridging oxygen atoms. By analogy with pure SiO_2, which is composed of SiO_4^{2-} tetrahedra that share all four oxygen atoms with adjacent tetrahedra, it is reasonable to expect that an increase in γ_{SiO_2} in a melt is related to an increase in the number of bridging oxygens. Raman, nuclear magnetic resonance (NMR), and X-ray absorption (XAS) spectroscopic data on silicate glasses in the systems CaO-Al_2O_3-SiO_2 and MgO-Al_2O_3-SiO_2 indicate that Al^{3+} is also a network-former in melts, where it is charge-balanced by Ca^{2+} or Mg^{2+} (Seifert et al., 1982; Sharma et al., 1983; Murdoch et al., 1985; Sharma et al., 1988; Merzbacher and White, 1991; Landron et al., 1992). Because Al^{3+} is subordinate to Si^{4+} in the melts in this study and may be randomly dispersed in the network, it is unclear what species increases in response to a rise in $\gamma_{Al_2O_3}$. However, because Al^{3+} is a network-former, an increase in $\gamma_{Al_2O_3}$ is probably also related to a rise in the overall degree of polymerization. In contrast, components such as MgO or CaO, when present in excess

of that needed to charge-balance Al^{3+}, serve to depolymerize the melt by reacting with Si–O or Al–O bonds to produce non-bridging oxygens (NBO) charge-balanced by Mg^{2+} or Ca^{2+}.

Fig. 9 shows the relationship between activity coefficient and composition for the network-forming components in the CAI and POI liquids. Fig. 9a demonstrates that, as expected, there is a strong positive correlation between γ_{SiO_2} and X_{SiO_2}. Since Si^{4+} is the dominant network-former in these melts, an increase in SiO_2 should increase polymerization in the liquid and raise γ_{SiO_2}. Fig. 9b shows that the activity coefficient of Al_2O_3 has a weak but positive correlation with $X_{Al_2O_3}$. This indicates that Al^{3+} also participates in polymerization but due to lower abundances does not control it to the same degree as Si^{4+}. Fig. 10 shows the relationship between activity coefficient and composition for the components CaO and MgO. The total CaO and MgO in the experimental compositions exceeds that needed to charge-balance the Al^{3+} in the network, so it is evident that some of the CaO and MgO must function as network-modifiers, although it is unknown what proportion of the CaO or MgO serves each function. Fig. 10a shows a strong negative correlation between γ_{MgO} and X_{SiO_2}, indicating decreasing basicity in the melt with increasing SiO_2. The relationship between γ_{MgO} and polymerization of the network is not completely straightforward, however, as can be seen in a plot of γ_{MgO} against non-bridging oxygen divided by total oxygen (NBO/ΣO; Fig. 10b). Although there is a general increase in γ_{MgO} with NBO, the FOB liquids deviate from the main trend. This indicates a possible change in the speciation of the melts between FOB and the others. The failure of γ_{MgO} in FOB to

Figure 9. Thermodynamic properties of network-forming components as a function of composition. (a) Activity coefficient of SiO_2 versus mole fraction of SiO_2. (b) Activity coefficient of Al_2O_3 versus mole fraction of Al_2O_3.

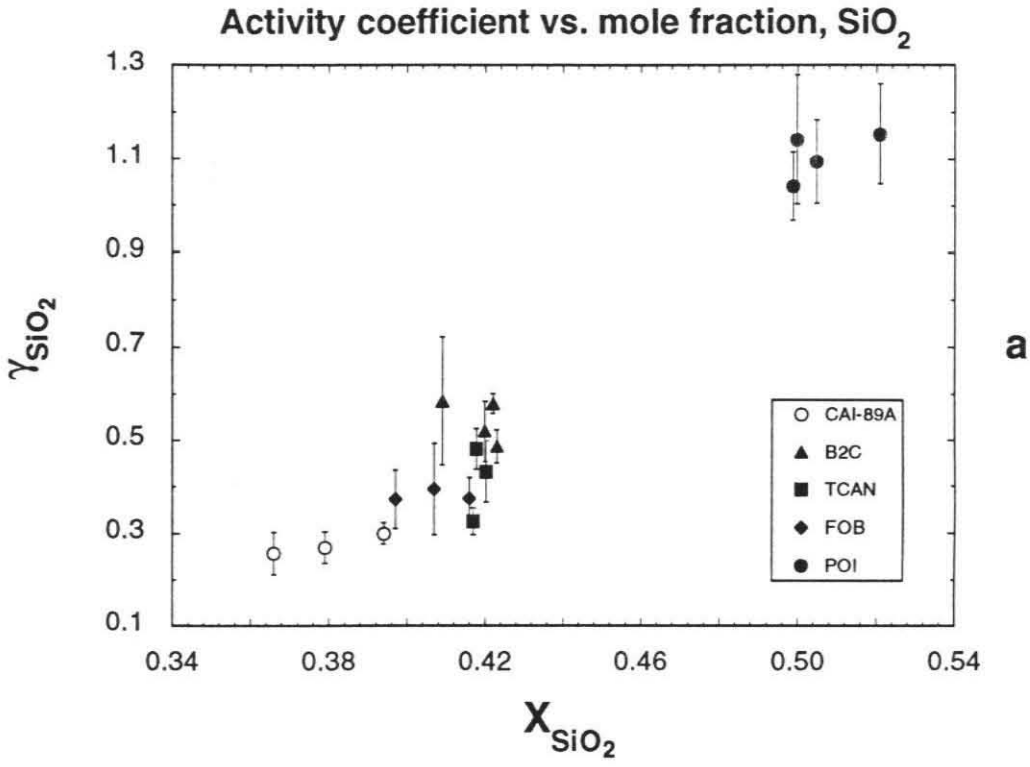
Activity coefficient vs. mole fraction, SiO_2
γ_{SiO_2}
X_{SiO_2}
1.3
1.1
0.9
0.7
0.5
0.3
0.1
0.34
0.38
0.42
0.46
0.50
0.54
CAI-89A
B2C
TCAN
FOB
POI
a

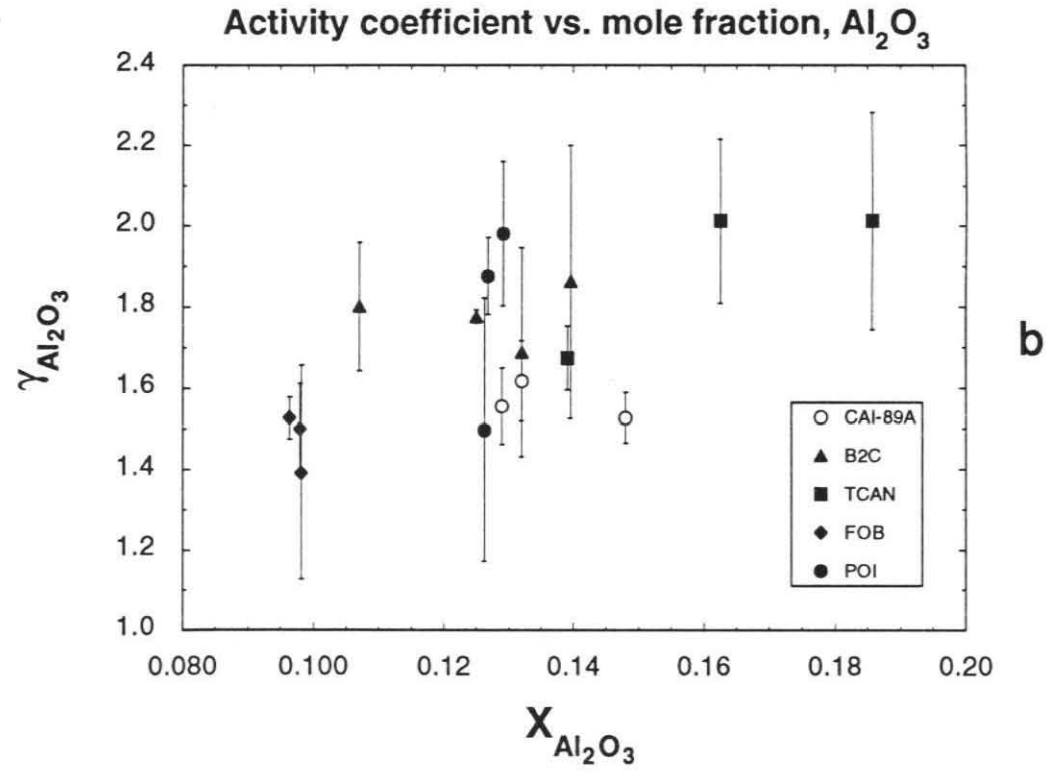
Activity coefficient vs. mole fraction, Al_2O_3
$\gamma_{Al_2O_3}$
$X_{Al_2O_3}$
2.4
2.2
2.0
1.8
1.6
1.4
1.2
1.0
0.080
0.100
0.12
0.14
0.16
0.18
0.20
CAI-89A
B2C
TCAN
FOB
POI
b

Figure 10. Thermodynamic properties of network-modifying components as a function of composition. (a) Activity coefficient of MgO versus mole fraction of SiO_2. (b) Activity coefficient of MgO versus NBO/ΣO.

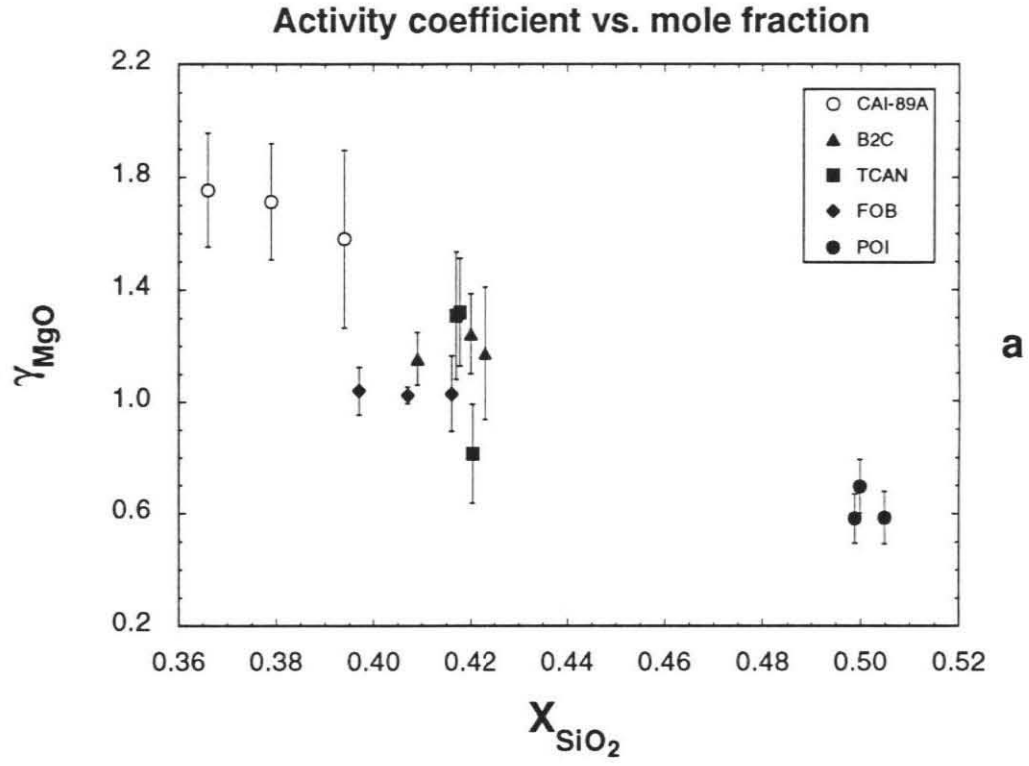
Activity coefficient vs. mole fraction
CAI-89A
B2C
TCAN
FOB
POI
γ_{MgO}
X_{SiO_2}
2.2
1.8
1.4
1.0
0.6
0.2
0.36
0.38
0.40
0.42
0.44
0.46
0.48
0.50
0.52
a

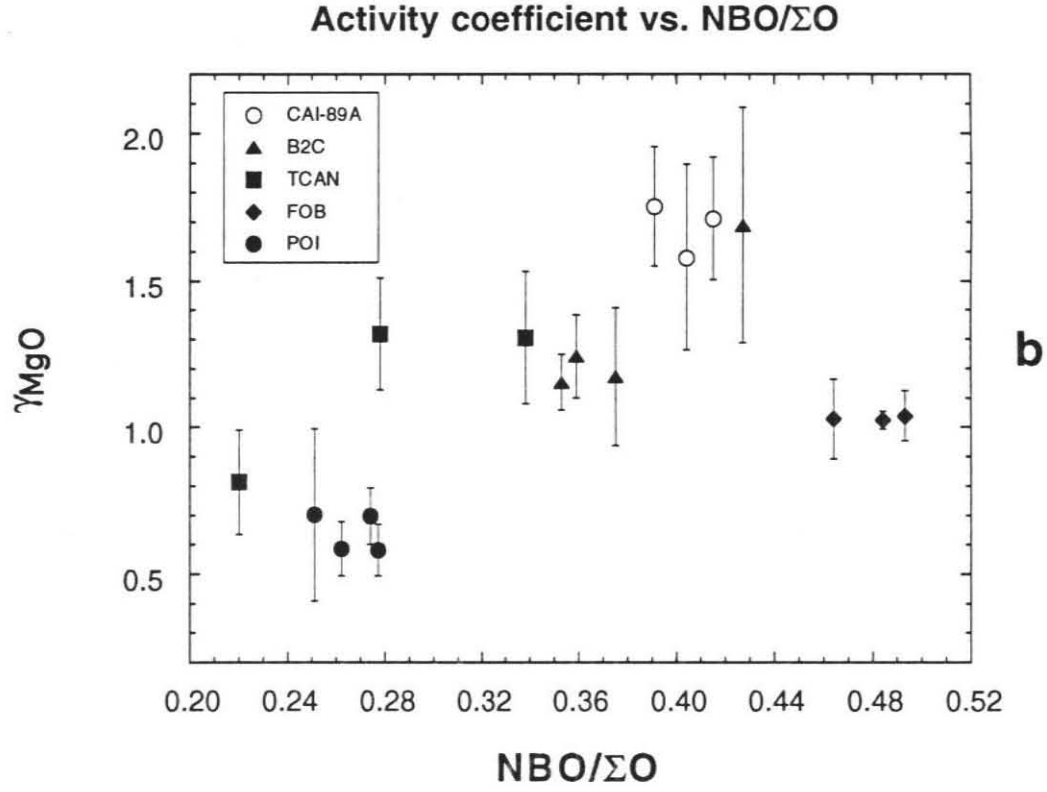
Activity coefficient vs. NBO/ΣO
CAI-89A
B2C
TCAN
FOB
POI
γMgO
NBO/ΣO
2.0
1.5
1.0
0.5
0.20
0.24
0.28
0.32
0.36
0.40
0.44
0.48
0.52
b

continue to increase with increasing NBO may indicate a change in the proportion of Mg^{2+} acting as charge-balancer versus network modifier, possibly related to the fact that the FOB composition has a higher ratio of network-modifiers to Al^{3+} than the other compositions. There is some indication that Ca^{2+} may exert a controlling influence on the role of alkaline earth cations in the melts, as the activity coefficient of MgO correlates poorly with X_{MgO} (Fig. 11a) but well with X_{CaO} (Fig. 11b).

The effect of the network-modifiers on the silicate framework can be judged by plotting $\gamma_{Al_2O_3}$ and γ_{SiO_2} against NBO/ΣO. An increase in the concentration of the network-modifiers should correlate with a decrease in the activity coefficient of one or both of the network-formers. Fig. 12a shows that there is a strong negative correlation between $\gamma_{Al_2O_3}$ and NBO/ΣO. All of the measured values fall on the same decreasing trend except for POI, which crosscuts the main trend at a steeper angle. There is a negative correlation also in γ_{SiO_2} versus NBO/ΣO (Fig. 12b), but the experimental points fall into groups. POI and FOB lie along a steeply decreasing trend, TCAN and CAI-89A follow an almost flat trend, and B2C is intermediate. The trends observed in Fig. 12b correlate with Al:Si ratio, becoming flatter as the ratio increases. The experimental data points can be divided into groups characterized by Al:Si < 0.6, 0.6 < Al:Si < 0.8, and Al:Si > 0.8. The relationships in Fig. 12 suggest that Ca^{2+} and Mg^{2+} prefer to react with the longer, weaker Al–O bonds, although they may also react with the Si–O bonds. Most of the liquids follow the main trend in Fig. 12a because they have similar Al:Si ratios and hence undergo similar degrees of depolymerization as NBO/ΣO increases. POI crosscuts this trend because there is very little Al^{3+} in the

Figure 11. Thermodynamic properties of network-modifying components as a function of concentration of network-modifiers. (a) Activity coefficient of MgO versus X_{MgO}. (b) Activity coefficient of MgO versus X_{CaO}.

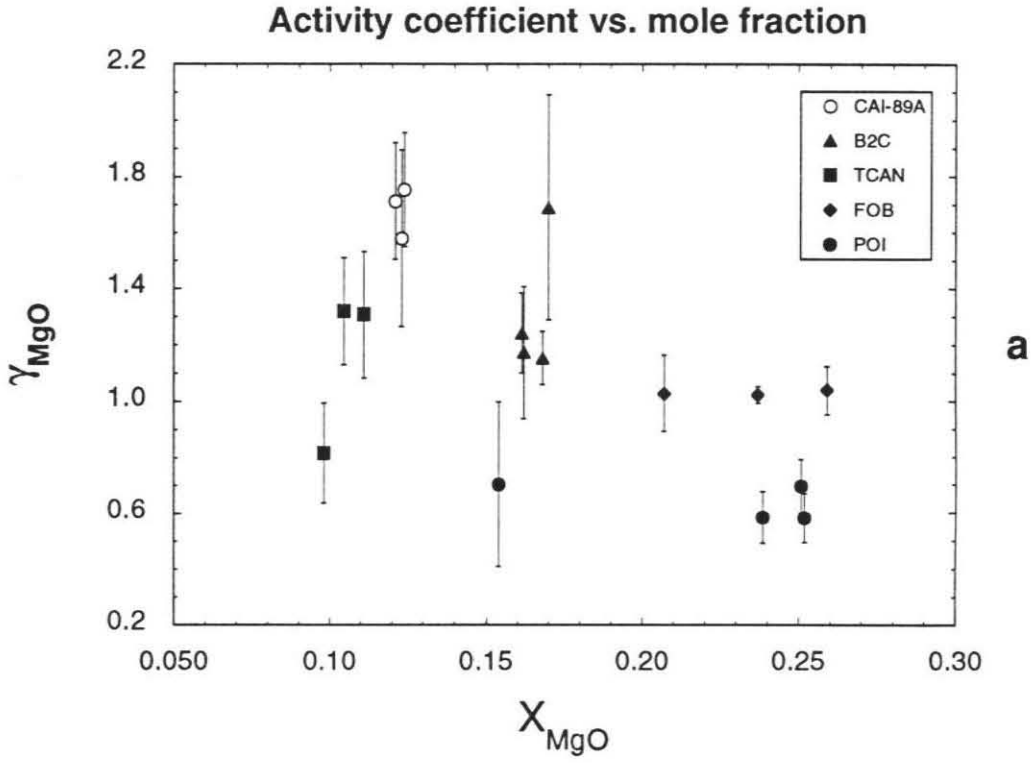
Activity coefficient vs. mole fraction
2.2
1.8
1.4
1.0
0.6
0.2
γ_{MgO}
0.050
0.10
0.15
0.20
0.25
0.30
X_{MgO}
CAI-89A
B2C
TCAN
FOB
POI
a

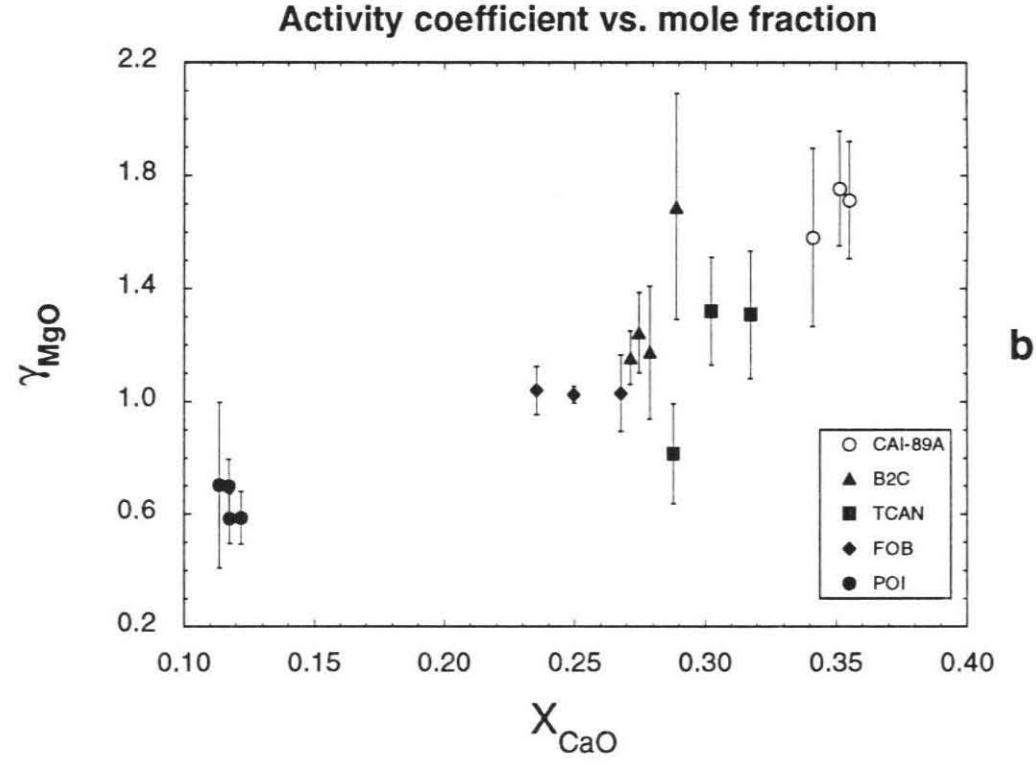
Activity coefficient vs. mole fraction
2.2
1.8
1.4
1.0
0.6
0.2
γ_{MgO}
0.10
0.15
0.20
0.25
0.30
0.35
0.40
X_{CaO}
CAI-89A
B2C
TCAN
FOB
POI
b

Figure 12. Thermodynamic properties of network-forming components as a function of NBO/ΣO. (a) Activity coefficient of Al_2O_3 versus NBO/ΣO. (b) Activity coefficient of SiO_2 versus NBO/ΣO.

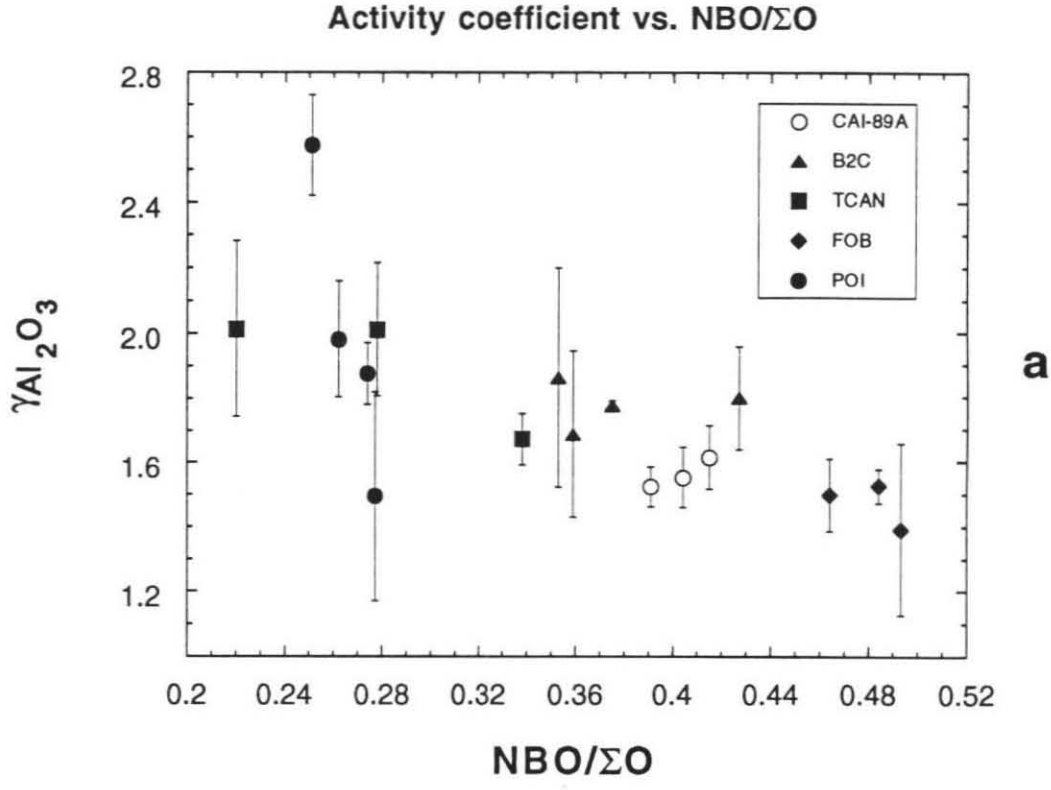
Activity coefficient vs. NBO/ΣO
γAl_2O_3
2.8
2.4
2.0
1.6
1.2
0.2
0.24
0.28
0.32
0.36
0.4
0.44
0.48
0.52
NBO/ΣO
CAI-89A
B2C
TCAN
FOB
POI
a

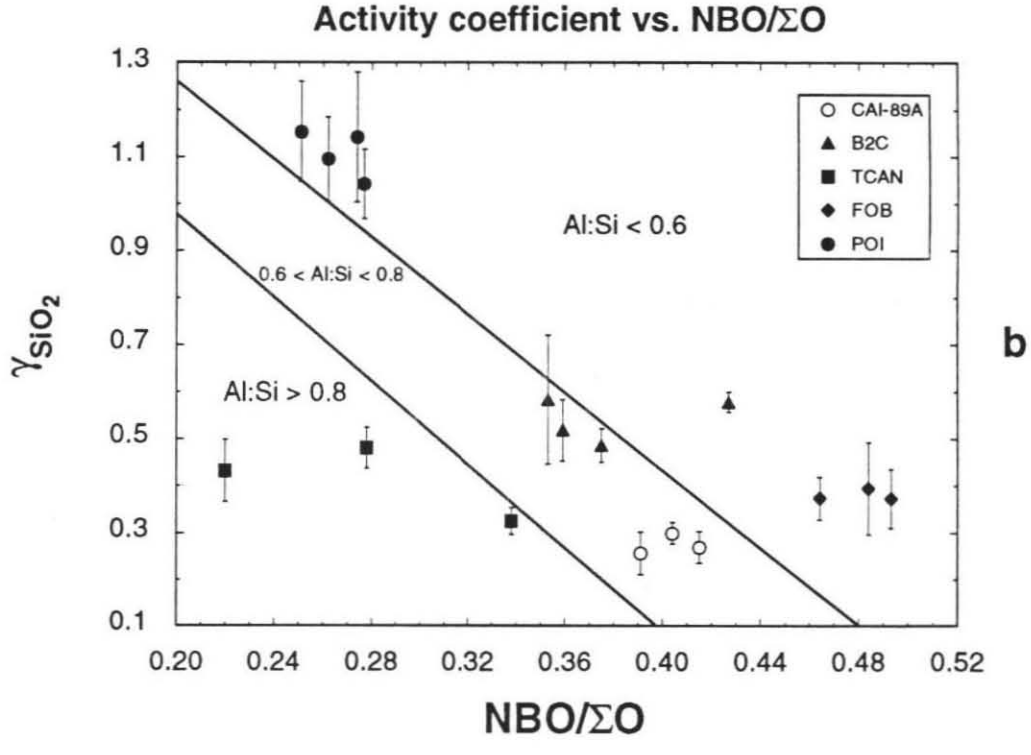
Activity coefficient vs. NBO/ΣO
γ_{SiO_2}
1.3
1.1
0.9
0.7
0.5
0.3
0.1
0.20
0.24
0.28
0.32
0.36
0.40
0.44
0.48
0.52
NBO/ΣO
Al:Si < 0.6
0.6 < Al:Si < 0.8
Al:Si > 0.8
CAI-89A
B2C
TCAN
FOB
POI
b

framework, and the $\gamma_{Al_2O_3}$ therefore drops very rapidly when the Al–O bonds are attacked. Although FOB also has a low Al:Si ratio, no rapid drop in $\gamma_{Al_2O_3}$ is seen because FOB has a much higher concentration of network modifiers and is therefore already depolymerized relative to POI. In Fig. 12b, the flat trend indicates that in the high Al:Si compositions relatively few Si–O bonds are broken as network modifiers are added. In contrast, the steep trend defined by POI-FOB indicates that as network modifiers are added to relatively low-alumina compositions, Si–O bonds are attacked. The observed relationship between γ_{SiO_2}, NBO/ΣO, and Al:Si ratio holds in general for other melts in CMAS where the activity of SiO_2 can be inferred (cristobalite-saturated melts, Longhi, 1987) or has been measured (Rein and Chipman, 1965), but it seldom holds for the simpler systems MAS and CAS (Kay and Taylor, 1960; Rein and Chipman, 1965). This indicates that the melt structure and speciation varies according to the nature and proportions of alkaline earth cations present in the melt.

It is difficult to ascertain what species are present in these liquids, as there are no spectroscopic studies of glasses in the mixed alkaline earth CMAST system. The structure of the high Al:Si compositions in this study may be similar to that of anorthite glass, since the Al:Si ratio in anorthite is similar. Seifert et al. (1982) state based on Raman spectroscopic evidence that anorthite glass is composed of the species $Al_2Si_2O_8^{2-}$ in four-membered rings plus SiO_2 and $Al_2O_4^{2-}$ in six-membered rings. However, the CAI and POI liquids must exhibit distinct differences from anorthite glass, as the thermodynamic data in this study and Raman spectroscopic data on the simpler systems CAS and MAS imply that the presence of Mg^{2+} affects the speciation.

Raman studies indicate that Mg^{2+} in a melt leads to a wider distribution of silicate polymer species because of its higher charge density relative to Ca^{2+} (Murdoch et al., 1985; Merzbacher and White, 1991). Mg^{2+} can also cause clustering of aluminate tetrahedra into areas of locally higher negative charge density (Merzbacher and White, 1991), resulting in the creation of Al-rich and Si-rich regions in the melt. Therefore, compared to anorthite glass, the high Al:Si liquids in this study likely have a wider range of polymer species and may be inhomogeneous on the microscopic scale. If clusters of Mg^{2+} with aluminate tetrahedra are present in the melt structure, they may serve as nucleation points for the $MgAl_2O_4$ spinel that crystallizes abundantly from the CAI compositions. The low Al:Si CAI liquids must be more depolymerized than the others, since more of the CaO and MgO function as modifiers instead of charge balancers. POI, however, is probably highly polymerized due to its high SiO_2 content, although again the presence of large amounts of Mg^{2+} may lead to the existence of a range of species in the liquid.

Comparison with model of Berman (1983)

It is instructive to compare the measured activities with those predicted for these liquid compositions through thermodynamic modeling. One recent model for the four-component system CaO-MgO-Al_2O_3-SiO_2 (CMAS) is that of Berman (1983). It was calibrated by applying linear programming to a series of phase equilibria and calorimetric constraints via a simple Margules solution model. Although the synthetic CAI liquids in this study were actually in the five-component system CMAS + TiO_2,

the measurements can be compared to his predictions because the concentrations of TiO_2 in the liquids are less than 2 wt%. The presence of TiO_2 was allowed for by recalculating Berman's activities assuming that TiO_2 acts only as a diluent (that is, all Margules parameters involving TiO_2 were set to zero).

Experimentally determined activities and values predicted by the melt model of Berman (1983) are given in Table 10 and compared in Fig. 13. Although the agreement is good, it is evident that the experimentally measured activities of MgO and Al_2O_3 are systematically lower than predicted by Berman's model, and the experimental SiO_2 activities are systematically higher. These differences are attributable to inaccuracies in the thermodynamic data incorporated into Berman's melt model. For example, the higher MgO and Al_2O_3 activities predicted by his model for the spinel-saturated compositions are linked to a ΔG_f° of $MgAl_2O_4$ spinel 3-5 kJ/mole more positive than determined in Chapter 2. In addition, Berman's model uses liquid end-member oxides for standard states even though the thermodynamic properties of the pure liquid oxides are only poorly known. Models such as Berman's may be refined using the experimental measurements, which provide important new constraints for the modeling of silicate liquids that are independent of knowledge of phase equilibria and thermodynamic properties of solid phases.

Free energy of formation of crystalline phases

The measured activities of MgO, Al_2O_3, and SiO_2 in the spinel- and forsterite-saturated liquids can be used to calculate the free energies of formation from the ox-

Figure 13. Comparison between experimental activities and those predicted by the model of Berman (1983). Experimental activities derived from data in Table 8.

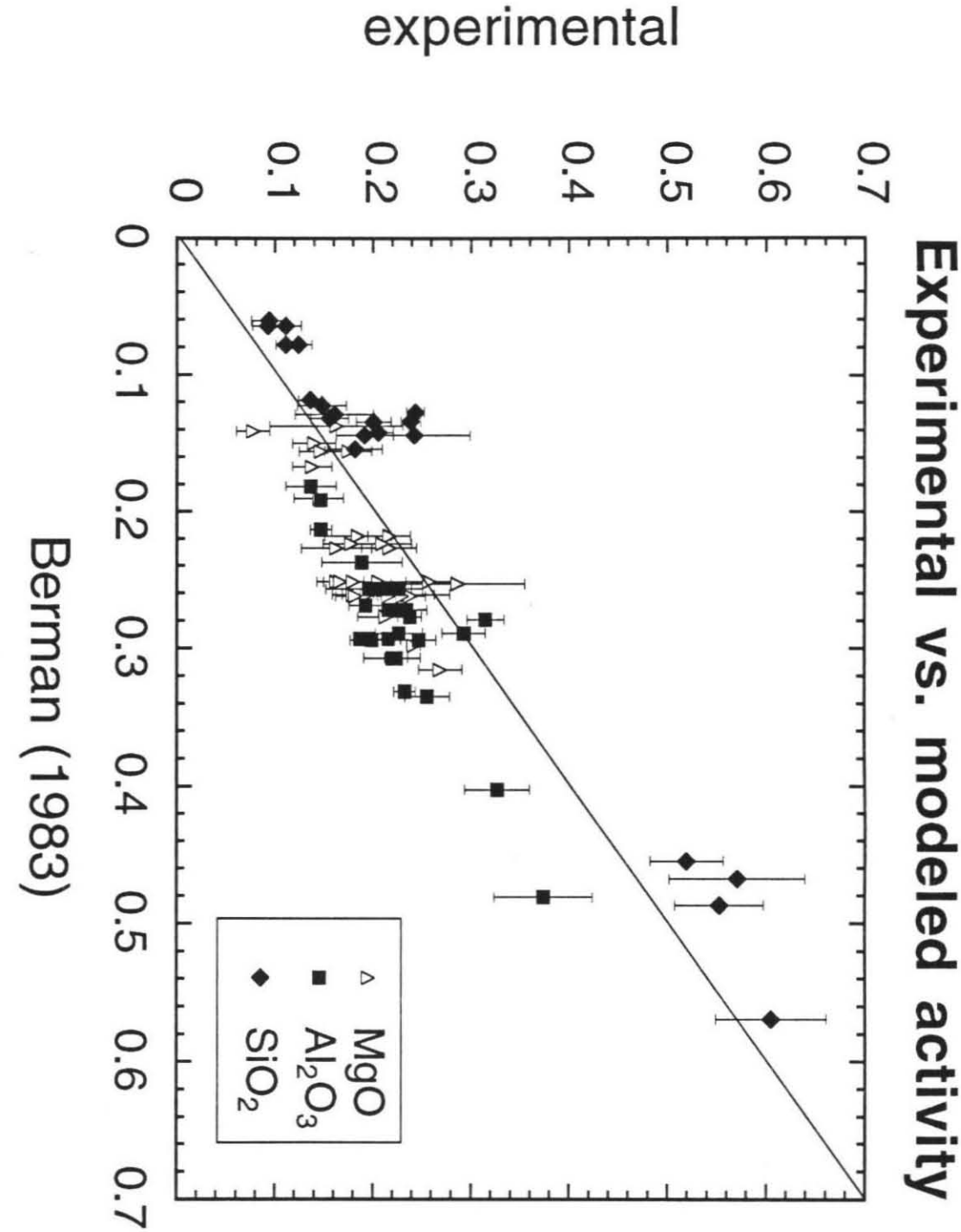
Experimental vs. modeled activity
experimental
Berman (1983)
0
0.1
0.2
0.3
0.4
0.5
0.6
0.7
MgO
Al_2O_3
SiO_2

ides, ΔG_f°, of $MgAl_2O_4$ and Mg_2SiO_4. If the phases are essentially stoichiometric ($a^{spinel}_{MgAl_2O_4} \equiv 1$, $a^{forsterite}_{Mg_2SiO_4} \equiv 1$), then one can calculate ΔG_f° from the relations:

$$\Delta G_f^\circ(\text{spinel}) = -\,RT \ln \frac{1}{a^{spinel}_{MgO}\, a^{spinel}_{Al_2O_3}} \qquad (1)$$

and

$$\Delta G_f^\circ(\text{forsterite}) = -\,RT \ln \frac{1}{(a^{forsterite}_{MgO})^2\, a^{forsterite}_{SiO_2}} \,. \qquad (2)$$

Table 12 and Fig. 14 show the values of ΔG_f° calculated for the CMAST liquids that were saturated with spinel, forsterite, or both. The ΔG_f°'s of spinel overlap with the values determined from stoichiometric $MgAl_2O_4$ in the binary system MgO–Al_2O_3 (Chapter 2), although they are up to 4-5 kJ/mole more negative. The ΔG_f°'s of forsterite determined from POI are in excellent agreement with values we determined for olivines in the binary system MgO-SiO_2 (see Chapter 5) as well as the data sets of Robie et al. (1978) and Berman (1988), but the ΔG_f°'s determined from FOB are about 10 kJ/mole more negative. This discrepancy may be due to the substantial amount of CaO (~1.1 wt%) present in the FOB forsterites. The 10 kJ/mole difference in ΔG_f° implies an activity of Mg_2SiO_4 as low as 0.65 in these olivines, a value much lower than that predicted by current models for solution of CaO in olivine (~0.97, Davidson and Mukhopadhyay, 1984). This may indicate a heretofore unsuspected complexity in dilute olivine solid solutions that may be linked to changes in defect concentrations or ordering properties produced by the entry of Ca ions into the lattice (see Chapter 5).

Table 12. ΔG_f° from the oxides of spinel and forsterite (J).

Table 12. ΔG_f° from the oxides of spinel and forsterite (J).			
liquid	T (°C)	$\Delta G_f^\circ(sp)^{a,b}$	$\Delta G_f^\circ(fo)^{a,c}$
CAI-89A	1300	-42429 (2732)	-------
CAI-89A	1350	-42085 (1826)	-------
CAI-89A	1400	-41940 (1678)	-------
B2C	1250	-36686 (3202)	-------
B2C	1300	-41404 (2619)	-------
B2C	1350	-41900 (2574)	-------
B2C	1400	-41549 (2765)	-------
TCAN	1300	-44307 (2339)	-------
TCAN	1350	-41809 (2385)	-------
FOB	1300	-45301 (1980)	-64750 (3795)
FOB	1350	-45019 (609)	-62937 (3444)
FOB	1400	-44869 (2875)	-63105 (3273)
POI	1280	-------	-53335 (10774)
POI	1300	-------	-59176 (4248)

a. Calculated from mean activities in Table 10. 1σ errors based on propagation of errors in activities in Table 10.

b. sp = spinel.

c. fo = forsterite.

Figure 14. (a) ΔG_f° of $MgAl_2O_4$ spinel vs. T(K) in CMAST liquids. Solid squares and circles are stoichiometric and periclase-saturated spinel from Chapter 2 (Chamberlin et al., 1993b); open symbols are from this study (Table 12). Lines are data sets from the literature: 1) Robie et al. (1978), 2) Helgeson et al. (1978), 3) Holland and Powell (1990), 4) Berman (1988), 5) Chapter 2, 6) JANAF (1985), and 7) Hallstedt (1992).

(b) ΔG_f° of Mg_2SiO_4 forsterite vs. T(K) in CMAST liquids. Solid squares and circles are stoichiometric forsterite and forsterite in equilibrium with protoenstatite (Chapter 5); open symbols are from this study (Table 12). Lines are data sets from the literature: Róg et al., 1974; Robie et al. (1978); Berman (1988); JANAF (1985); Gillet et al. (1991).

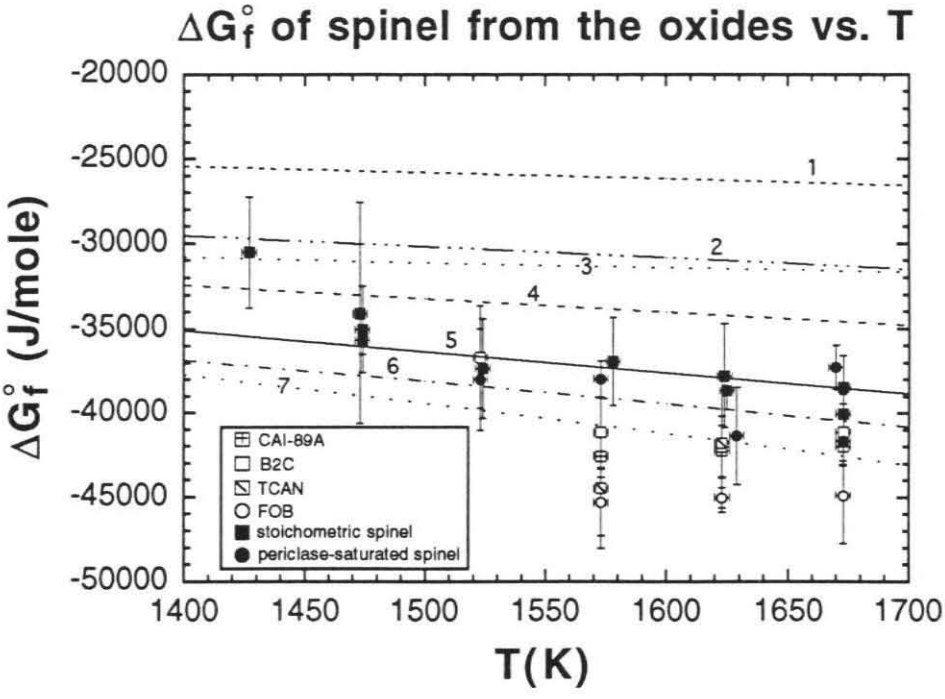
ΔG°f of spinel from the oxides vs. T
ΔG°f (J/mole)
T(K)
-20000
-25000
-30000
-35000
-40000
-45000
-50000
1400
1450
1500
1550
1600
1650
1700
1
2
3
4
5
6
7
CAI-89A
B2C
TCAN
FOB
stoichometric spinel
periclase-saturated spinel

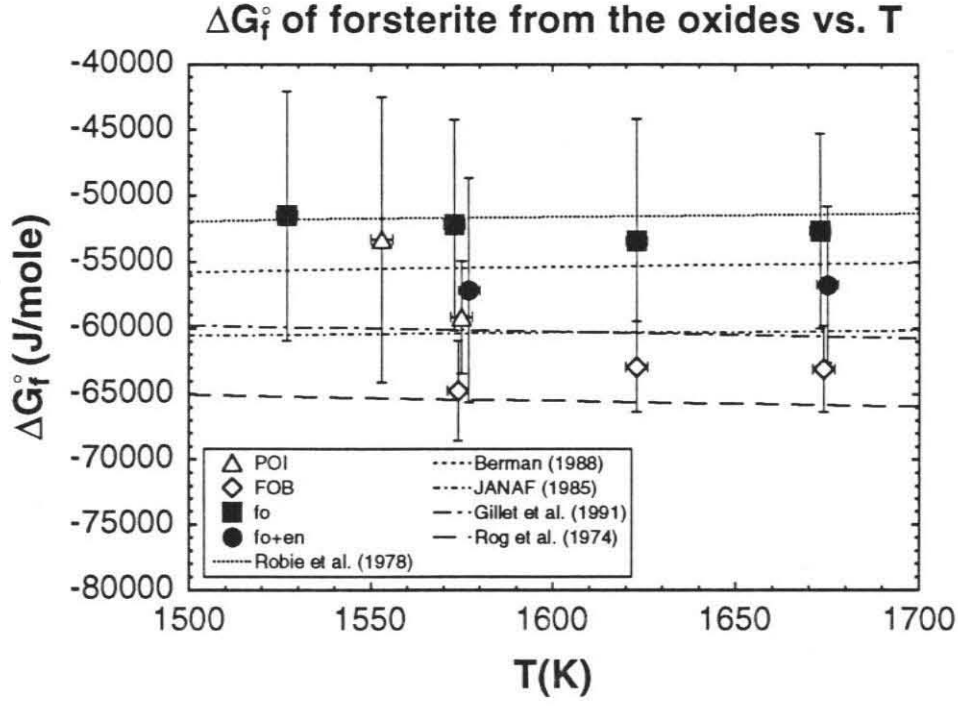
ΔG°f of forsterite from the oxides vs. T
ΔG°f (J/mole)
T(K)
-40000
-45000
-50000
-55000
-60000
-65000
-70000
-75000
-80000
1500
1550
1600
1650
1700
POI
FOB
fo
fo+en
Robie et al. (1978)
Berman (1988)
JANAF (1985)
Gillet et al. (1991)
Rog et al. (1974)

The ability to measure the activity of CaO in melts and minerals through Pd-oxide equilibration has not been developed, but one can constrain the value of a_{CaO} in anorthite-saturated melts using literature values for the ΔG_f° of anorthite and the measurements of Al_2O_3 and SiO_2 as long as the anorthite is stoichiometric. Electron microprobe analysis shows that anorthites crystallized from B2C and TCAN are indeed stoichiometric (J. Paque, unpublished data), although anorthite may dissolve up to 8 wt% excess SiO_2 in solid solution (Longhi and Hays, 1979). For the anorthite-saturated liquids, (B2C at 1250°C, TCAN at 1300 to 1400°C), one has the reaction:

$$CaO_{(lime)} + Al_2O_{3(corundum)} + 2\ SiO_{2(cristobalite)} = CaAl_2Si_2O_{8(anorthite)} \qquad (3)$$

with the relation:

$$\Delta G_f^\circ(\text{anorthite}) = -\ RT\ \ln \frac{1}{a_{CaO}^{anorthite}\ a_{Al_2O_3}^{anorthite}\ (a_{SiO_2}^{anorthite})^2}\ , \qquad (4)$$

where $a_{CaAl_2Si_2O_8}^{anorthite} \equiv 1$ for stoichiometric anorthite. Eqn. (4) and the ΔG_f° of anorthite from Berman (1988) give CaO activities in coexisting melts of 0.003 for B2C at 1250°C, and 0.008, 0.003, and 0.005 for TCAN at 1300, 1350, and 1400°C. These results compare favorably with the calculated values from the model of Berman (1983), which are respectively 0.005, 0.006, 0.005, and 0.004.

Equilibrium with the solar nebula

Table 13 lists the calculated equilibrium partial pressures of Mg, Al, and SiO over the synthetic melt compositions at f_{O_2}'s corresponding to a gas of solar composition (Fegley and Palme, 1985). Thermodynamic data for the oxides are taken from Robie

Table 13. Partial pressures of Mg, Al, and SiO in equilibrium with CMAST liquids and in the solar nebula.

Table 13. Partial pressures of Mg, Al, and SiO in equilibrium with CMAST liquids and in the solar nebula.

			liquid[a]			solar[b]		
liquid	T (°C)	$\log_{10} f_{O_2}$ [b]	P_{Mg}	P_{Al}	P_{SiO}	P_{Mg}	P_{Al}	P_{SiO}
CAI-89A	1300	-17.19	2×10^{-6}	5×10^{-12}	3×10^{-6}	7×10^{-10}	1×10^{-11}	6×10^{-10}
CAI-89A	1350	-16.68	8×10^{-6}	4×10^{-11}	9×10^{-6}	7×10^{-10}	3×10^{-11}	3×10^{-9}
CAI-89A	1400	-16.19	2×10^{-5}	2×10^{-10}	2×10^{-5}	7×10^{-10}	3×10^{-11}	2×10^{-9}
B2C	1300	-17.19	2×10^{-6}	6×10^{-12}	5×10^{-6}	7×10^{-10}	1×10^{-11}	6×10^{-10}
B2C	1350	-16.68	7×10^{-6}	4×10^{-11}	2×10^{-5}	7×10^{-10}	3×10^{-11}	3×10^{-9}
B2C	1400	-16.19	2×10^{-5}	2×10^{-10}	7×10^{-5}	7×10^{-10}	3×10^{-11}	2×10^{-9}
TCAN	1300	-17.19	2×10^{-6}	6×10^{-12}	3×10^{-6}	7×10^{-10}	1×10^{-11}	6×10^{-10}
TCAN	1350	-16.68	5×10^{-6}	5×10^{-11}	2×10^{-5}	7×10^{-10}	3×10^{-11}	3×10^{-9}
TCAN	1400	-16.19	8×10^{-6}	3×10^{-10}	5×10^{-5}	7×10^{-10}	3×10^{-11}	2×10^{-9}
POI	1300	-17.19	2×10^{-6}	6×10^{-12}	1×10^{-5}	7×10^{-10}	1×10^{-11}	6×10^{-10}
POI	1350	-16.68	7×10^{-6}	4×10^{-11}	5×10^{-5}	7×10^{-10}	3×10^{-11}	3×10^{-9}
POI	1400	-16.19	1×10^{-5}	2×10^{-10}	1×10^{-4}	7×10^{-10}	3×10^{-11}	2×10^{-9}
FOB	1300	-17.19	2×10^{-6}	4×10^{-12}	4×10^{-6}	7×10^{-10}	1×10^{-11}	6×10^{-10}
FOB	1350	-16.68	9×10^{-6}	3×10^{-11}	1×10^{-5}	7×10^{-10}	3×10^{-11}	3×10^{-9}
FOB	1400	-16.19	2×10^{-5}	2×10^{-10}	4×10^{-5}	7×10^{-10}	3×10^{-11}	2×10^{-9}

a. K(T) for the oxides from Robie et al. (1978).

b. L. Grossman pers. comm., 1993 (see text). $P_{tot} = 10^{-5}$ atm.

et al. (1978). Shown for comparison are the partial pressures of the same gas species calculated for equilibrium condensation in a cooling gas of solar bulk composition at the same temperatures and a total pressure P_{tot} of 10^{-5} bars (L. Grossman, 1993, pers. comm.). This pressure is the highest likely P_{tot} in the solar nebula based on accretion models, where estimates range from 10^{-5} to 10^{-7} bars (Wood and Morfill, 1988). Assuming that all partial pressures in Table 13 are correct to within at least an order of magnitude, it is evident that the partial pressures of Al in equilibrium with CAI melts are comparable at 1350°C to those in the solar nebula, but the partial pressures of Mg and SiO in equilibrium with these melts at 1300 to 1400°C are many orders of magnitude higher than expected in the solar nebula. If the model of Berman (1983) is used to estimate a_{CaO} in these liquids at 1300 to 1400°C, it yields values ranging from $\sim 10^{-3}$ in POI to $\sim 10^{-2}$ in CAI-89A. This gives P_{Ca} over the liquids as 10^{-10} to 10^{-8} bar, at least an order of magnitude higher than expected in this temperature range for the solar nebula (4×10^{-11} bar, L. Grossman, 1993, pers. comm.). These observations imply that a liquid of CAI or POI composition would not condense from a solar gas but instead would require an environment of higher Ca, Mg, and Si content. Alternatively, P_{Ca}, P_{Mg}, and P_{SiO} could be increased to levels equal or in excess of those over CAI melts by increasing the total pressure by about 4 to 5 orders of magnitude, or to almost 1 bar. Possible errors in the estimates of f_{O_2} in the solar nebula do not alter the conclusions about the disequilibrium. Because P_{Mg} and P_{SiO} are proportional to $f_{O_2}^{-1/2}$, the nebular f_{O_2} would have to be eight orders of magnitude lower than assumed in Table 13 to bring the partial pressures into equilibrium with CAI melts. Since such

high total pressures and extremely reducing conditions are not plausible (Fegley and Palme, 1985; Wood and Morfill, 1988), it is likely that CAIs and POIs in meteorites probably acquired their present forms through secondary melting events.

On the basis of the partial pressures of Ca, Mg, and SiO calculated for the solar nebula, it appears that any liquid condensate would be characterized by extremely low CaO, MgO, and SiO_2 activities (at 1400°C, $a_{CaO} = 3.1x10^{-5}$, $a_{MgO} = 1.8x10^{-5}$, and $a_{SiO_2} = 3.6x10^{-5}$). Fig. 15 shows contours of oxide activity at 1400°C projected through spinel onto the plane anorthite-gehlenite-forsterite. Trends at lower temperatures are similar and so are not shown. From the isoactivity contours in this figure, a_{MgO} and a_{SiO_2} tend toward zero as the gehlenite apex is approached, suggesting that Type A CAIs might be possible candidates for liquid condensates. However, the activities of CaO, MgO, and SiO_2 in Type A liquids estimated from the model of Berman (1983) are about 0.02, 0.2, and 0.04, low but much larger than 10^{-5}. Moreover, only a few Type As exhibit textures consistent with crystallization from a melt (the "compact" Type As), and these inclusions may have attained their present textures through a secondary melting event. There are other inclusions, similar in composition to CAIs, that are also possible candidates for liquid condensates, as they contain glass or have microporphyritic textures that indicate they were once molten (Marvin et al, 1970; Reid et al., 1974; Kurat, 1975; Nagahara and Kushiro, 1982; Grossman et al., 1988; Ireland et al., 1991; MacPherson pers. comm., 1991), but these also lie according to our contours and Berman's model at CaO, MgO, and SiO_2 activities too high to have condensed from a solar gas. The model of Berman (1983) indicates that a liquid

Figure 15. Contours of (a) MgO, (b) Al_2O_3, and (c) SiO_2 activity at 1400°C projected onto the plane anorthite-gehlenite-forsterite. Letters by each bulk composition give the measured activities. TCAN is spinel-saturated within 15°C of this projection and so is considered in the 1400°C data base.

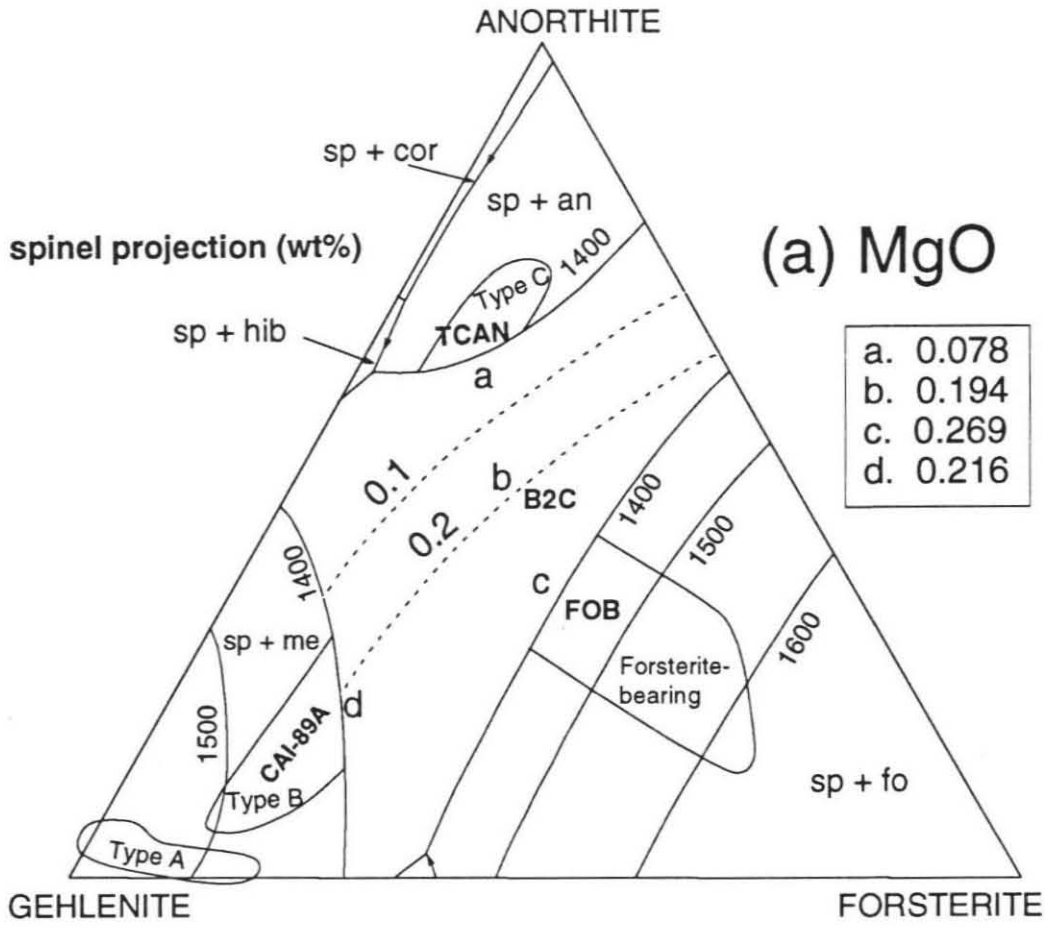
ANORTHITE
sp + cor
sp + an
spinel projection (wt%)
(a) MgO
a. 0.078
b. 0.194
c. 0.269
d. 0.216
sp + hib
Type C
TCAN
1400
a
0.1
b
B2C
0.2
1400
1500
c
FOB
Forsterite-
bearing
1600
1400
sp + me
1500
CAI-89A
d
Type B
Type A
sp + fo
GEHLENITE
FORSTERITE

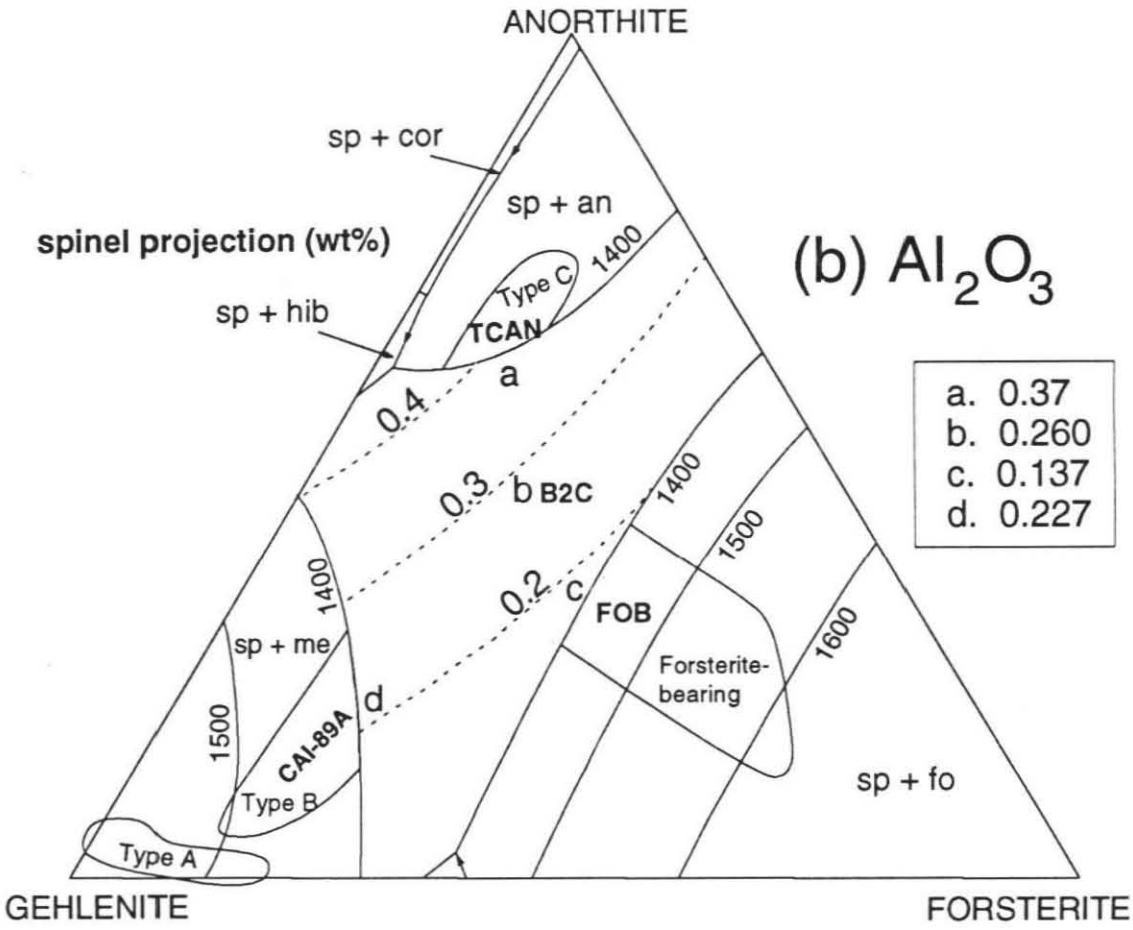
ANORTHITE
sp + cor
sp + an
spinel projection (wt%)
(b) Al_2O_3
sp + hib
Type C
TCAN
1400
a
0.4
0.3
b B2C
1400
1500
0.2
c
FOB
Forsterite-
bearing
1600
sp + me
1400
1500
CAI-89A
d
Type B
Type A
sp + fo
a. 0.37
b. 0.260
c. 0.137
d. 0.227
GEHLENITE
FORSTERITE

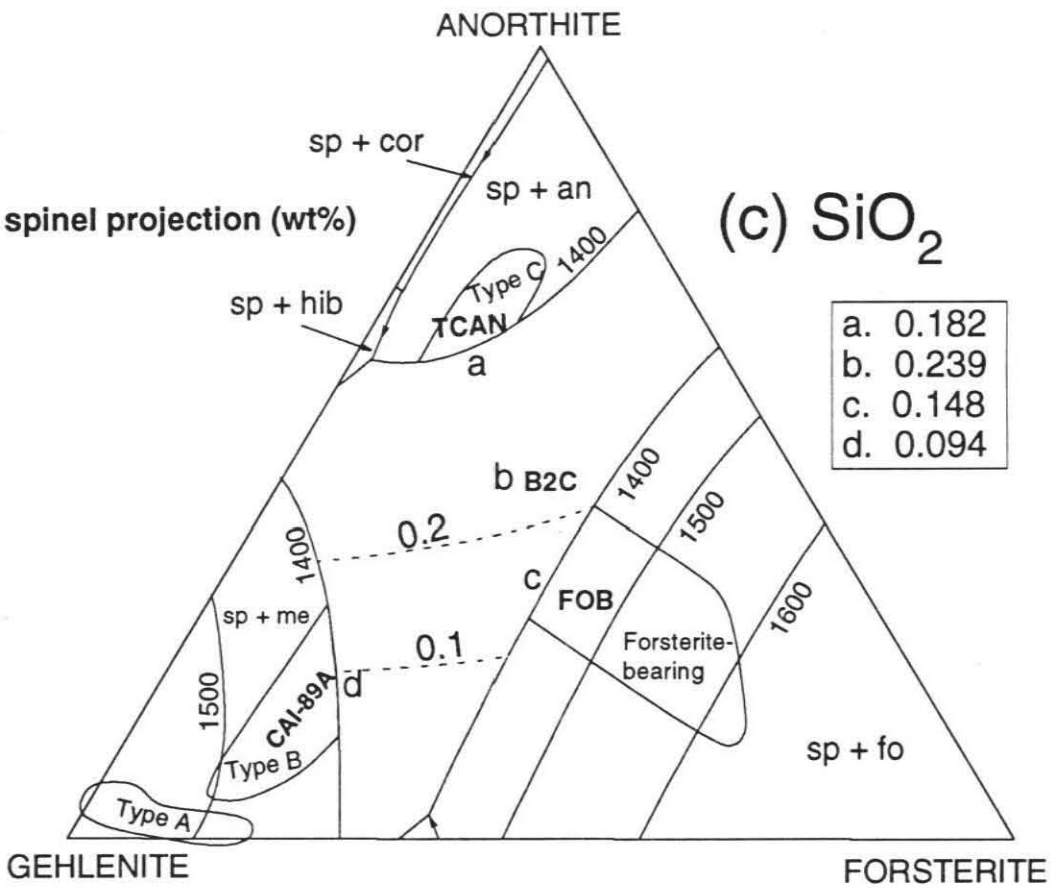
ANORTHITE
sp + cor
sp + an
spinel projection (wt%)
(c) SiO2
sp + hib
Type C
1400
TCAN
a
a. 0.182
b. 0.239
c. 0.148
d. 0.094
b B2C
1400
1500
0.2
1400
c
FOB
sp + me
0.1
Forsterite-
bearing
1600
1500
CAI-89A
d
Type B
sp + fo
Type A
GEHLENITE
FORSTERITE

in which a_{CaO}, a_{MgO}, and a_{SiO_2} are all on the order of 10^{-5} would have to be essentially pure Al_2O_3, a substance unlikely to condense as a liquid in this temperature range because of its high melting point (2054°C; JANAF, 1985). Because the expected partial pressures of key species are so low, it appears unlikely that liquids could have condensed directly from the solar nebula unless there were regions either enriched in Ca, Mg, and Si or several orders of magnitude higher in P_{tot} than 10^{-5} bar.

It is evident that if CAIs melted in a solar gas, they would have been out of thermodynamic equilibrium and should have volatilized Mg, SiO, and to a lesser degree Ca, producing more aluminous compositions. This is a fact of some significance, as many CAIs were at least partially molten at some time in their histories (Stolper, 1982; Stolper and Paque, 1986; MacPherson and Davis, 1993). Some inclusions exhibit enrichment in the heavy isotopes of Mg and Si, namely forsterite-bearing CAIs and FUN inclusions (Wark et al., 1987; Brigham, 1990), but the Mg and Si isotopic systematics of CAIs in general do not unambiguously indicate volatilization (MacPherson et al., 1988; Brigham, 1990), perhaps a reflection of later reequilibration with a reservoir of isotopically light material. The lack of a volatilization signature may also be due to briefness of melting, a factor suggested in some CAIs by the retention of sodium in anorthite (MacPherson and Davis, 1993). However, in certain cases, volatilization may have played a significant role in producing the observed chemical diversity of inclusions in meteorites (Hashimoto, 1983; Hashimoto et al., 1979; Wark et al., 1987).

Summary

Pd-oxide equilibration has been used to measure activities of MgO, Al_2O_3, and SiO_2 in melts in the system CMAST relevant to the formation of CAIs and POIs in carbonaceous chondrites. Five bulk compositions were studied, corresponding to synthetic analogs of Type B, Type C, and forsterite-bearing CAIs and an average Group 2 POI. Measured MgO activities ranged from 0.08 to 0.29, Al_2O_3 activities from 0.15 to 0.32, and SiO_2 activities from 0.09 to 0.61, with precision ranging from 1 to 25%, depending on the magnitude of the activity determined. There are correlated variations between activity coefficient and liquid composition that reflect the thermodynamic effects of changing melt structure. The measured activities are within 10-35% of those calculated using Berman's (1983) model and are therefore generally consistent with known phase equilibria in CMAS, although MgO and Al_2O_3 activities are systematically lower and SiO_2 activities higher than predicted. The ΔG_f°'s of spinel and forsterite from the oxides determined from the measured activities in spinel- and forsterite-saturated melts generally agree with those determined for the pure minerals. The measured activities indicate that the CAI and POI liquids would be out of equilibrium with a gas of solar nebula composition; estimated partial pressures of key species in the solar nebula indicate that only essentially pure Al_2O_3 liquids could have coexisted at equilibrium with such a gas. The experimental data presented here provide important new modeling constraints for silicate liquids that are independent of knowledge of phase equilibria and thermodynamic properties of crystalline phases in CMAS.

Chapter 4. The thermodynamics of spinel-alumina solutions at 1400°C

In this chapter, the technique of Pd-oxide equilibration is used to experimentally determine the activities of MgO and Al_2O_3 across the join $MgAl_2O_4$–$Al_{8/3}O_4$ at 1400°C and 1 bar. The chapter first outlines the complexities of mineral solutions along the join $MgAl_2O_4$–γ-$Al_{8/3}O_4$ and explains the usefulness of the Pd-oxide equilibration technique for studying solid solutions. The experimental procedure for measuring oxide activities in this system is described, and the activities and free energies of formation across the join are reported. The experimentally determined oxide activities are used in calibrating a thermochemical model for aluminous spinels based on Landau theory, and finally the measured activities are used to make inferences about the condensation of magnesium aluminate spinel in the solar nebula.

Solid solution phenomena in spinel

$MgAl_2O_4$, one of the important end-members in the spinel series, exhibits solid solution towards the defect spinel γ-$Al_{8/3}O_4$ (Fig. 16). A number of factors suggest complex behavior on the microscopic level in this solid solution. For example, the end-member $MgAl_2O_4$ manifests temperature-dependent, energetically significant Mg-Al disordering on the tetrahedral and octahedral sites; adding excess alumina to the spinel lattice introduces vacancies whose distribution also affects the energetics. The disorder present in aluminous spinels at high temperature may also be only partially

Figure 16. Phase diagram for the system MgO-Al_2O_3. MgO_{ss} = MgO solid solution, $spinel_{ss}$ = spinel solid solution. After Hallstedt (1992).

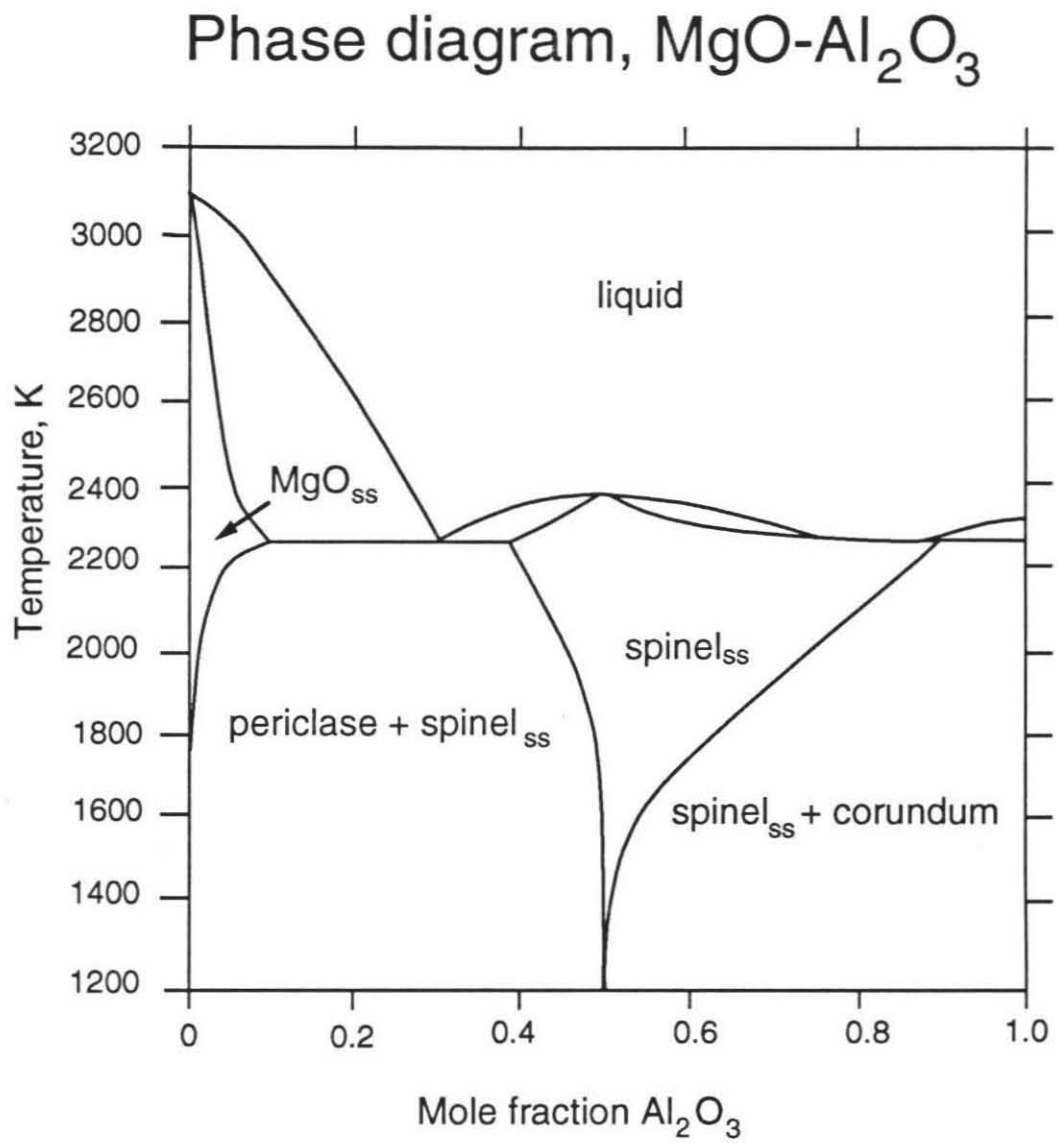
Phase diagram, MgO-Al2O3
Temperature, K
3200
3000
2800
2600
2400
2200
2000
1800
1600
1400
1200
0
0.2
0.4
0.6
0.8
1.0
Mole fraction Al2O3
liquid
MgOss
periclase + spinelss
spinelss
spinelss + corundum

quenchable, as is the case in the $MgAl_2O_4$ end-member (Wood et al., 1986; Millard et al., 1992). In addition, the size mismatch between $MgAl_2O_4$ (a_0 = 0.8085 nm) and γ-$Al_{8/3}O_4$ (a_0 = 0.7905 nm) (Navrotsky et al., 1986) should result in lattice strain in the solid solution. Nonconfigurational effects such as charge coupling or short-range order may also play a role (Navrotsky et al., 1986). It is important to understand how the microscopic factors affect the thermodynamics of the solid solution if spinel is to be included in the calibration of geothermometers and geobarometers.

In order to create a thermodynamic model that can describe macroscopic thermodynamic properties of spinel in terms of its microscopic parameters, one must obtain accurate measurements of equilibrium thermochemical properties in this mineral system. The method of Pd-oxide equilibration is ideal for the study of disordered mineral solutions because it yields direct information on the dependence of free energy on composition and because the measured activities reflect the equilibrium state of order at 1400°C.

Experimental procedure

Sample preparation

Spinel solid solutions were prepared at composition intervals of approximately 0.03 mole fraction of $Al_{8/3}O_4$, from about 0.03 to 0.17 (corundum saturation at 1400°C). Powdered reagent-grade MgO and Al_2O_3 (Alfa Products) were dried overnight at 800°C before weighing. The powders were shaken for 10-15 minutes in ethanol in a SPEX mill, dried, pressed into pellets, and sintered at 1400°C for 48

hours. Mg:Al ratios were determined in the run products by electron microprobe analysis (Table 14). The spinel compositions were powdered and pressed into pellets around 3-4 mm lengths of 0.25 mm-diameter 99.997% pure Pd wire. The pellets were placed in ¼-inch diameter Pd foil buckets. The pure oxide standards were prepared by pressing analytical-grade MgO and Al_2O_3 (JMC Puratronic) around 3-4 mm lengths of pure Pd wire. Before pressing, the initially amorphous Al_2O_3 was converted to corundum (confirmed by XRD) by heating for about 6 hours at 1500°C in a Pt crucible. The Pd + periclase or Pd + corundum pellets were placed in open capsules made from ¼-inch diameter crushable magnesia or alumina rods (Ozark Technical Ceramics) that were drilled out to form open capsules.

Experimental methods

Experiments were conducted in a 1-atmosphere home-built furnace with $MoSi_2$ heating elements. Temperature was controlled to within 1-2°C by a Eurotherm 812 Controller/Programmer and measured by a Type S thermocouple calibrated at the melting point of gold. Stated temperatures are believed accurate to ± 3°C. Oxygen fugacity was set using mixtures of H_2 and CO_2 and measured by an yttria-doped zirconia solid electrolyte oxygen sensor (Ceramic Oxide Fabricators Pty. Ltd., Australia). The sensor was calibrated at the iron-wüstite (IW) buffer at 1200 and 1400°C by measuring changes in the resistance of pure iron wire as f_{O_2} was varied. Drift of the emf of the sensor during a run was typically 1 mV or less.

The samples and standards were suspended from Ir hanging wire and placed adja-

cent to each other in a 1-atmosphere gas-mixing furnace. The f_{O_2} of the experiments was typically an order of magnitude below IW. Experiments were run at 1400°C for 38-52 hours and drop-quenched into deionized water. The pellets were removed from their containers, mounted in epoxy, and rough-polished to expose a length-wise cross section through the Pd wire. The Pd was then fine-polished with diamond paste using an automatic polisher.

Analytical techniques

The Pd alloys were analyzed as described in Chapter 1. Analysis of Mg and Al in the spinel solid solutions was performed at 15 keV, 40°, 10 nA, and 30 s. A stoichiometric Union Carbide $MgAl_2O_4$ laser crystal served as a standard. Signal loss due to the porosity of the spinel pellets resulted in low totals for most samples, but the measured Mg:Al ratios are accurate because the overvoltage is virtually identical for Mg and Al (P. Carpenter, pers. comm.). Several grains from each composition were analyzed; Mg per 4 oxygens varies by 0.5 to 2%, and Al per 4 oxygens varies by 0.1 to 0.6%.

Activities and free energies across the join

Table 14 gives the compositions of the spinel solid solutions as determined by electron microprobe analysis. Table 15 gives experimental run conditions and analyses of Pd alloys equilibrated with each spinel composition. Table 16 gives the experimental activities of MgO relative to periclase and Al_2O_3 relative to corundum (α-Al_2O_3) derived from the concentrations of Mg and Al in the alloys. The free energy expres-

Table 14. Compositions of spinel solid solutions.

Table 14. Compositions of spinel solid solutions[a] (mole fraction).				
run	Mg^{b}	Al^{b}	$MgAl_2O_4$	$Al_{8/3}O_4$
1	1.000 (0.013)	1.996 (0.008)	1.000 (0.013)	0.000 (0.010)
2	1.012 (0.012)	1.991 (0.009)	1.012 (0.012)	0.000 (0.012)
3	0.964 (0.011)	2.024 (0.007)	0.964 (0.011)	0.036 (0.009)
4	0.944 (0.018)	2.037 (0.012)	0.944 (0.018)	0.056 (0.014)
5	0.918 (0.016)	2.055 (0.010)	0.918 (0.016)	0.082 (0.013)
6	0.902 (0.013)	2.065 (0.009)	0.902 (0.013)	0.098 (0.011)
7	0.900 (0.004)	2.067 (0.003)	0.900 (0.004)	0.100 (0.003)
8	0.871 (0.013)	2.086 (0.009)	0.871 (0.013)	0.129 (0.010)
9	0.830 (0.010)	2.114 (0.007)	0.830 (0.010)	0.170 (0.008)

a. Electron microprobe: 15 keV, 10 nA, 30s, standardized on spinel. Numbers in parentheses indicate 1σ errors in the last digits.

b. Cations per 4 oxygens.

Table 15. Experimental data for spinel solid solutions.

Table 15. Experimental data for spinel solid solutions[a]							
run	T (°C)	log f_{O_2}	time (hrs.)	$X_{Mg}^{Pd,spinel}$	$X_{Mg}^{Pd,periclase}$	$X_{Al}^{Pd,spinel}$	$X_{Al}^{Pd,corundum}$
1	1400	-10.170	38	0.00261 (11)	0.00281 (11)	0.00120 (9)	0.00459 (7)
2	1405	-10.836	46	0.00129 (8)	0.00666 (11)	0.00761 (6)	0.01359 (10)
3	1404	-10.915	47	0.00061 (8)	0.00674 (19)	0.01117 (12)	0.01418 (15)
4	1400	-10.893	44	0.00044 (9)	0.00598 (10)	0.00980 (6)	0.01168 (7)
5	1400	-10.893	40	0.00044 (11)	0.00617 (10)	0.01057 (6)	0.01138 (11)
6	1405	-10.860	44	0.00042 (9)	0.00712 (26)	0.01324 (7)	0.01407 (7)
7	1406	-10.734	45	0.00040 (9)	0.00648 (9)	0.01243 (16)	0.01277 (6)
8	1404	-10.842	48	0.00039 (7)	0.00677 (18)	0.01294 (9)	0.01383 (10)
9	1405	-10.836	52	0.00034 (8)	0.00656 (11)	0.01334 (7)	0.01343 (25)

a. Numbers in parentheses indicate 1σ errors in the last digits based on heterogeneity. Temperatures are believed accurate to ± 3°C and f_{O_2}'s to ± 0.05 log units.

Table 16. Derived data for spinel solid solutions.

Table 16. Derived data for spinel solid solutions[a]						
run	T (°C)	a_{MgO}	$a_{Al_2O_3}$	$a_{MgAl_2O_4}$	$a_{Al_{8/3}O_4}$	ΔG_f° (J/mole)
1	1400	0.929 (0.053)	0.068 (0.010)	1.00[b]	0.015 (0.016)	-38418 (1876)
2	1405	0.194 (0.013)	0.314 (0.007)	0.975 (0.156)	0.113 (0.009)	-39242 (310)
3	1404	0.091 (0.012)	0.621 (0.019)	0.905 (0.179)	0.281 (0.025)	-38940 (1138)
4	1400	0.074 (0.015)	0.704 (0.012)	0.836 (0.208)	0.330 (0.027)	-39162 (1973)
5	1400	0.071 (0.018)	0.863 (0.020)	0.984 (0.288)	0.433 (0.036)	-35882 (3032)
6	1405	0.059 (0.013)	0.885 (0.012)	0.836 (0.220)	0.451 (0.036)	-37316 (2710)
7	1406	0.062 (0.014)	0.947 (0.026)	0.939 (0.253)	0.494 (0.042)	-35721 (2981)
8	1404	0.057 (0.011)	0.875 (0.018)	0.802 (0.193)	0.444 (0.037)	-36732 (2342)
9	1405	0.052 (0.012)	0.987 (0.038)	0.826 (0.228)	0.522 (0.049)	-34428 (3176)

a. Numbers in parentheses indicate 1σ errors in the last digits from propagation of errors based on heterogeneity. Temperatures are believed accurate to ± 3°C and f_{O_2}'s to ± 0.05 log units.

b. Standard state is defined as pure stoichiometric spinel.

sions of Chapter 2 for $MgAl_2O_4$ and Navrotsky et al. (1986) for γ-$Al_{8/3}O_4$ were used to convert to activities of $MgAl_2O_4$ and γ-$Al_{8/3}O_4$ (Table 16) using the reactions:

$$4/3\ Al_2O_{3(\alpha)} = Al_{8/3}O_{4(\gamma)}\ , \tag{1a}$$

with

$$a_\gamma = a_\alpha^{4/3} \exp\left[\frac{-\Delta G_1^\circ}{RT}\right]\ , \tag{1b}$$

and

$$MgO_{(periclase)} + Al_2O_{3(\alpha)} = MgAl_2O_{4(spinel)}\ , \tag{2a}$$

with

$$a_{MgAl_2O_4} = a_\alpha\ a_{MgO} \exp\left[\frac{-\Delta G_2^\circ}{RT}\right]\ , \tag{2b}$$

where a_γ is the activity of γ-$Al_{8/3}O_4$, a_α is the activity of corundum, ΔG_1° is the free energy of reaction (1a), R is the gas constant, T is temperature, $a_{MgAl_2O_4}$ is the activity of $MgAl_2O_4$, a_{MgO} is the activity of periclase, and ΔG_2° is the free energy of reaction (2a). The activities of $MgAl_2O_4$ and γ-$Al_{8/3}O_4$ are plotted as a function of mole fraction of $Al_{8/3}O_4$ in Fig. 17. The compositional dependence of the free energy of formation of spinel, ΔG_f°, was also calculated through the reaction:

$$i\,MgO_{(periclase)} + j/2\ Al_2O_{3(\alpha)} = Mg_i\,Al_j\,O_{4(spinel)}\ , \tag{3}$$

with

$$\Delta G_f^\circ = -RT \ln \frac{1}{a_{MgO}^{i}\ a_\alpha^{j/2}} \tag{4}$$

Figure 17. Experimental activities of $MgAl_2O_4$ and γ-$Al_{8/3}O_4$ versus mole fraction of $Al_{8/3}O_4$ in spinel solid solution. Circles are $MgAl_2O_4$ activities, and squares are γ-$Al_{8/3}O_4$ activities. 1σ error bars from propagation of errors based on heterogeneity.

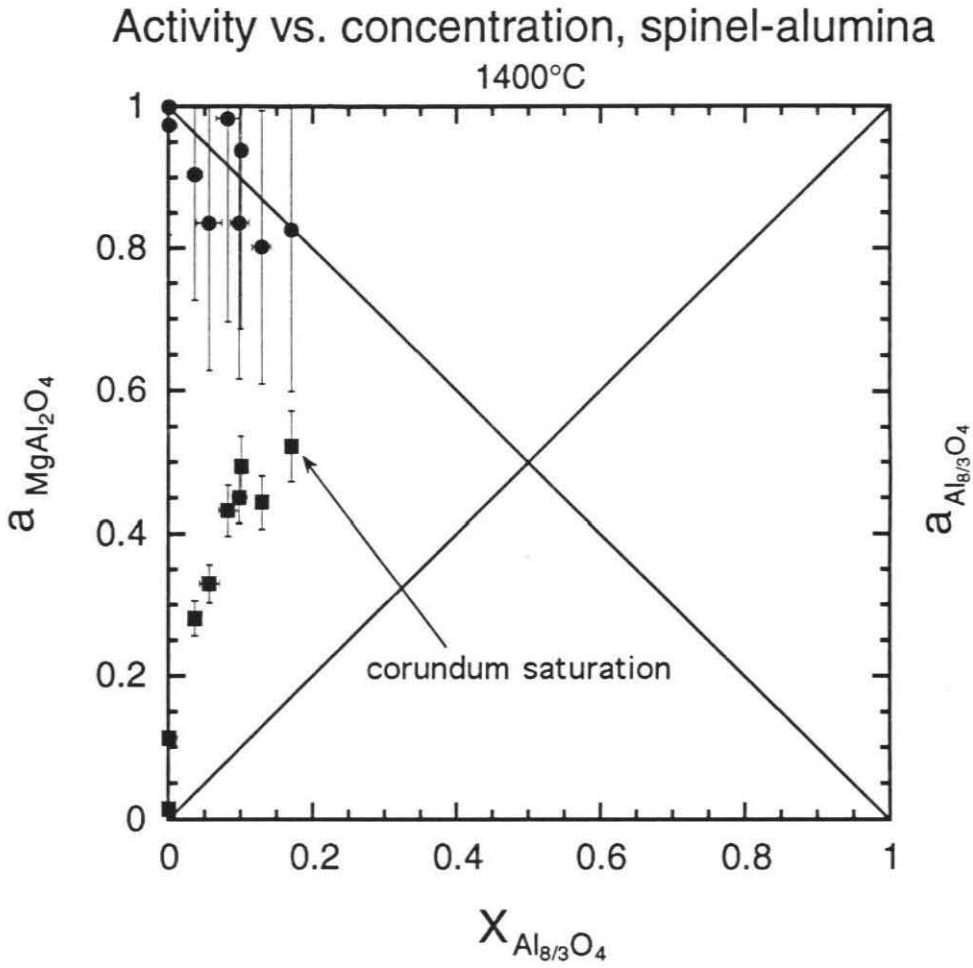
Activity vs. concentration, spinel-alumina
1400°C
1
0.8
0.6
0.4
0.2
0
0
0.2
0.4
0.6
0.8
1
a MgAl2O4
a Al8/3O4
X Al8/3O4
corundum saturation

where i is Mg per 4 oxygens, j is Al per 4 oxygens (Table 14), and $a^{spinel}_{Mg_i Al_j O_4} \equiv 1$. The results are shown in Table 16 and Fig. 18.

Several features of the thermochemistry of aluminous spinels are evident in Fig. 17. First, the activities of γ-$Al_{8/3}O_4$ exhibit a strong positive deviation from ideality, whereas the activities of $MgAl_2O_4$ appear closer to Raoultian. In addition, the errors on the activities of γ-$Al_{8/3}O_4$ are only about 8% (except in the stoichiometric mineral, where the error is higher), while those on the $MgAl_2O_4$ activities are much higher, 20-40%. The errors on a_γ are low because the activity of Al_2O_3 rapidly approaches one as alumina is added to the spinel lattice and Al concentrations in the Pd alloys are consequently high. In contrast, MgO activities drop rapidly to less than 0.1 as alumina content increases, and Mg contents in the alloys likewise drop considerably. The significant background correction for Mg in Pd makes it particularly difficult to determine these low MgO activities precisely. Fig. 18 shows that there is a slight increase in ΔG_f° with increasing alumina content, with ΔG_f° being about 4 kJ/mole higher at corundum saturation than in stoichiometric $MgAl_2O_4$. The correlation seems well-defined in spite of the scatter and large error bars, which are attributable to the uncertainties on the values of a_{MgO}.

Thermodynamic model

A microscopically consistent description of the thermodynamic properties of $MgAl_2O_4$–γ-$Al_{8/3}O_4$ solutions must be able to incorporate effects due to the distribution of cations and vacancies and a lattice size mismatch. It is difficult to produce an

Figure 18. ΔG_f° of spinel from the oxides versus mole fraction of $Al_{8/3}O_4$. 1σ error bars from propagation of errors based on heterogeneity. Curve is the predicted ΔG_f° based on the model discussed in the text (see Eqn. 24).

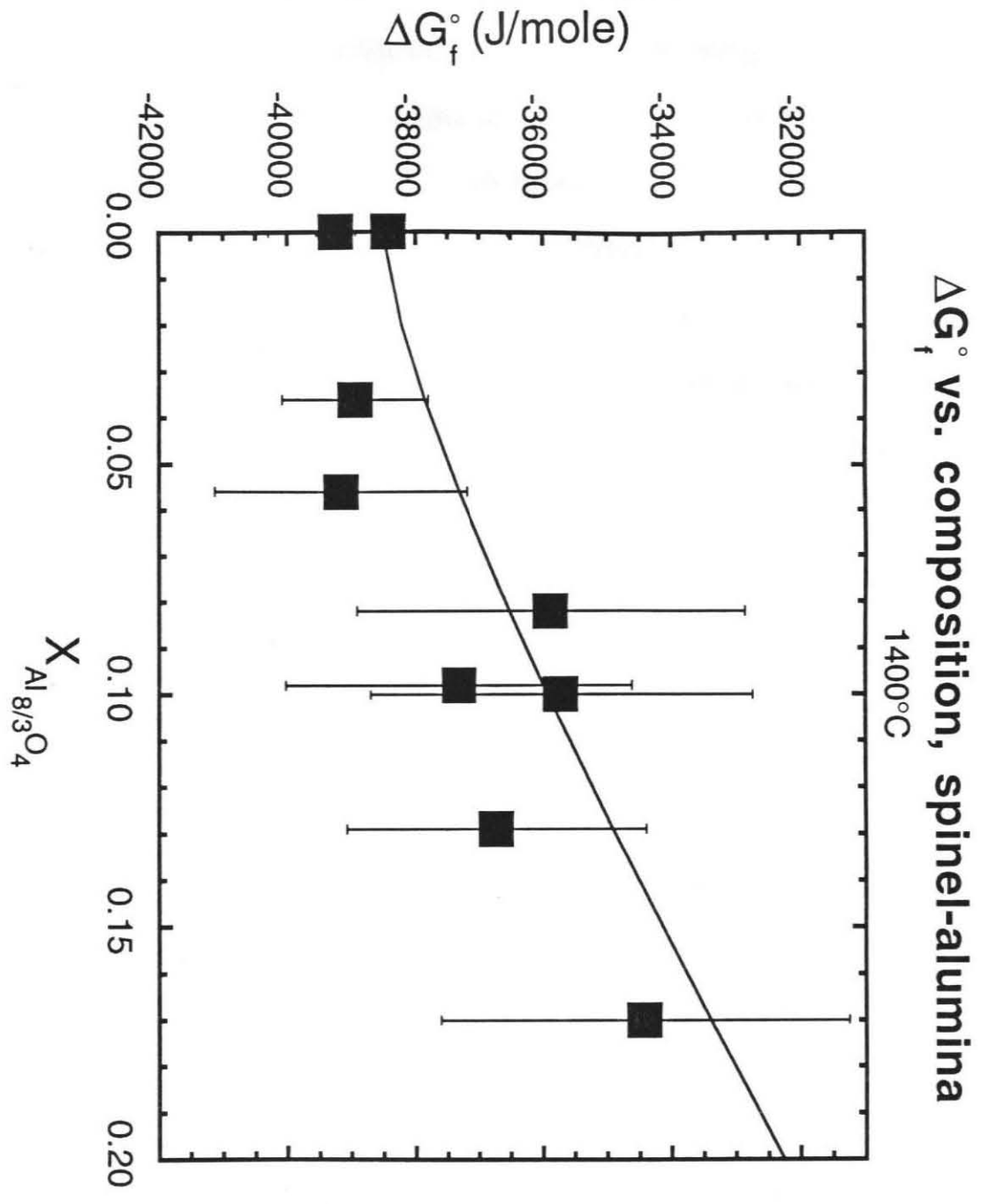
ΔG_f° vs. composition, spinel-alumina
1400°C
ΔG_f° (J/mole)
-32000
-34000
-36000
-38000
-40000
-42000
0.00
0.05
0.10
0.15
0.20
$X_{Al_{8/3}O_4}$

accurate description of aluminous spinels because the data base on site occupancies is inadequate to support detailed structural models. However, if the site occupancies can be estimated, one can use Landau theory (Carpenter et al., 1993a,b) to construct a simple model for excess-alumina spinels at 1400°C that incorporates measured oxide activities, calorimetric data, and structural information. Landau theory, which is normally used to describe the thermodynamics of phase transitions in minerals, can be applied to non-convergent ordering (where no transition occurs) if a term linear in the order parameter Q is included in the free energy of ordering expression. For non-convergent ordering at constant P, the free energy of ordering in an end-member mineral from a completely disordered (random) to an equilibrium state, G_{ord}, is given by (Carpenter et al., 1993a):

$$G_{ord} = -hQ + \tfrac{1}{2}a\,(T - T_c)Q^2 + e_n/nQ^n \qquad (5)$$

where h, a (italicized to distinguish it from activity), T_c, n, and e_n are constants. The entropy due to ordering, S_{ord}, is therefore equal to:

$$S_{ord} = -\tfrac{1}{2}a\,Q^2\ . \qquad (6)$$

The free energy of mixing of a mineral solution with an equilibrium state of order, $\Delta G_{mix,o}$, is given by (Carpenter et al., 1993b):

$$\Delta G_{mix,o} = \Delta H_{mix,o} + T(\tfrac{1}{2}a\,Q^2 - \Delta S_{mix,d}) \qquad (7)$$

where $\Delta H_{mix,o}$ is the enthalpy of mixing of the mineral solution with equilibrium order, $\Delta S_{mix,d}$ is the configurational entropy of mixing for the completely disordered mineral solution, the quantity $-\tfrac{1}{2}a\,Q^2 + \Delta S_{mix,d}$ is equal to the total entropy of mixing $\Delta S_{mix,o}$,

and a is now a function of composition.

The enthalpy of mixing has been measured by Navrotsky et al. (1986) at 975 K in compositions along the two-phase boundary between spinel solid solution and corundum. They obtained negative heats of mixing, described by the regular solution formulation (where for simplicity the mole fraction of $Al_{8/3}O_4$ in solution is referred to as x):

$$\Delta H_{mix,o} = -16573x(1-x) \qquad \text{(J/mole)} . \tag{8}$$

They also determined by transposed-temperature drop calorimetry that no energetically significant reordering takes place in the solid solution upon annealing, unlike in end-member $MgAl_2O_4$.

The order parameter Q in the solid solution is currently unknown, as there are at present no comprehensive measurements of cation and vacancy occupancy in this system. However, the work of Jagodzinski and Saalfeld (1958) and Basso et al. (1991) suggest that vacancies prefer the octahedral site in Mg-Al spinels. If one assumes that vacancies are confined to the octahedral sites for all bulk compositions and that the vacancies are randomly distributed on these sites, then the distribution of vacancies in the lattice contributes nothing to the entropy of ordering because it is the same in the ordered and disordered states. The disordered mineral then has the distribution $Mg_{1/3(1-x)}Al_{1/3(2+x)}[Mg_{2/3(1-x)}Al_{1/3(4+x)}\square_{x/3}]O_4$, where $\square$ represents a vacancy and brackets enclose the cations on octahedral sites, and the cation disorder in the solid solution can be described using the one order parameter:

$$Q = \left[\frac{-3}{2+x}\right] x_{Al}^{tet} + 1 \ , \qquad (9)$$

where x_{Al}^{tet} is the mole fraction of Al on the tetrahedral site. This compositionally dependent expression for Q reduces at x = 0 to that given for stoichiometric $MgAl_2O_4$ by Carpenter et al. (1993b) (see also Chapter 2).

The end-member mixing components are chosen as $Mg_{0.55}Al_{0.45}[Mg_{0.45}Al_{1.55}]O_4$, the predicted equilibrium state of order in $MgAl_2O_4$ at 1400°C from neutron activation measurements (Peterson et al., 1992 via Carpenter et al., 1993b), and $Al[Al_{5/3}\square_{1/3}]O_4$. It is not strictly true that vacancies are confined to octahedral sites in γ-$Al_{8/3}O_4$, where vacancies are thought to prefer tetrahedral sites (Jayaram and Levi, 1989), but this assumption is made for simplicity in the model. If vacancies are located on both sites, then two order parameters would be needed to describe the solid solution, an approach more complicated than is justified by current knowledge of site occupancies. One then has the mixing reaction:

$$\begin{aligned} &xAl[Al_{5/3}\square_{1/3}]O_4 + (1-x)Mg_{0.55}Al_{0.45}[Mg_{0.45}Al_{1.55}]O_4 \\ &\quad = Mg_{0.55(1-x)}Al_{0.45+0.55x}[Mg_{0.45(1-x)}Al_{1.55(1-x)+5x/3}\square_{x/3}]O_4 \end{aligned} \qquad (10)$$

and the order parameter:

$$Q = \frac{-3}{2+x}(0.45 + 0.55x) + 1 \ . \qquad (11)$$

Here it is assumed that the ratio of tetrahedral to octahedral Mg is constant at 1400°C across the join because there are no measurements of cation site occupancy in the solid solution. The configurational entropy of the disordered solid solution is given by:

$$S_{conf,d} = -R[1/3(1-x)\ \ln\ 1/3(1-x) + 1/3(2+x)\ \ln\ 1/3(2+x) + 2/3(1-x)\ \ln\ 1/3(1-x) + 1/3(4+x)\ \ln 1/6(4+x) + x/3\ \ln\ x/6]\ , \quad (12)$$

and the configurational entropies of the end members are:

$$S_{conf}(Mg_{0.55}Al_{0.45}[Mg_{0.45}Al_{1.55}]O_4) = 14.587 \quad (13)$$

and

$$S_{conf}(Al[Al_{5/3}\square_{1/3}) = 7.492\ . \quad (14)$$

Therefore:

$$\Delta S_{mix,d} = S_{conf,d} - 7.492x - 14.587(1-x)\ . \quad (15)$$

Substituting Eqns. (8), (10), (12), and (15) into (7) leads to (with T = 1673 K):

$$\Delta G_{mix,o} = -16573x(1-x) + \tfrac{1}{2}\ 1673\ a(x)\left[\frac{-3}{2+x}(0.45 + 0.55x) + 1\right]^2 - 1673\Delta S_{mix,d}\ . \quad (16)$$

The functional dependence of a on x is not known, but a suitable approximation can be chosen by examining a plot of $a(x)$ versus x. Rearranging (16), one may determine $a(x)$ at each x through the relation:

$$a(x) = [\Delta G_{mix,o} + 16573x(1-x) + 1673\Delta S_{mix,d}]/\{(\tfrac{1}{2}\ 1673)\left[\frac{-3}{2+x}(0.45 + 0.55x) + 1\right]^2\}\ , \quad (17)$$

where $\Delta G_{mix,o}$ is obtained from our measurements of a_γ and $a_{MgAl_2O_4}$ using the relation:

$$\Delta G_{mix,o} = RT[x\ \ln\ a_\gamma + (1-x)\ln\ a_{MgAl_2O_4}]\ . \quad (18)$$

These calculated values are plotted against x in Fig. 19. An excellent empirical

Figure 19. Plot of Landau coefficient *a(x)* (Eqn. 17) versus x for the experimental compositions, showing that a second-order polynomial provides an excellent approximation to the relationship between *a(x)* and x. The best-fit curve (Kaleidagraph, Abelbeck Software) is for illustrative purposes only and is not used in the model in the text. R is the linear correlation coefficient.

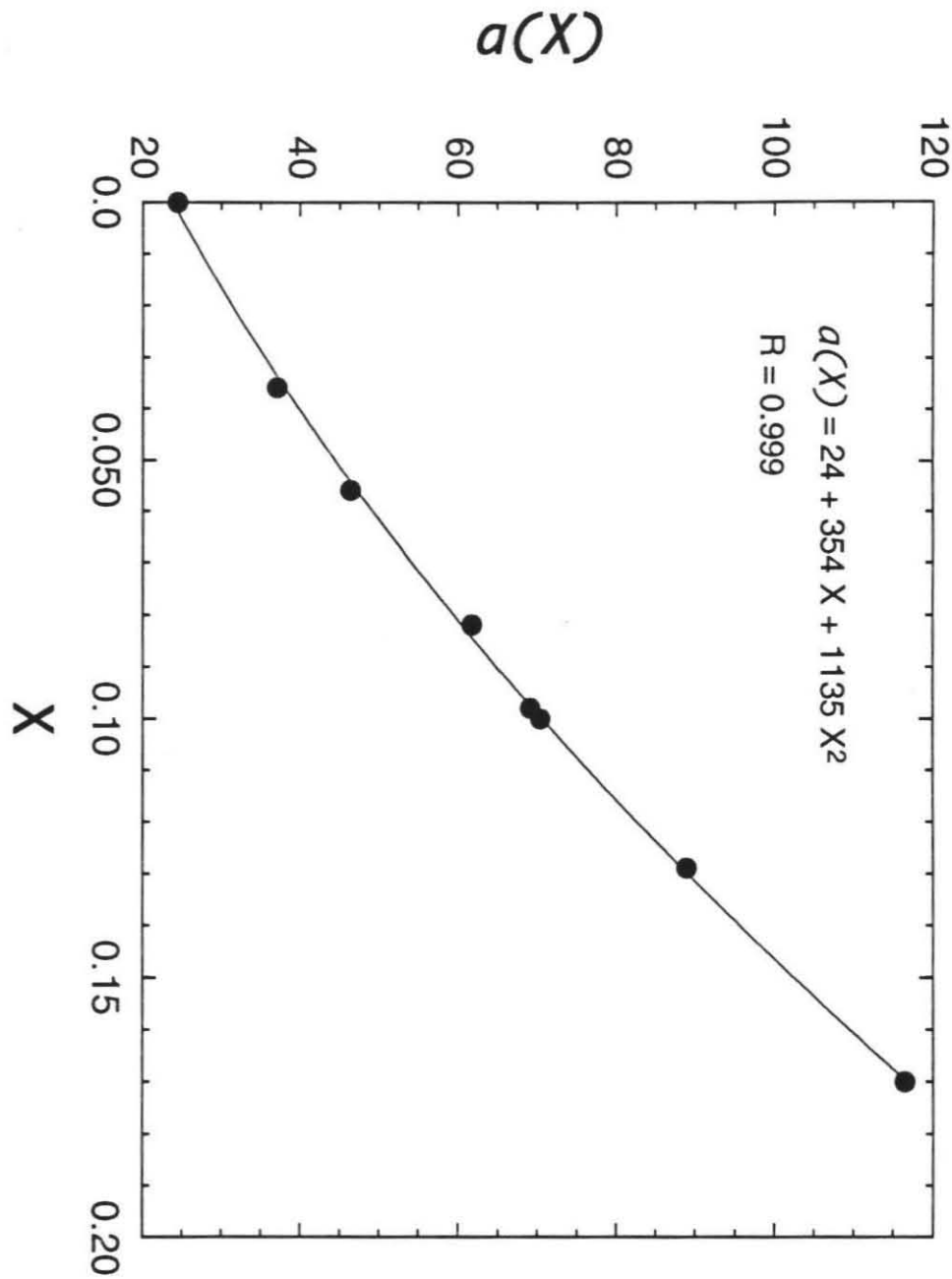
a(X) vs. X (Eqn. 17)
a(X)
X
a(X) = 24 + 354 X + 1135 X²
R = 0.999
120
100
80
60
40
20
0.0
0.050
0.10
0.15
0.20

description of the dependence of a on x is provided by a second-order polynomial with intercept:

$$a(x=0) = \frac{2\Delta S_{mix,d}(x=0)}{Q^2(x=0)} \ . \qquad (19)$$

This is equal in the model to 24.4, a value within error of the a parameter found by Carpenter et al. (1993b) for stoichiometric $MgAl_2O_4$ (19.7 ± 11.6). It is therefore assumed that $a(x)$ has the form:

$$a(x) = 24.4 + bx + cx^2 \qquad (20)$$

where b and c are constants.

From simple graphical principles, it is known that:

$$RT \ln a_\gamma = \Delta\mu_\gamma = \Delta G_{mix,o} + \frac{\partial \Delta G_{mix,o}}{\partial x}(1-x) \ , \qquad (21)$$

where $\Delta\mu_\gamma$ is the difference in chemical potential of γ-$Al_{8/3}O_4$ between the spinel solution and pure γ-$Al_{8/3}O_4$. Combining Eqns. (16), (17), and (21), the activity data can be fit for the parameters b and c through linear regression. This gives the values (Kaleidagraph, Abelbeck Software) b = 299.5 ± 3.3 and c = 1114.7 ± 7.8. The fit is excellent and is shown in Fig. 20, with values for the activities of $MgAl_2O_4$ calculated from:

$$RT \ln a_{MgAl_2O_4} = \Delta G_{mix,o} - \frac{\partial \Delta G_{mix,o}}{\partial x} x \ . \qquad (22)$$

Plots of $\Delta G_{mix,o}$, $\Delta H_{mix,o}$, and $\Delta S_{mix,o}$ are shown in Figs. 21 and 22. The configura-

Figure 20. Activities of $MgAl_2O_4$ and γ-$Al_{8/3}O_4$ versus mole fraction of $Al_{8/3}O_4$, showing fit to activity model discussed in text. Solid lines show regions of stable solid solution and dashed lines show model extension into metastable and unstable regions.

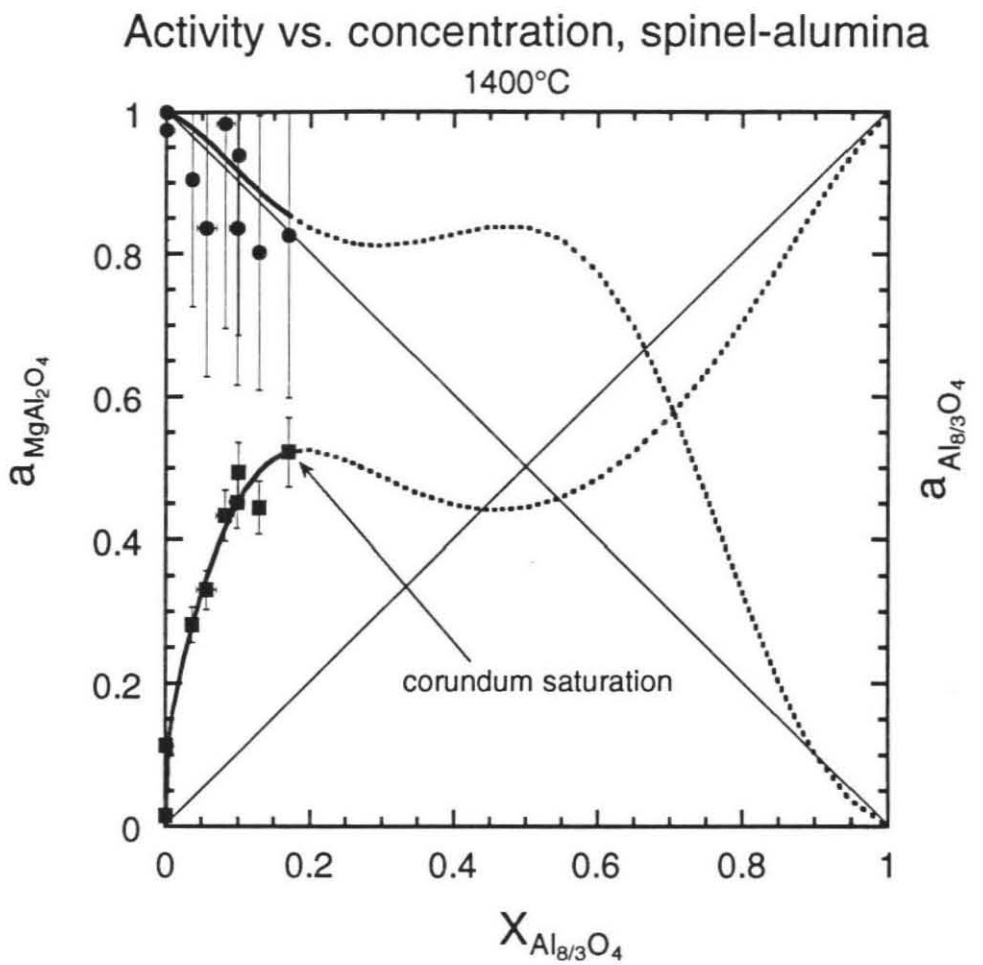
Activity vs. concentration, spinel-alumina
1400°C
1
0.8
0.6
0.4
0.2
0
0
0.2
0.4
0.6
0.8
1
$a_{MgAl_2O_4}$
$a_{Al_{8/3}O_4}$
$X_{Al_{8/3}O_4}$
corundum saturation

Figure 21. $\Delta G_{mix,o}$ (Eqn. 16) and $\Delta H_{mix,o}$ (Eqn. 8) versus mole fraction of $Al_{8/3}O_4$. The two curves are very similar in the region of stable solid solution ($x \leq 0.17$), implying the entropy of mixing is close to zero. The inflection in $\Delta G_{mix,o}$ between $x \sim 0.2$ and $x \sim 0.5$ implies that unmixing into Mg- and Al-rich phases would occur if not for the intervention of the stability field of spinel + corundum.

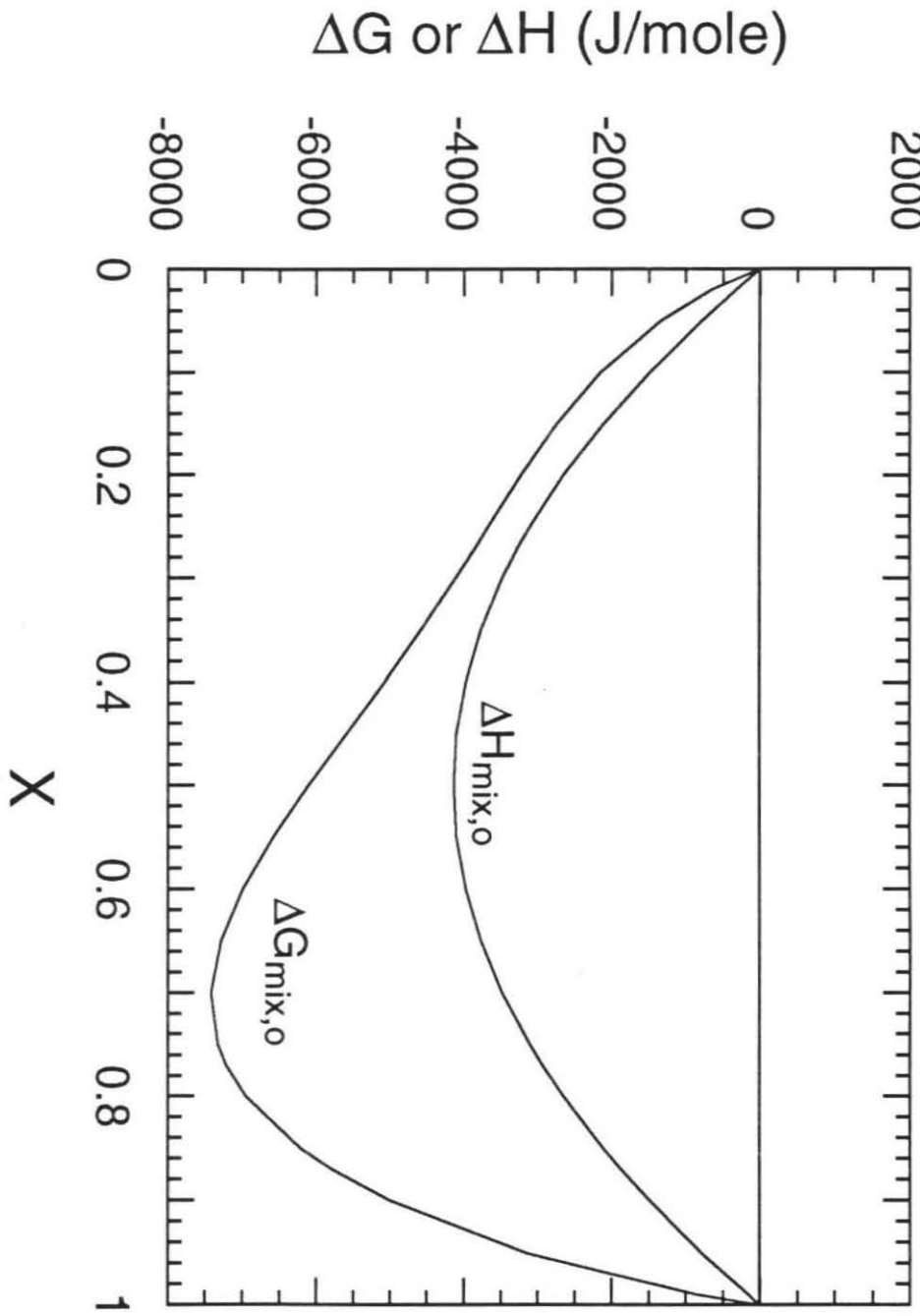
ΔG and ΔH of mixing, spinel-alumina
1400°C
ΔG or ΔH (J/mole)
2000
0
-2000
-4000
-6000
-8000
0
0.2
0.4
0.6
0.8
1
X
ΔH mix,o
ΔG mix,o

Figure 22. Entropy of mixing in spinel solid solution as a function of x. $\Delta S_{mix,o(conf)}$ is the configurational entropy of mixing (Eqn. 23), $\Delta S_{mix,o}$ is the total entropy of mixing of the crystal with equilibrium order (Eqn. 4 + Eqn. 10), and ΔS_{xs} is the excess entropy of mixing $\Delta S_{mix,o} - \Delta S_{mix,o(conf)}$. ΔS_{xs} is negative, indicating a tendency toward short-range order in the solid solution.

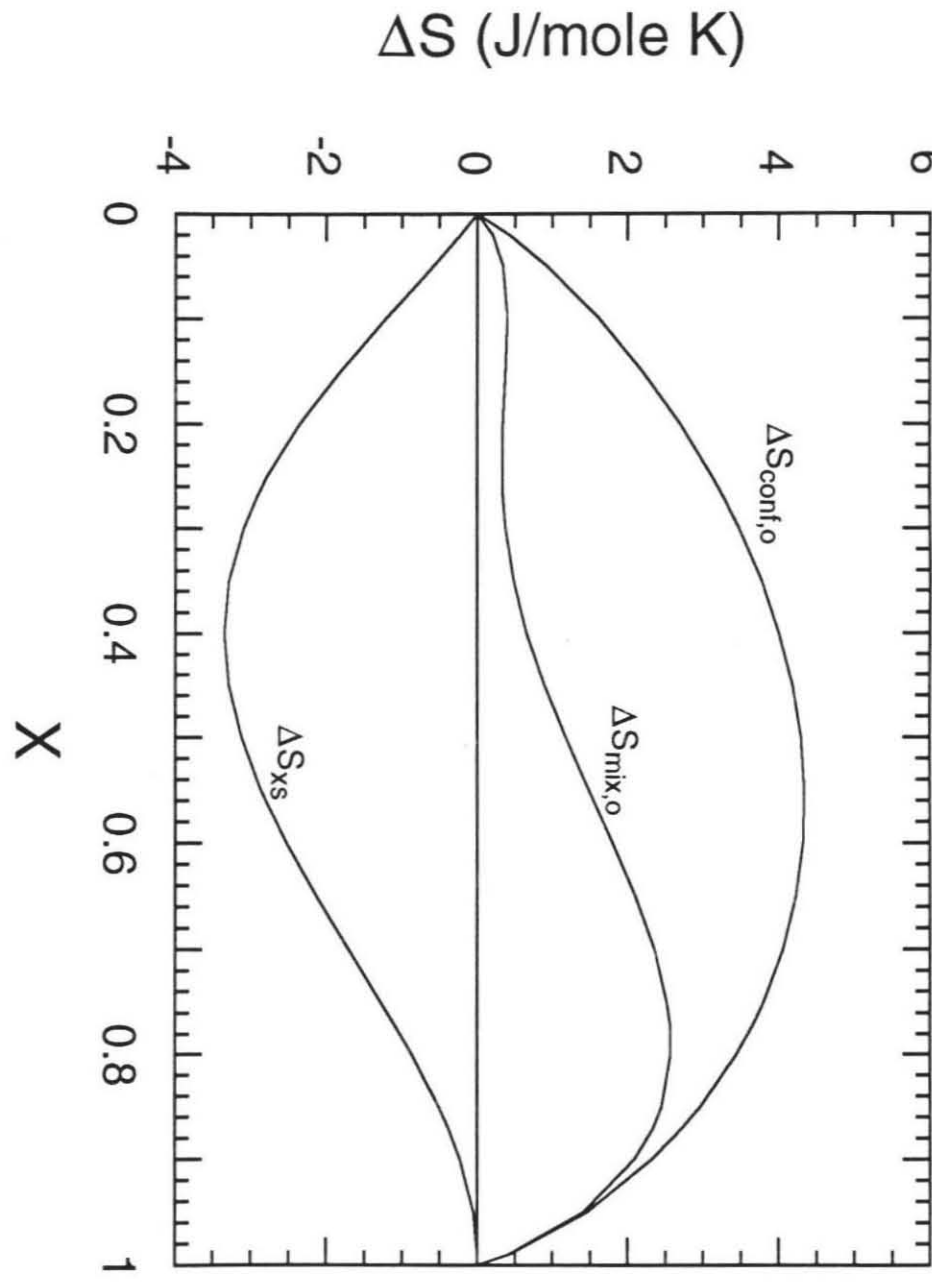
ΔS of mixing vs. X, spinel-alumina
1400°C
ΔS (J/mole K)
6
4
2
0
-2
-4
0
0.2
0.4
0.6
0.8
1
X
ΔSconf,o
ΔSmix,o
ΔSxs

tional entropy of mixing of the ordered solid solution in our model is given by:

$$\Delta S_{mix,o(conf)} = -R\{0.55(1-x)\ \ln\ 0.55(1-x) + (0.45+0.55x)\ \ln\ (0.45+0.55x) \quad (23)$$
$$+ 0.45(1-x)\ \ln\ 0.225(1-x) + [1.55(1-x)+5x/3]\ \ln\ [0.775(1-x)+5x/6]$$
$$+ x/3\ \ln\ x/6\} - 7.492x - 14.587(1-x)$$

and is also shown in Fig. 22 along with ΔS_{xs}, the excess entropy of mixing given by $\Delta S_{mix,o} - \Delta S_{mix,o(conf)}$. Predicted values of ΔG_f° for the spinel solutions are given by the curve in Fig. 18, calculated from (c.f. Eqns. 1b and 2b):

$$\Delta G_f^\circ = \Delta G_{mix,o} + (1-x)\Delta G_2^\circ + x\Delta G_1^\circ \ . \quad (24)$$

The cation and vacancy distributions adopted for the solid solution are of course only speculative, so some of the implications of the model may be incorrect in detail. However, some of the broader conclusions to be drawn about the thermodynamics of the spinel solution are independent of the assumed cation and vacancy distributions. As shown in Fig. 20, $\Delta G_{mix,o}$ and $\Delta H_{mix,o}$ are very similar in magnitude in the region $x < 0.3$, indicating that $\Delta S_{mix,o}$ is close to zero in the stable solid solution. This conclusion stems directly from the measured activities (Eqn. 18) and enthalpies of mixing (Eqn. 8) rather than the assumed distributions. As demonstrated by Navrotsky et al. (1986), no purely configurational entropy model based on the components $Al_{8/3}O_4$ and $MgAl_2O_4$ can account for such low entropies, indicating that nonconfigurational effects play an important role. It is likely therefore that the short-range order inferred by Carpenter et al. (1993) in the $MgAl_2O_4$ end-member persists into the excess-alumina spinels. The nature of this short-range order is difficult to explore without the benefit of actual measurements of site occupancies, but could be related to the association of

Al^{3+} and vacancies or tetrahedral Al^{3+} with neighboring octahedral Mg^{2+} and vice versa. In any case, the solid solution is evidently stabilized by a negative $\Delta H_{mix,o}$ associated with the formation of a very ordered structure rather than by a significant $\Delta S_{mix,o}$, a conclusion also reached by Navrotsky et al. (1986).

Necessarily more model-dependent are inferences about the energetics of the metastable region. According to the model, there are inflections in the $\Delta G_{mix,o}$ curve between x ~ 0.2 and ~ 0.5 that indicate that there would be a solvus in the $MgAl_2O_4$–γ-$Al_{8/3}O_4$ system were it not for the intervention of the spinel + corundum stability field at x = 0.17. Figs. 19 and 20 indicate that the spinel solution on the Al-rich side of the solvus would be stabilized by entropy considerations, in contrast to the Mg-rich stable solid solution. This suggests that the short-range order characteristic of the stable spinel solution may be associated with Mg-Al interactions, which become minimized as Mg decreases. Although it is probable that there is indeed a metastable solvus in this system because of the increase in ΔG_f° with increasing alumina content (Fig. 18), its location and the microscopic nature of the Al-rich solid solution will depend on the actual site occupancies. Fig. 23 shows schematically how the free energy curves for the various phases in MgO–Al_2O_3 are expected to lie relative to one another based on the phase relations and measured thermodynamic properties.

The model presented in this chapter can be contrasted with that of Eriksson et al. (1993), who optimized thermodynamic properties of the various phases in the system MgO-Al_2O_3 based on phase equilibria and the measured thermodynamic properties of selected mineral end-members. They chose a simple regular solution model to des-

Figure 23. Schematic illustration of the molar free energy $\overline{G}$ at ~ 1400°C as a function of composition for the system $MgO\text{-}Al_2O_3$. The stable phase assemblage at any bulk composition is the one with the lowest free energy, given by the tangent to the $\overline{G}$ curves. Between A and B, the stable assemblage is periclase plus stoichiometric $MgAl_2O_4$ spinel; between B and C, it is spinel solid solution; between C and D it is spinel solid solution of composition C plus corundum.

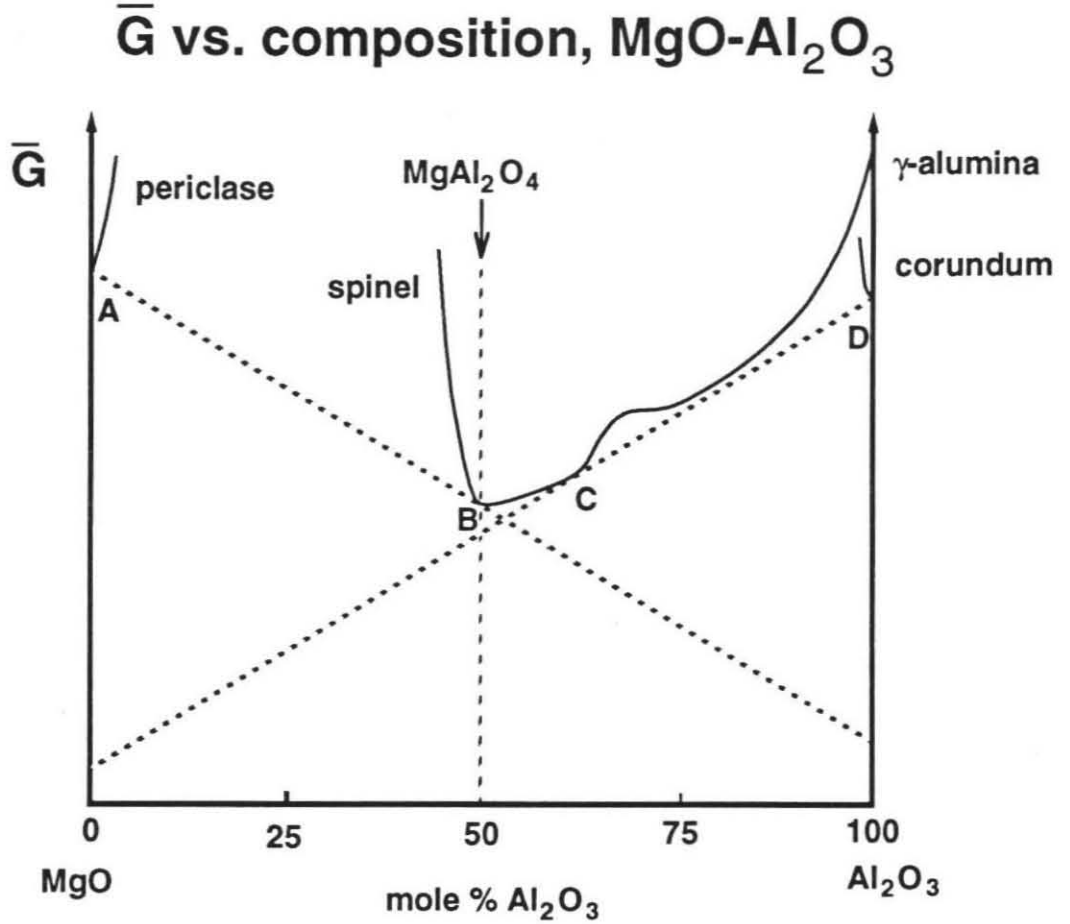
$\overline{G}$ vs. composition, MgO-Al_2O_3
$\overline{G}$
periclase
$MgAl_2O_4$
spinel
γ-alumina
corundum
A
B
C
D
0
25
50
75
100
MgO
mole % Al_2O_3
Al_2O_3

cribe excess-alumina spinel based on the components $MgAl_2O_4$ and Al_8O_{12} (γ-alumina) with no regard for either cation or vacancy distribution. This regular solution model fits the experimental activities of γ-$Al_{8/3}O_4$ in this study well at mole fractions of $Al_{8/3}O_4$ less than or equal to 0.074 but underestimates the experimental values by 6% at corundum saturation. Although this model may describe the data fairly well, it provides an inadequate description of the thermodynamics of the solid solution because it does not take into account the complex behavior at the microscopic level. Eriksson et al. (1993) reproduce the observed near-zero entropy of mixing simply by choosing a large molecule for γ-alumina, thereby minimizing the mole fraction of excess alumina and the configurational entropy. So although the model may reproduce the data adequately, it offers no insight into the energetics of cation or defect distribution or the possibility of interactions between the species. It is therefore ultimately less likely to be useful for extrapolation to higher pressure or more complex composition than a model based on a microscopic understanding of the spinel.

Finally, although the common convention of modeling excess-alumina spinels with γ-$Al_{8/3}O_4$ as one of the end-members has been followed, it may be more proper to choose σ-$Al_{8/3}O_4$, a newly-discovered cubic alumina phase (Guse and Saalfeld, 1990). This approach would have advantages in that σ-$Al_{8/3}O_4$ is truly cubic, as opposed to γ-$Al_{8/3}O_4$, which is actually tetragonal (Navrotsky et al. 1986), and the vacancies in σ-$Al_{8/3}O_4$ are believed to be octahedral as was assumed in the model. However, no one has yet measured the thermodynamic properties of σ-$Al_{8/3}O_4$, so it cannot be used as an end-member. Although the model will require refinement when

measurements of Q and the thermodynamic properties of σ-$Al_{8/3}O_4$ become available, it is nevertheless possible to create a plausible working model for this complex mineral solution that incorporates available thermodynamic data and information on the microscopic structure.

Mg-Al spinel in meteorites

Pure magnesium aluminate spinel is rare in terrestrial environments but is a common constituent of calcium-aluminum-rich inclusions (CAIs) in carbonaceous chondrites. CAIs are mm- to cm-sized mineral aggregates that have long been interpreted to contain high-temperature material produced during the very first stages of solid condensation of the solar nebula (Grossman, 1972; 1973). Understanding of the phase assemblage in CAIs may shed light on the nature and variety of early solar system processes.

The spinels reported in CAIs are often described as stoichiometric $MgAl_2O_4$, but excess-alumina spinel has been reported in the rimming sequence of a CAI from CM2 chondrite Essebi (El Goresy et al., 1984). The mole fraction of excess $Al_{8/3}O_4$ in these spinels ranges from 0.01 to 0.097, with the majority at around 0.035. There is no corundum present in the CAIs, but the point of corundum saturation may be used to estimate minimum temperatures of formation of these spinels. These minimum temperatures range from about 1400 K at x = 0.01 to about 1600 K at x = 0.1, with most being formed at 1450 K or higher (c.f. Navrotsky et al., 1986; Hallstedt, 1992).

It has been suggested that excess alumina in solid solution will raise the conden-

sation temperature of spinel (El Goresy et al., 1984). This is a matter of some importance, as condensation calculations place the formation of melilite at about 100 K above that of spinel, but petrographic considerations occasionally imply that spinel formed first (MacPherson and Grossman, 1984). Based on its free energy of formation, stoichiometric $MgAl_2O_4$ is thought to condense at about 1470 K (L. Grossman, 1993, pers. comm.). According to Fig. 18, the ΔG_f° of spinel increases with alumina content, indicating that excess-alumina spinel is in general less stable than stoichiometric spinel. If the compositional dependence of ΔG_f° at any other temperature is similar to that at 1400°C (1673 K), the presence of excess alumina should lower rather than raise the condensation temperature of spinel. However, the increase in ΔG_f° with alumina content appears rather slow, with ΔG_f° at 1400°C (1673 K) remaining close to the stoichiometric value until approximately x = 0.09. If the shape of the ΔG_f° versus x curve is similar at other temperatures, it appears that spinel solid solution may be condensed as easily as stoichiometric spinel at low levels of excess alumina. In order to predict what composition of spinel would be likely to condense from a gas of solar composition, it is necessary to examine the equilibrium activities of MgO and Al_2O_3 in such a gas at the condensation temperature of spinel. One can calculate these activities using the partial pressures of Mg, Al, and O_2 expected at this temperature for a cooling gas of solar nebula composition. According to calculations of the equilibrium condensation sequence of a solar gas at a total pressure of 10^{-5} bar, $P_{Mg} = 7 \times 10^{-8}$ bar, $P_{Al} = 2 \times 10^{-13}$ bar, and $P_{O_2} = 5 \times 10^{-19}$ bar at 1470 K (L. Grossman, 1993, pers. comm.). Based on the free energies of formation of the oxides from

the JANAF Tables (1985), $a_{MgO} = 0.084$ and $a_{Al_2O_3} = 1$ with an overpressure of Al relative to that needed to stabilize corundum. Above 1470 K, $a_{Al_2O_3} = 1$ over a large range of temperature, so the controlling factor in stabilizing spinel is P_{Mg}, which is too low to stabilize spinel at higher temperatures. Because $a_{Al_2O_3}$ is high, it is likely that excess-alumina spinel would condense before stoichiometric spinel as long as ΔG_f° is the same for both. The fact that the majority of excess-alumina spinels reported in Essebi have minimum formation temperatures around 1450 K (that is, compositions appropriate to corundum saturation at this temperature) suggests that it may well be appropriate to regard them as primary condensates. The range of compositions found may be the result of fluctuations in P_{Mg} that result in spinel condensation at a range of temperatures. Excess alumina is not diagnostic of solid condensation, however, as excess-alumina spinels may crystallize from aluminous melts at high temperatures, and excess-alumina spinels have been found in CAIs with igneous textures (Simon et al., 1993).

Summary

The technique of Pd-oxide equilibration has been used to measure the activities of MgO and Al_2O_3 in spinel solid solutions in the system $MgAl_2O_4$–$Al_{8/3}O_4$ at 1400°C. Eight compositions were studied, ranging from stoichiometric $MgAl_2O_4$ to corundum-saturated spinel at 0.17 ± 0.01 mole fraction $Al_{8/3}O_4$. MgO activities decrease with increasing alumina content from 0.93 ± 0.05 to 0.048 ± 0.02 at corundum saturation; Al_2O_3 activities relative to corundum (α-Al_2O_3) increase from 0.07 ± 0.01 to 0.99 ±

0.03. Activities of $MgAl_2O_4$ and γ-$Al_{8/3}O_4$ were calculated from the experimental values of a_{MgO} and $a_{Al_2O_3}$ using the free energy expressions of Chapter 2 and Navrotsky et al. (1986). The $MgAl_2O_4$ activities range from 1.0 (standard state is stoichiometric spinel) to 0.74 ± 0.31, and γ-$Al_{8/3}O_4$ activities range from 0.02 ± 0.02 to 0.50 ± 0.04. The $MgAl_2O_4$ activities are approximately Raoultian, whereas the $Al_{8/3}O_4$ activities show a strong positive deviation from ideality. A plausible model has been set forth for spinel solid solution at 1400°C based on Landau theory, with an assumed cation and vacancy distribution. This model provides an excellent fit to the observed activities in the region of solid solution and predicts that there would be unmixing at $x > 0.2$ if not for the intervention of the stability field of corundum at $x = 0.17$. The similarity of the $\Delta G_{mix,o}$ calculated from the activities and the $\Delta H_{mix,o}$ measured by Navrotsky et al. (1986) imply that entropies of mixing are virtually zero and that the mineral solution is affected by significant short-range order. The free energy of formation of spinel increases with increasing alumina content from about -39 kJ/mole in end-member $MgAl_2O_4$ to about -34 kJ/mole in corundum-saturated spinel, indicating that excess alumina does not lower the condensation temperature of spinel in the solar nebula. However, at low levels of excess alumina ($x < 0.09$), the free energy of formation of spinel is virtually the same as that for end-member $MgAl_2O_4$. Because of the high P_{Al} in the solar nebula, the first spinel condensates should therefore have been aluminous.

Chapter 5. The thermodynamics of forsterite and protoenstatite

In this chapter, Pd-oxide equilibration is used to determine the activities of MgO and SiO_2 in forsterite from a variety of environments and in protoenstatite. It begins with a description of solid solution behavior in forsterite and of the difficulty of determining the equilibrium free energy of formation of protoenstatite. This is followed by an outline of experiments using Pd-oxide equilibration to measure oxide activities in forsterite and protoenstatite and by the measured values and derived free energies of formation of both minerals. The effect of trace constituents on the thermodynamics of olivine is explored with emphasis on the effect of minor CaO solution. Finally, the possible effect of defects on the rheology of forsterite solid solutions is discussed.

Forsterite solid solutions and protoenstatite

Olivine is a very common mineral in the earth's crust, occurring in rocks ranging from gabbro, diabase, andesite, and basalt to thermally metamorphosed limestone. In addition, Mg-rich olivine is thought to comprise a good portion of the earth's upper mantle and therefore plays a crucial role in determining its petrology and rheology. The olivine mineral group exhibits a wide range of solid solution, the most well-known case being the complete solution series between the Mg end-member forsterite (Mg_2SiO_4) and the Fe end-member fayalite (Fe_2SiO_4). Forsterite forms solid solutions in other, less studied systems as well. It can dissolve as much as 1.1 mole% excess SiO_2, producing Mg vacancies in the structure that increase the electrical conductivity

(Pluschkell and Engell, 1968). Forsterite can dissolve up to 16 wt% $CaMgSiO_4$ also (Biggar and O'Hara, 1969), but the microscopic-level effect of Ca dissolution on the lattice is unknown, especially at low concentrations (Warner and Luth, 1973; Mohanan et al., 1993). The presence of defects and minor constituents may exert a significant influence on the thermodynamics and rheology of forsterite.

The pyroxene end-member enstatite ($MgSiO_3$) has at least four polymorphs: orthoenstatite, protoenstatite, and high and low clinoenstatite (Deer et al., 1978). At 1 bar, orthoenstatite is stable from 600 to 1000°C, and protoenstatite is stable from 1000 to 1557°C, the melting point of $MgSiO_3$. Low clinoenstatite is probably the stable form below 600°C, but the stability region of high clinoenstatite is unclear. Protoenstatite is metastable at low temperature and tends to invert to low clinoenstatite when quenched rapidly or to orthoenstatite when quenched slowly. As a result, the thermodynamic properties of protoenstatite are difficult to characterize through conventional drop calorimetric techniques. If one wishes to assess the thermodynamic effect of defects and minor constituents in forsterite and the equilibrium free energy of formation of protoenstatite, a method is needed that can determine both activity as a function of composition and free energy of formation at high temperature. The method of Pd-oxide equilibration is ideal for the study of mineral solutions and high-temperature phases because it yields direct information on activities and equilibrium free energies at high temperature.

Experimental procedure

Sample preparation

Powdered stoichiometric forsterite (fo) was prepared from mixtures of reagent-grade MgO and SiO_2 (JMC Puratronic) ground for 5 hours under ethanol in an agate mortar and sintered for 48 hours at 1400°C. XRD analysis of the sintered material confirmed the presence of forsterite. Powdered $MgSiO_3$ enstatite was prepared from mixtures of MgO and SiO_2 (JMC Puratronic) ground for 5 hours under ethanol in an agate mortar and sintered for 48 hours at 1400°C. XRD analysis revealed the presence of forsterite as well as enstatite in the sample, so the sample was reground and resintered at 1400°C for another 48 hours. XRD analysis revealed the sample had quenched to a mixture of orthorhombic and monoclinic enstatite. A portion of the synthetic forsterite and enstatite were mixed together in an agate mortar and sintered at 1400°C for 44 hours to produce forsterite in equilibrium with enstatite (fo+en). XRD analysis revealed the presence of both minerals. In addition, forsterite-saturated liquids in the system CaO-MgO-Al_2O_3-SiO_2-TiO_2 prepared for the study on oxide activities in silicate melts in Chapter 3 were examined. Details of the synthesis are given in that chapter. The first composition (POI) is a synthetic analog of an average Group 2 plagioclase-olivine inclusion from carbonaceous chondrite meteorites (Sheng et al., 1991). The other (FOB) is a synthetic analog of a forsterite-bearing calcium-aluminum-rich inclusion from carbonaceous chondrites (Wark et al., 1987). Compositions of these liquids as a function of temperature are given in Table 17.

Samples were prepared by pressing the powdered mineral or glassy starting material into pellets around 3-4 mm lengths of 0.25 mm diameter 99.997% pure Pd

Table 17. Compositions of forsterite-saturated silicate liquids (wt%).

Table 17. Compositions of forsterite-saturated silicate liquids (wt%).[a]							
	POI[b]			FOB[c]			
	1280°C	1300°C	bulk	1300°C	1350°C	1400°C	bulk
CaO	10.52	11.31	11.04	25.38	23.91	22.39	20.5
MgO	15.45	15.92	16.73	14.11	16.25	17.71	19.1
Al_2O_3	20.61	21.80	21.88	16.89	16.76	17.02	22.2
SiO_2	52.07	50.22	49.25	42.31	41.82	40.47	36.8
TiO_2	1.05	0.74	0.81	1.49	1.42	1.44	1.37
Total	99.70	99.99	99.71	100.18	100.16	99.03	99.97

a. Electron microprobe analyses: 15 keV, 10 nA, 20 μm beam, 30 s; standardized on anorthite, forsterite, and rutile. Averages of several analyses of two runs at each temperature. Variations at each temperature are within 1 wt%.

b. Forsterite-saturated.

c. Spinel- and forsterite-saturated.

wire (Alfa Products). No binder was used because of the tendency of organic binders to leave a carbon residue in the sample at low f_{O_2}. The mineral pellets were placed in ¼-inch diameter Pd foil buckets. The POI and FOB pellets were melted onto Pd wire loops with a small H_2/O_2 torch. The pure oxide standards were prepared by pressing analytical-grade MgO and SiO_2 (JMC Puratronic) around 3-4 mm lengths of pure Pd wire. Before pressing, the initially amorphous SiO_2 was converted to cristobalite (confirmed by XRD) by heating for about 6 hours at 1500°C. The Pd + periclase pellets were placed in open capsules made from ¼-inch diameter crushable magnesia rods. The Pd + cristobalite pellets were placed in open capsules made from silica glass tubes sealed at one end using a torch.

Experimental methods

Experiments were conducted in a 1-atmosphere home-built furnace with $MoSi_2$ heating elements. Temperature was controlled to within 1-2°C by a Eurotherm 812 Controller/Programmer and measured by a Type S thermocouple calibrated at the melting point of gold. Stated temperatures are estimated to be accurate to ± 3°C. Oxygen fugacity was set using mixtures of H_2 and CO_2 and measured by an yttria-doped zirconia solid electrolyte oxygen sensor (Ceramic Oxide Fabricators Pty. Ltd., Australia). The sensor was calibrated at the iron-wüstite (IW) buffer at 1200 and 1400°C by measuring changes in the resistance of pure iron wire as f_{O_2} was varied. Drift of the emf of the sensor during a run was typically 1 mV or less.

The samples and standards were suspended from Ir or Rh hanging wire and

placed adjacent to each other in a 1-atmosphere gas-mixing furnace. Except for POI, runs were done in the temperature range 1250 to 1400°C, at approximately 50°C intervals. POI becomes forsterite-saturated only below 1305°C, so the experiments on POI were done at 1300 and 1280°C, the lowest temperatures at which forsterite was present but there was still appreciable liquid left (> 50%). The oxygen fugacity of the experiments was typically between IW and an order of magnitude below. Run times varied from 2 days at 1400°C to 7 days at 1250°C. Experiments were terminated by drop-quenching into deionized water. The samples were removed from their containers, mounted in epoxy, and rough-polished to expose a length-wise cross section through the Pd wire. The Pd was then fine-polished with diamond paste using an automatic polisher.

Analytical techniques

Analysis of the Pd alloys was performed as described in Chapter 1. Post-run analyses were performed on the forsterites to determine their Mg:Si ratios, and in the case of POI and FOB olivines, their CaO contents. The analyses of Mg:Si ratio were performed at 15 keV, a 40° takeoff angle, a 10 nA beam current, and a counting time of 100 s. Standardization was done on stoichiometric forsterite. Signal loss due to pellet porosity was minimal, with totals ranging from 99 to 101%. The CaO analyses were performed at 15 keV, 40°, 50 nA, and 255 s. Standardization was done on Boyd forsterite and wollastonite. Sample concentrations were determined through ZAF correction procedures (Armstrong, 1988).

Activities and free energies

The analyzed Mg:Si ratios and estimated CaO contents of the forsterites are shown in Table 18. Due to the energetic unfavorability of the incorporation of excess Mg into the forsterite lattice (Pluschkell and Engell, 1968), the apparent surplus of Mg in the fo and fo+en samples is probably not actually present but rather is an artifact of the calibration. The variation in Mg:Si in these forsterites is only about ± 1 to 1.5%, and the Mg:Si ratio in the standard is known to be stoichiometric to only ± 1% (J.T. Armstrong, pers. comm.). The Si excess that was found by Pluschkell and Engell (1968) in forsterite in equilibrium with enstatite is not observed in the fo+en composition, perhaps because fo+en was prepared by sintering a mixture of the two minerals rather than from a mix of MgO and SiO_2. The CaO contents of the POI and FOB olivines were hard to determine accurately because of fluorescence from the surrounding glass, which may have slightly influenced the analyzed concentrations of 0.2 and 1.3 wt% for POI and FOB respectively. However, the analytical results are consistent with those of Jurewicz and Watson (1988), who took a number of measures to eliminate or correct for fluorescence. They predict contents of ~0.2 and ~1.1 wt% for olivines that crystallize from liquids with CaO contents of 10 (POI) and 23 (FOB) wt% in the system $CaO\text{-}MgO\text{-}Al_2O_3\text{-}SiO_2$.

Experimental run conditions and analyses of the Pd alloys are given in Table 19. Table 20 shows the derived activities of MgO and SiO_2 relative to periclase and cristobalite for the experimental compositions. The measured activities are shown as a function of Ca:Mg ratio in Fig. 24. Table 20 also shows the free energies of formation

Table 18. Compositions of forsterites.

Table 18. Compositions of forsterites.				
type	T (°C)	Mg:Si[a]	CaO (wt%)[b]	Ca:Mg[c]
fo[d]	1350	2.004 (0.004)	NA	0
fo	1400	2.023 (0.007)	NA	0
fo+en[e]	1304	2.023 (0.004)	NA	0
fo+en	1402	2.036 (0.013)	NA	0
POI	1278	2.000 (0.004)	0.23 (0.2)	0.00289 (43)
POI	1282	2.008 (0.007)	NA	0.00289 (43)
POI	1301	1.988 (0.017)	NA	0.00290 (43)
POI	1304	2.003 (0.004)	NA	0.00289 (43)
FOB	1300	1.982 (0.006)	1.32 (0.2)	0.01684 (253)
FOB	1302	1.974 (0.004)	1.32 (0.2)	0.01687 (253)
FOB	1350	1.980 (0.004)	NA	0.01685 (253)
FOB	1351	2.000 (0.010)	1.27 (0.2)	0.01614 (253)

a. Electron microprobe analyses: 15 keV, 30 nA, 30 s; standardized on forsterite. Averages of 2-3 analyses at each temperature. Numbers in parentheses indicate 1σ errors from propagation of errors based on heterogeneity.

b. Electron microprobe analyses: 15 keV, 50 nA, 255 s; standardized on forsterite and wollastonite. Averages of 2-3 analyses at each temperature. Numbers in parentheses indicate 1σ errors based on counting statistics. NA = not analyzed.

c. Numbers in parentheses indicate 1σ errors based on counting statistics. Where not analyzed, CaO content is assumed to be 0.23 wt% in POI and 1.32 wt% in FOB.

d. Forsterite.

e. Forsterite plus protoenstatite.

Table 19. Experimental data for Mg_2SiO_4 and $MgSiO_3$.

Table 19. Experimental data for Mg_2SiO_4 and $MgSiO_3$[a,b]

type	T (°C)	$\log_{10} f_{O_2}$	time (hrs.)	$X_{Mg}^{Pd,fo}$	$X_{Mg}^{Pd,periclase}$	$X_{Si}^{Pd,fo}$	$X_{Si}^{Pd,cristobalite}$
fo	1254	-12.15	165	0.00038 (14)	0.00210 (9)	0.00317 (8)	0.00601 (6)
fo	1300	-11.19	93	0.00030 (9)	0.00166 (10)	0.00149 (5)	0.00264 (11)
fo	1350	-10.38	48	0.00033 (12)	0.00181 (9)	0.00131 (6)	0.00228 (13)
fo	1400	-9.68	60	0.00031 (8)	0.00177 (8)	0.00168 (5)	0.00227 (7)
fo+en	1304	-11.16	93	0.00022 (7)	0.00176 (9)	0.00257 (6)	0.00324 (5)
fo+en	1402	-9.64	46	0.00025 (5)	0.00168 (6)	0.00170 (4)	0.00216 (4)
POI	1282	-11.32	85	0.00025 (10)	0.00153 (7)	-------	-------
POI	1278	-11.33	36	-------	-------	0.00127 (11)	0.00210 (7)
POI	1301	-11.44	60	0.00035 (5)	0.00250 (12)	-------	-------
POI	1304	-10.97	68	-------	-------	0.0104 (4)	0.00188 (13)
FOB	1302	-11.72	60	0.00073 (8)	0.00343 (24)	-------	-------
FOB	1300	-11.25	68	-------	-------	0.00051 (6)	0.00328 (7)
FOB	1351	-11.31	45	0.00118 (8)	0.00488 (15)	-------	-------
FOB	1350	-10.38	45	-------	-------	0.00033 (8)	0.00205 (10)
FOB	1402	-10.30	45	0.00098 (8)	0.00364 (7)	-------	-------
FOB	1400	-9.68	39	-------	-------	0.00037 (6)	0.00250 (7)

a. Numbers in parentheses indicate 1σ errors in the last digits based on heterogeneity. Temperatures are estimated to be accurate to ± 3°C and f_{O_2}'s to ± 0.05 log units.

b. $X_i^{Pd,j}$ defined as mole fraction of solute i dissolved in Pd alloy in equilibrium with phase j.

Table 20. Derived data for Mg_2SiO_4 and $MgSiO_3$.

Table 20. Derived data for Mg_2SiO_4 and $MgSiO_3$[a]					
type	T (°C)	a_{MgO}	a_{SiO_2}	ΔG_f°(fo) (J/mole)[b]	ΔG_f°(pren) (J/mole)[c]
fo	1254	0.181 (0.067)	0.527 (0.014)	-51534 (9426)	-------
fo	1300	0.181 (0.055)	0.564 (0.028)	-52199 (7975)	-------
fo	1350	0.182 (0.062)	0.575 (0.041)	-53449 (9253)	-------
fo	1400	0.175 (0.046)	0.740 (0.034)	-52678 (7341)	-------
fo+en	1304	0.127 (0.041)	0.793 (0.024)	-57155 (8476)	-30098 (4252)
fo+en	1402	0.147 (0.031)	0.787 (0.022)	-56739 (5888)	-30038 (2963)
POI	1280	0.163 (0.068)	0.605 (0.056)	-53335 (10774)	-------
POI	1303	0.140 (0.022)	0.553 (0.045)	-59176 (4248)	-------
FOB	1301	0.213 (0.028)	0.156 (0.019)	-64750 (3791)	-------
FOB	1351	0.242 (0.007)	0.161 (0.040)	-62937 (3444)	-------
FOB	1401	0.269 (0.022)	0.148 (0.025)	-63105 (3273)	-------

a. Numbers in parentheses indicate 1σ errors from propagation of errors based on heterogeneity.

b. Free energy of formation of forsterite from the oxides.

c. Free energy of formation of protoenstatite from the oxides.

Figure 24. Measured activities of (a) MgO relative to periclase and (b)SiO_2 relative to cristobalite versus Ca:Mg ratio in forsterite. Error bars are 1σ from propagation of errors based on heterogeneity.

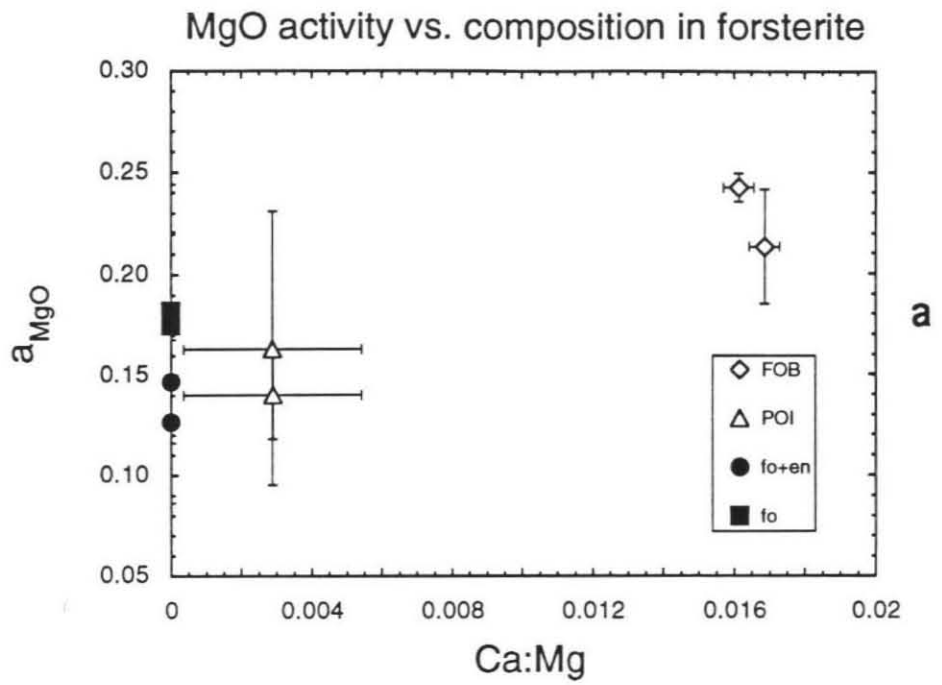
MgO activity vs. composition in forsterite
0.30
0.25
0.20
0.15
0.10
0.05
a_{MgO}
0
0.004
0.008
0.012
0.016
0.02
Ca:Mg
FOB
POI
fo+en
fo
a

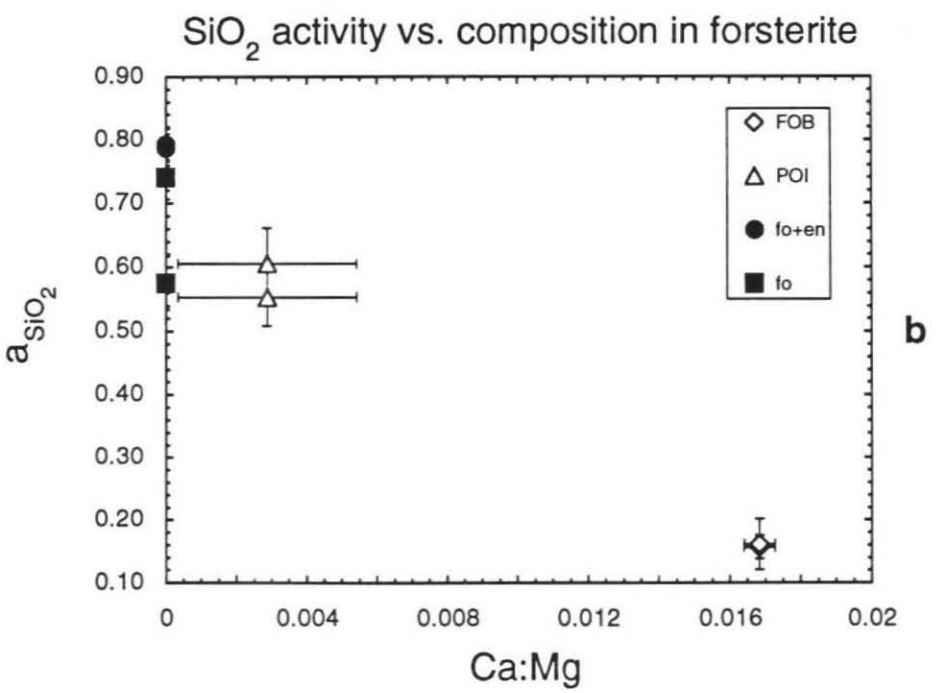
SiO_2 activity vs. composition in forsterite
0.90
0.80
0.70
0.60
0.50
0.40
0.30
0.20
0.10
a_{SiO_2}
0
0.004
0.008
0.012
0.016
0.02
Ca:Mg
FOB
POI
fo+en
fo
b

from the oxides of Mg_2SiO_4, and where appropriate, of $MgSiO_3$ (protoenstatite), calculated from the reactions:

$$2\ MgO_{(periclase)} + SiO_{2(cristobalite)} = Mg_2SiO_{4(forsterite)} \quad (1)$$

and:

$$MgO_{(periclase)} + SiO_{2(cristobalite)} = MgSiO_{3(protoenstatite)}\ , \quad (2)$$

and the relations:

$$\Delta G_f^\circ(fo) = -\ RT\ \ln \frac{1}{(a_{MgO}^{fo})^2\ a_{SiO_2}^{fo}} \quad (3)$$

and:

$$\Delta G_f^\circ(pren) = -\ RT\ \ln \frac{1}{a_{MgO}^{pren}\ a_{SiO_2}^{pren}}\ , \quad (4)$$

where "fo" stands for forsterite, "pren" stands for protoenstatite, $a_{Mg_2SiO_4}^{fo} \equiv 1$ for pure end-member forsterite, and $a_{MgSiO_3}^{pren} \equiv 1$ for pure protoenstatite. The experimental ΔG_f°'s for forsterite are shown in Fig. 25 with ΔG_f°'s from five sets of thermodynamic data from the literature (Róg et al., 1974; Robie et al., 1978; JANAF, 1985; Berman, 1988; Gillet et al., 1991). All the measured values fall between the Robie et al. and JANAF data sets except for the Ca-rich FOB forsterites, which lie between JANAF (1985) and Róg et al. (1974). The ΔG_f°'s for protoenstatite are shown in Fig. 26 with the estimates for protoenstatite from Berman (1988) and JANAF (1985). The experimental values show excellent agreement with the Berman and JANAF values.

Figure 25. ΔG_f° of forsterite from the oxides versus temperature. Error bars are 1σ from propagation of errors based on heterogeneity. Dashed lines are ΔG_f°'s from the literature (Róg et al., 1974; Robie et al., 1978; JANAF, 1985; Berman, 1988; Gillet et al., 1991).

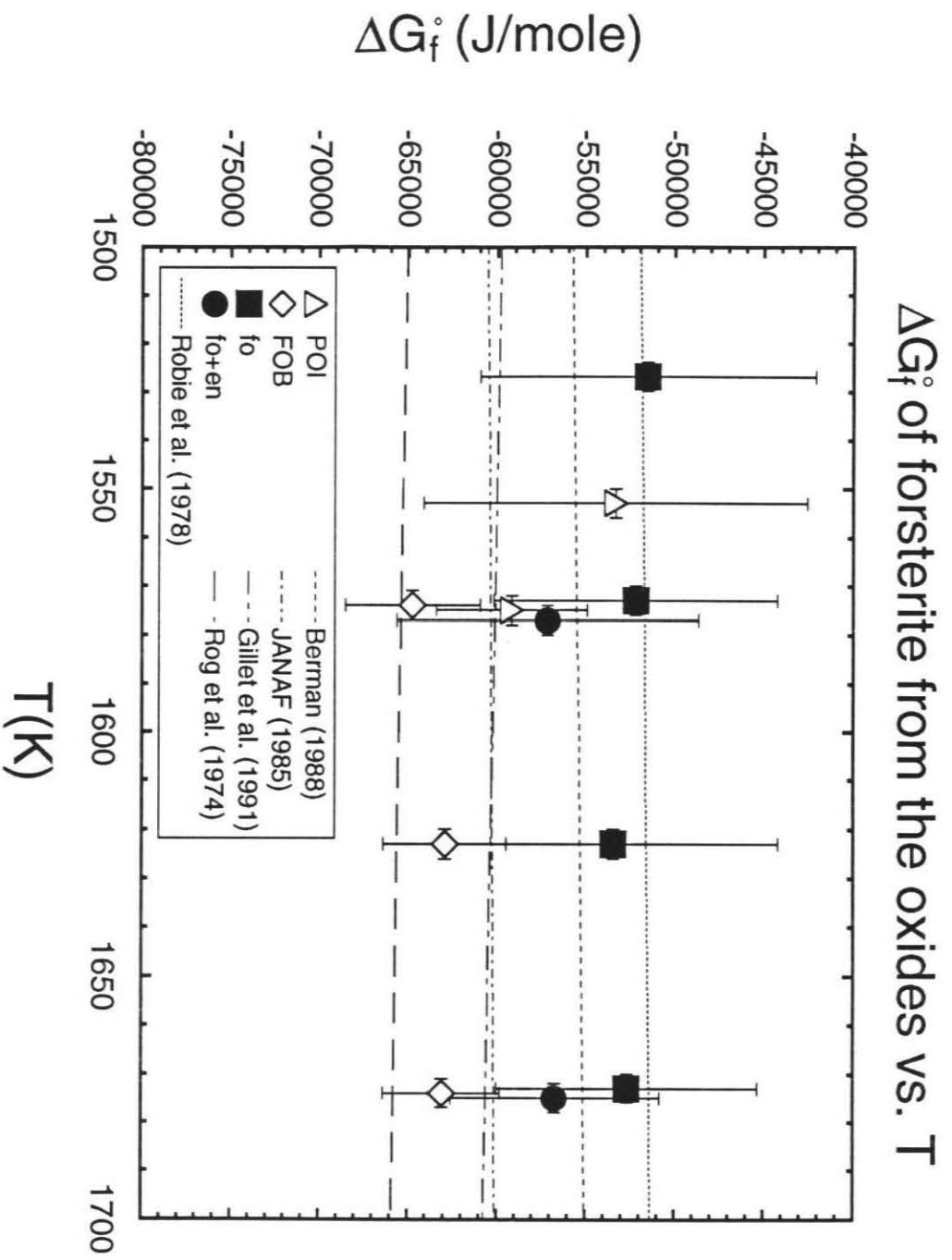
ΔG°f of forsterite from the oxides vs. T
ΔG°f (J/mole)
-40000
-45000
-50000
-55000
-60000
-65000
-70000
-75000
-80000
1500
1550
1600
1650
1700
T(K)
POI
FOB
fo
fo+en
Robie et al. (1978)
Berman (1988)
JANAF (1985)
Gillet et al. (1991)
Rog et al. (1974)

Figure 26. ΔG_f° of protoenstatite from the oxides versus temperature. Error bars are 1σ from propagation of errors based on heterogeneity. Dashed lines are ΔG_f°'s from the literature (JANAF, 1985; Berman, 1988).

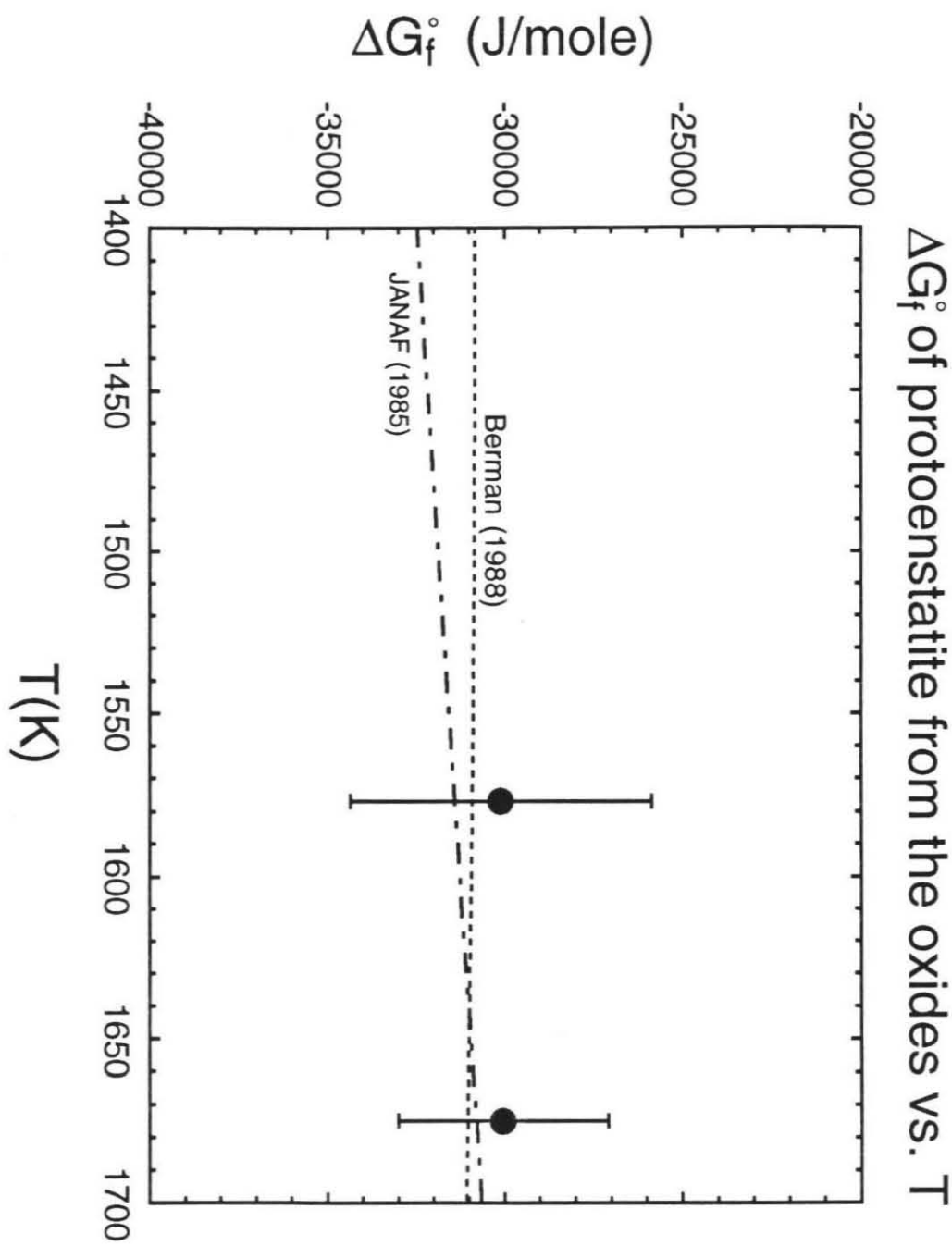
ΔG°f of protoenstatite from the oxides vs. T
ΔG°f (J/mole)
-20000
-25000
-30000
-35000
-40000
Berman (1988)
JANAF (1985)
1400
1450
1500
1550
1600
1650
1700
T(K)

Activities

Table 20 and Fig. 24 show that the activities of MgO and SiO_2 vary even though all of the olivine compositions are very close to stoichiometric Mg_2SiO_4. The activity of MgO ranges from 0.24 in FOB to 0.13 in fo+en, and the activity of SiO_2 varies from 0.8 in fo+en to 0.15 in FOB. For a phase in the binary system MgO-SiO_2, the Gibbs-Duhem equation requires that variations in a_{MgO} be coupled with variations in a_{SiO_2}. For forsterite, this gives:

$$\frac{d\mu^{fo}_{MgO}}{d\mu^{fo}_{SiO_2}} = \frac{d \ln a^{fo}_{MgO}}{d \ln a^{fo}_{SiO_2}} = - \frac{X^{fo}_{SiO_2}}{X^{fo}_{MgO}} , \qquad (5)$$

where chemical potential μ is given by $\mu_i^{fo} = \mu_i^{fo\,\circ} + RT\ln a_i^{fo}$. For stoichiometric forsterite,

$$\frac{d \ln a^{fo}_{MgO}}{d \ln a^{fo}_{SiO_2}} = -½ . \qquad (6)$$

A plot of ln a_{MgO} versus ln a_{SiO_2} for olivines at 1300 and 1400°C is shown in Fig. 27, together with best-fit lines at each temperature fixed at a slope of -½. At both temperatures, the FOB olivines deviate at the 1σ level from the best-fit lines, whereas the fo, fo+en, and POI olivines all fall very close to them. This deviation indicates a compositional difference in the FOB olivines that can be linked to the Ca in the lattice. The FOB olivines do overlap with the best-fit lines at the 2σ level, however, indicating that although they are compositionally more complex than the other olivines, they are still close to stoichiometric forsterite.

Figure 27. Ln a_{MgO} versus ln a_{SiO_2} in forsterite for (a) 1300 and (b) 1400°C. Data at each temperature is fit to a line with slope -½. The Ca-rich olivines (FOB) deviate from the Gibbs-Duhem relationship, suggesting that they are compositionally more complex.

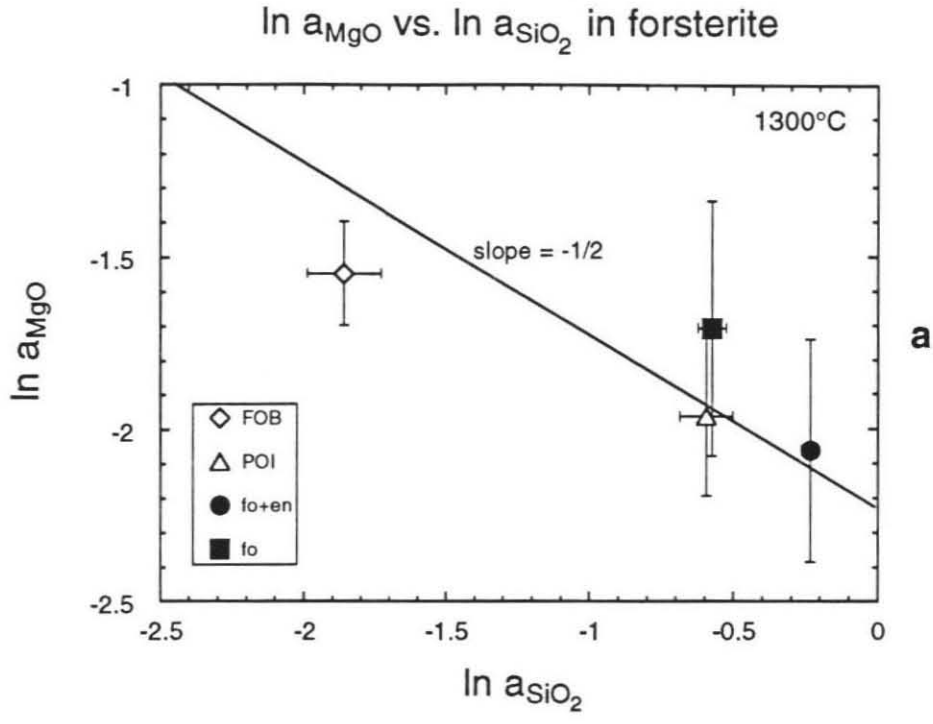
ln a_{MgO} vs. ln a_{SiO_2} in forsterite
1300°C
slope = -1/2
FOB
POI
fo+en
fo
ln a_{MgO}
ln a_{SiO_2}
-1
-1.5
-2
-2.5
-2.5
-2
-1.5
-1
-0.5
0

a

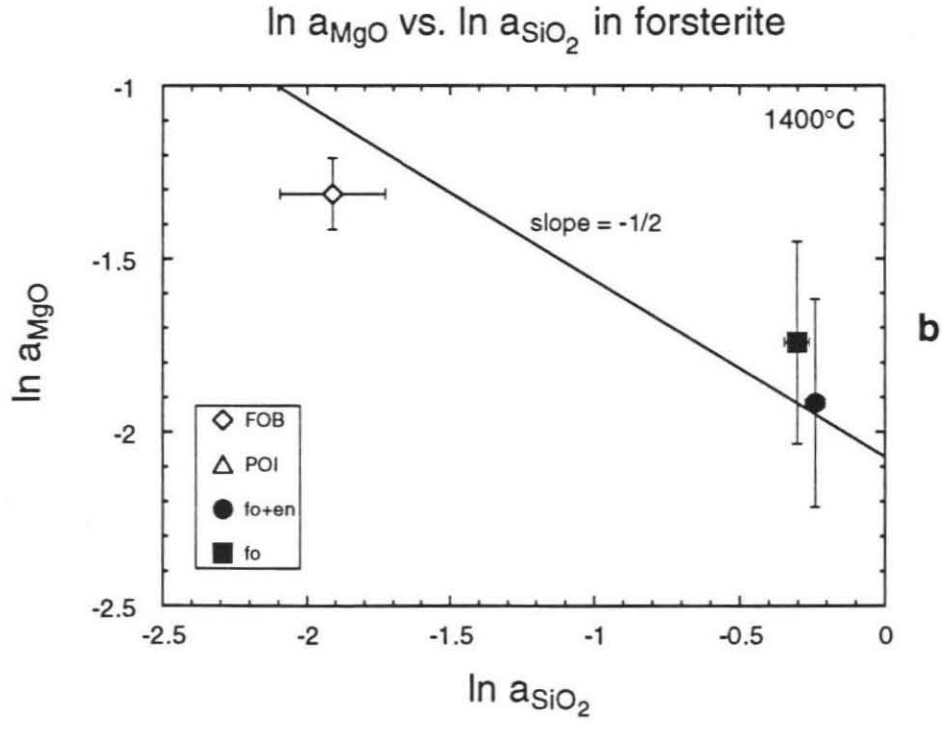
ln a_{MgO} vs. ln a_{SiO_2} in forsterite
1400°C
slope = -1/2
FOB
POI
fo+en
fo
ln a_{MgO}
ln a_{SiO_2}
-1
-1.5
-2
-2.5
-2.5
-2
-1.5
-1
-0.5
0

b

Fig. 24 reveals, however, that there are small variations in composition that accompany the changes in oxide activities in the olivines. There is a positive correlation between a_{MgO} and Ca content and a negative correlation between a_{SiO_2} and Ca content, especially pronounced in the latter case, where the range of activity is larger and the trend is clearer. The microscopic expression of these changes is unknown, but the rise in a_{MgO} with CaO content indicates that solution of Ca affects the distribution of Mg in more than a random configurational manner. The Ca-bearing olivine may be inhomogeneous on a microscopic scale, a process that leads at higher Ca contents to the unmixing into forsterite and monticellite ($CaMgSiO_4$)-rich phases that is observed in the Mg_2SiO_4–$CaMgSiO_4$ compositional system.

Although the greatest changes in activity are linked to changes in Ca content, the binary forsterites (fo, fo+en,) also exhibit a small range in MgO and SiO_2 activity. The range in activity in fo and fo+en occurs despite an essentially negligible difference in Mg:Si between the forsterites, indicating that the free energy curve of forsterite is very sharp at Mg_2SiO_4, as found also for $MgAl_2O_4$ (Chapter 2; Chamberlin et al., 1993c). This is illustrated schematically in Fig. 28a, which shows the molar free energy $\overline{G}$ of forsterite as a function of composition. The chemical potentials μ of MgO and SiO_2 are given by the intercepts at 100% MgO and 100% SiO_2 of the tangent line to the forsterite free energy curve at a given composition of forsterite. At stoichiometric Mg_2SiO_4, the tangent to the $\overline{G}$ curve and hence the activities can change greatly without significantly perturbing Mg:Si. The presence of a second phase, such

Figure 28. Schematic illustration of the relationship between molar free energy ($\overline{G}$) and composition of forsterite.

a.) Binary system MgO-SiO_2. Chemical potentials μ of the oxides are given by the intercepts of the tangent lines (dashed) to the free energy curves of the minerals. Because of the sharpness of the free energy surface, the activities of MgO and SiO_2 change markedly between pure forsterite and forsterite in equilibrium with protoenstatite without significantly changing composition.

b.) Ternary system CaO-MgO-SiO_2. Chemical potentials μ of the oxides are given by the intercepts of the tangent plane (shaded) to the free energy surface of forsterite. Dashed lines correspond to those in Fig. 28a. The free energy surface decreases toward CaO and the curvature changes such that the activity of MgO rises and the activity of SiO_2 falls from the values in the binary system.

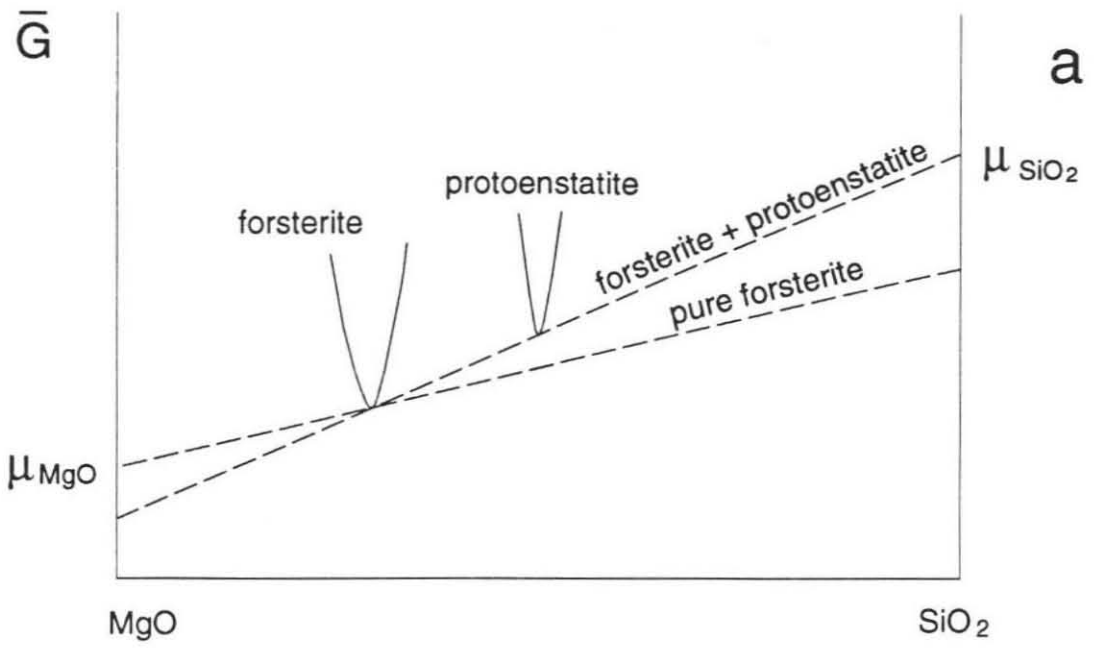
$\bar{G}$
a
μ_{SiO_2}
protoenstatite
forsterite
forsterite + protoenstatite
pure forsterite
μ_{MgO}
MgO
SiO_2

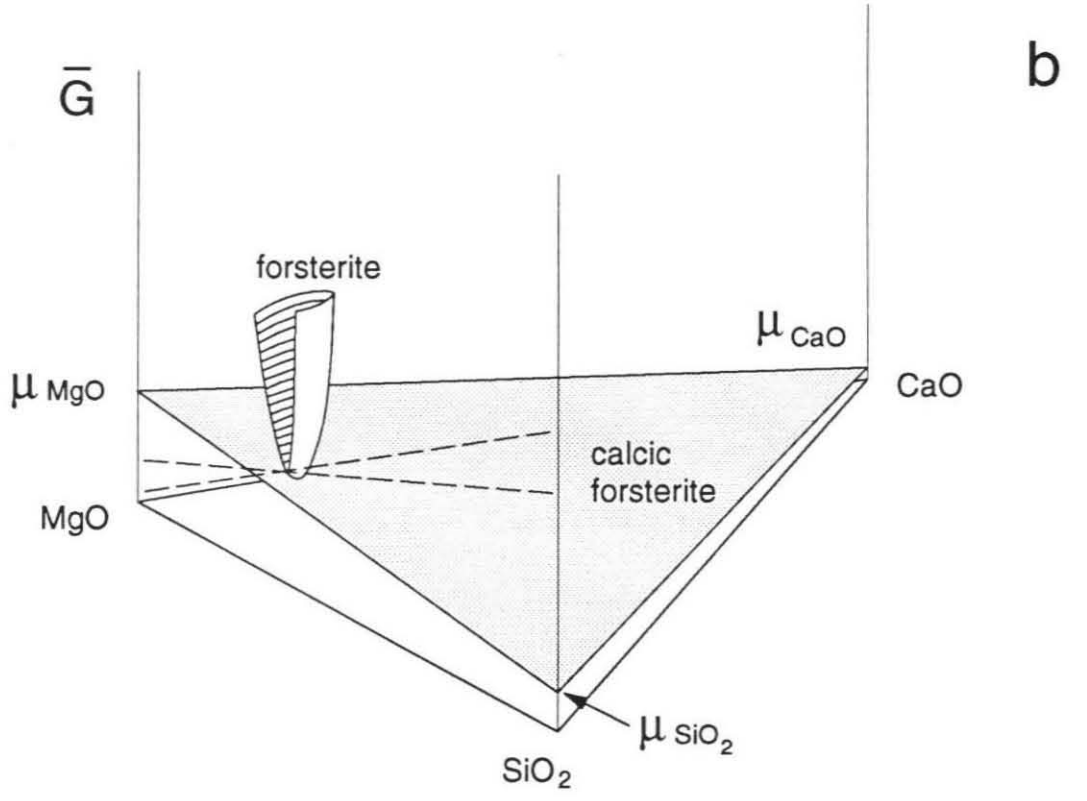
b
$\bar{G}$
forsterite
μ_{CaO}
μ_{MgO}
CaO
calcic
forsterite
MgO
μ_{SiO_2}
SiO_2

as protoenstatite (as shown in Fig. 28a), fixes the activities in forsterite at a particular value. When Ca is added to the lattice (Fig. 28b), the $\overline{G}$ curve becomes a surface, and the curvature of this surface must change toward CaO such that the tangent plane to the free energy surface swings toward higher μ_{MgO} and lower μ_{SiO_2} than in the binary system.

Free energies of formation

In Fig. 25, although the error bars are large, there appears to be a systematic decrease in ΔG_f° from fo at about -52 kJ/mole, to fo+en at about -57 kJ/mole, to FOB at about -64 kJ/mole. The literature values cover the same range, from Robie et al. (1978) at the high end to Róg et al. (1974) at the low end. The ΔG_f°'s of Robie et al. (1978), JANAF (1985), and Gillet et al. (1991) are all derived from calorimetric data. The difference between the values of Robie et al. (1978) and Gillet et al. (1991) is mainly due to the different values of entropy at 298 K (S_{298}°) used to calculate ΔG_f°. The Robie et al. (1978) data rely on an S_{298}° derived from the low temperature heat capacity measurements of Kelley (1943), whereas the Gillet et al. (1991) data set relies on an S_{298}° from the work of Robie et al. (1982), which is 1.1% lower. The JANAF (1985) data set uses the entropy from Kelley (1943) but relies on an enthalpy of formation (ΔH_f°) at 298 K from Torgeson and Sahama (1948), whereas Robie et al. (1978) and Gillet et al. (1991) use a $\Delta H_f^\circ(298)$ from King et al. (1967). These variations in the calorimetric data yield a 10 kJ/mole spread in calculated ΔG_f°. The values of Berman (1988) are derived by optimization of phase equilibrium data with

calorimetric constraints and are consistent with the ΔG_f°'s measured for fo, fo+en, and POI. Róg et al. (1974) determined ΔG_f° through high temperature emf measurements, and their results are most consistent with the measured values for FOB. It is unknown why the emf measurements yield values 5 kJ/mole lower than the most negative estimates from calorimetric studies, but the answer may lie in the difficulty in achieving equilibrium noted by Róg et al. (1974) in the emf experiments.

The majority of both literature and experimental values lie above -60 kJ/mole, suggesting that there is a compositional effect on ΔG_f° in the CaO-bearing FOB olivines. The FOB values are calculated without taking the CaO contents into account, but the activity of forsterite would have to be as low as 0.65 to bring them into accordance with the others. Models for Ca solution in olivine based on the Mg_2SiO_4–$CaMgSiO_4$ phase diagram are not consistent with such low forsterite activities (Warner and Luth, 1973), suggesting that the observed ΔG_f° effect may be present only in very dilute forsterite solutions. The configurational entropy contribution of the Ca atoms can be calculated from:

$$\Delta S_{conf} = -R[X_{Mg}^{M1} \ln X_{Mg}^{M1} + X_{Mg}^{M2} \ln X_{Mg}^{M2} + X_{Ca}^{M1} \ln X_{Ca}^{M1} + X_{Ca}^{M2} \ln X_{Ca}^{M2}] , \qquad (7)$$

where ΔS_{conf} is the configurational entropy relative to pure forsterite, M1 and M2 refer to the two cation sites in olivine, and X_i^j is the fraction of species i on site j. Because in monticellite M2 is larger than M1, and Ca therefore partitions onto the M2 site, it is commonly assumed that Ca atoms occupy the M2 sites in dilute forsterite solutions also. However, the M1 and M2 sites are the same size in forsterite, and Raman spec-

troscopic evidence implies that Ca may occupy both sites in forsterite (Mohanan et al., 1993), contributing a greater positional disorder to the mineral. If half the Ca atoms are on M1 and half on M2, then at 1.1 wt% CaO, $X_{Ca}^{M1} = X_{Ca}^{M2} = 0.0137$, $X_{Mg}^{M1} = X_{Mg}^{M2} = 0.9863$, and $\Delta S_{conf} = 1.203$ J/mole. This contributes only -2.0 kJ/mole to ΔG_f° at 1673 K, indicating that the distribution of Ca alone cannot account for the lowering of ΔG_f°, and there must be other effects present in the lattice.

A possible source for additional entropy in nonstoichiometric forsterite is the creation of defects. Stoichiometric forsterite is thought to have a small amount of Mg Frenkel defects, that is, Mg cations that reside in interstitial sites, leaving vacancies in the M1 and M2 sites (Pluschkell and Engell, 1968; Stocker and Smyth, 1978). Stocker and Smyth (1978) suggest that the presence of minor and trace elements may have a significant effect on the point-defect chemistry of olivine. If the calcic olivines are viewed as a solution of forsterite and monticellite, it is apparent that there is a large size mismatch between the two end-members (forsterite: a = 4.756, b = 10.195, c = 5.891 A; monticellite: a = 4.815, b = 11.08, c = 6.37 A; Deer et al., 1978) due to the large size of the Ca atom relative to Mg. It may be that the entry of the first few Ca atoms into a forsterite solution distorts the crystal lattice such that more Mg Frenkel defects are created, increasing the configurational entropy of the crystal. The configurational entropy would then be given by:

$$\Delta S_{conf} = -R[X_{Mg}^{int} \ln X_{Mg}^{int} + X_{Mg}^{M1} \ln X_{Mg}^{M1} + X_{Mg}^{M2} \ln X_{Mg}^{M2} + X_{Ca}^{M1} \ln X_{Ca}^{M1} + X_{Ca}^{M2} \ln X_{Ca}^{M2}] , \quad (8)$$

where "int" refers to the interstitial site. If each Ca atom causes about two defects,

then $X_{Mg}^{int} = 0.05$, $X_{Mg}^{M1} = X_{Mg}^{M2} = 0.9363$, $X_{Ca}^{M1} = X_{Ca}^{M2} = 0.0137$, and $\Delta S_{conf} = 3.2$ J/mole K. At 1673 K, this produces a lowering of the ΔG_f° of 5.4 kJ/mole, very similar to the 7 kJ/mole gap between FOB and fo+en. The results are actually similar if it is assumed that Ca is distributed on only one site and/or the Mg cations are ejected preferentially from either M1 or M2. The enthalpy effect of CaO dissolution is unknown and may oppose the entropy effect, in which case a somewhat larger amount of disorder would be required. The treatment above is rather speculative, as there is no detailed knowledge of the actual cation site distributions or enthalpies of mixing, but it certainly suggests that solution of minor components can decrease the ΔG_f° appreciably by increasing the concentration of point defects. If present, the increase in Frenkel defects could be detected through conductivity measurements such as those of Pluschkell and Engell (1968). Because the effect of Ca solution on ΔG_f° seems rather extreme and because the cause is only poorly understood, further study on olivines in the system forsterite-monticellite is warranted.

In Fig. 26, the close agreement between the experimental ΔG_f°'s for protoenstatite and those predicted by Berman (1988) are most likely due to his incorporation of phase equilibrium data in constructing his thermodynamic data base. He assumed that the heat capacity C_p of protoenstatite was equal to that of orthoenstatite as measured by Krupka et al. (1985a,b), and Haselton (1979), and refined the 298 K properties to fit known phase equilibria involving protoenstatite. The JANAF (1985) data uses the heat capacity data of Wagner (1932), assuming it pertains to protoenstatite between 1258 and 1850 K, and an enthalpy of transition from orthoenstatite calculated from the

dT/dP of inversion of Boyd et al. (1964) and the densities of ortho- and protoenstatite of Stephenson et al. (1966) and Smith (1959). The ΔG_f°'s predicted by JANAF (1985) coincide with the experimental data but predict a stronger temperature dependence than Berman (1988) at lower temperatures.

Rheology

The existence of defects in a mineral such as olivine is typically associated with a change in the mechanical strength of the mineral (Evans and Dresen, 1991). The propagation of deformation in a crystal may depend on the distribution and diffusion of point defects including vacancies, interstitials, electrons, and electron holes (Evans and Dresen, 1991). Previous studies have shown that olivine is weakened by low levels of hydrogen (Mackwell et al., 1985), vanadium (Ricoult and Kohlstedt, 1986), and carbon (Green, 1988). The existence of a low level of Ca or any other impurity in forsterite may increase the number of defects in the lattice and therefore decrease the mechanical strength of forsterite. The presence of excess SiO_2 in the lattice probably also causes weakening, as it effectively creates Mg vacancies in the structure.

Summary

Pd-oxide equilibration has been used to measure the activities of MgO and SiO_2 in forsterite and protoenstatite. Four different types of forsterite were studied: nominally pure stoichiometric forsterite, forsterite in equilibrium with protoenstatite, and forsterites crystallized from liquids of two different bulk compositions in the system

CaO-MgO-Al_2O_3-SiO_2-TiO_2 (POI and FOB). Measured MgO activities range from ~0.14 in forsterite in equilibrium with protoenstatite to ~0.24 in the calcic FOB forsterites and SiO_2 activities range from ~0.16 in the FOB forsterites to ~0.8 in forsterite in equilibrium with protoenstatite. The ΔG_f°'s of forsterite are consistent with the data sets of Robie et al. (1978), Berman (1988), and JANAF (1985) in the experimental temperature range, except in FOB, where they are noticeably lower. The changes in oxide activities and free energies of formation are most likely due to small variations in composition in the forsterites. In particular, the solution of approximately 1 wt% CaO in the FOB olivines may cause an increase in Mg Frenkel defects that lowers the ΔG_f°. The ΔG_f°'s of protoenstatite determined from the MgO and SiO_2 activities agree with those of Berman (1988) to within 1 kJ/mole. The presence of low levels of Ca or other impurities in the forsterite lattice may cause defects that lower the mechanical strength of the mineral.

Conclusions

1.) A new technique, Pd-oxide equilibration, has been developed for the experimental determination of the activities of oxide components in melts and minerals using the equilibrium between Pd alloy, oxygen, and the oxide component in the sample of interest. Due to the extraordinary stability of dilute alloys of Pd with Mg, Al, and Si, these metals dissolve into the Pd in equilibrium with oxide-based materials in amounts easily measured with the electron microprobe at f_{O_2}'s near IW. Because Mg, Al, and Si have constant activity coefficients in Pd at low concentrations, the activity of the oxide of each metal is a simple function of the ratio of the concentration of the metal in Pd in equilibrium with the sample to that in Pd in equilibrium with the pure oxide. Therefore, if Pd plus a melt or mineral and Pd plus pure oxide standards are equilibrated simultaneously at fixed T and f_{O_2}, the precision of the analytical technique is the major limitation on the determination of oxide activities. With Pd-oxide equilibration, all measurements of thermodynamic properties reflect equilibration at the temperature of interest, so no phase, ordering, or structural changes upon quenching influence the results. In addition, the method can be precise because the only measurements involved in the determination of activities are the concentrations of various metals in the Pd.

2.) The technique of Pd-oxide equilibration was used to determine activities of MgO and Al_2O_3 and ΔG_f°'s from the oxides for stoichiometric $MgAl_2O_4$ spinel at 1150 to 1400°C. The results are in good agreement with those of JANAF (1985) but are distinct at the 1σ level from the ΔG_f°'s of Helgeson et al. (1978), Holland and Powell (1990), Berman (1988), and Hallstedt (1992), and at the 2σ level from Robie et al. (1978). This implies a larger residual entropy upon quenching than is accounted for

by most compilations of thermodynamic data. Heat contents corrected based on Landau theory and measured ΔG_f°'s have been used to produce a new, self-consistent C_p function that can account for the experimental data. The results imply that nonconfigurational entropy contributions are important in spinel.

3.) The technique was also used to measure the activities of MgO, Al_2O_3, and SiO_2 in melts in the five-component system CMAST. Five bulk compositions were studied, including four synthetic analogs of CAIs and one synthetic analog of a POI from carbonaceous chondrites. Correlated variations between activity coefficient and liquid composition are observed in the melts, possibly giving insights into relationships between thermodynamics and structure. The measured activities agree to within 10-35% of those calculated using Berman's (1983) model and are therefore generally consistent with known phase equilibrium data in CMAS. Measured activities indicate that liquids of CAI and POI composition would be out of equilibrium with a solar gas and should volatilize Mg, SiO, and lesser Ca if they melt in such a gas.

4.) The method was also used to measure the activities of MgO and Al_2O_3 in spinel solid solutions in the $MgAl_2O_4$–$Al_{8/3}O_4$ compositional system at 1400°C. Compositions were studied ranging from stoichiometric $MgAl_2O_4$ to corundum-saturated spinel. Activities of $MgAl_2O_4$ and γ-$Al_{8/3}O_4$ were calculated from the experimental values of a_{MgO} and $a_{Al_2O_3}$ using the free energy expressions of Chamberlin et al. (1993b) and Navrotsky et al. (1986). The $MgAl_2O_4$ activities are approximately Raoultian, whereas the γ-$Al_{8/3}O_4$ activities show a strong positive deviation from ideality. A plausible model for spinel solid solution at 1400°C based on Landau theory (Carpenter et al., 1993a,b) is set forth, with an assumed cation and vacancy distribution. The similarity between calculated free energies of mixing and measured enthalpies of mixing (Nav-

rotsky et al., 1986) imply that entropies of mixing are virtually zero and that the solid solution is affected by significant short-range order. The ΔG_f° of spinel increases with increasing alumina content, indicating that excess alumina does not increase the condensation temperature of spinel in the solar nebula. However, the high P_{Al} in the solar nebula and the fact that ΔG_f° remains relatively constant at low alumina contents imply that aluminous spinels may condense.

5.) Finally, Pd-oxide equilibration was used to measure the activities of MgO and SiO_2 in forsterite and protoenstatite. Studied compositions included nominally pure forsterite, forsterite in equilibrium with protoenstatite, and forsterites that crystallized from liquids of two different bulk compositions in the system CMAST (POI and FOB). Measured oxide activities and ΔG_f°'s vary systematically with Ca content. The ΔG_f°'s are consistent with the literature values of Robie et al. (1978), Berman (1988), JANAF (1985), and Gillet et al. (1991) in this temperature range except for FOB, where they are lower. ΔG_f° of protoenstatite determined from the MgO and SiO_2 activities agrees with that of Berman (1988) to 1 kJ/mole. Low levels of Ca dissolved in forsterite may increase the number of point defects in the lattice and thereby decrease the mechanical strength of the mineral.

6.) The Pd-oxide equilibration technique can be of considerable value in refining the existing thermodynamic data base due to its potential for directly and precisely determining oxide activities in melts and mineral solutions and free energies of formation of minerals.

References

Abraham, K.P., M.W. Davies, and F.D. Richardson (1960) Activities of manganese oxide in silicate melts. Journal of the Iron and Steel Institute, 196, 82-89.

Alper, A.M., R.N. McNally, P.H. Ribbe, and R.C. Doman (1962) The system MgO-$MgAl_2O_4$. Journal of the American Ceramic Society, 45, 263-268.

Armstrong, J.T. (1988) Quantitative analysis of silicate and oxide minerals: Comparison of Monte Carlo, ZAF, and $\phi(\rho z)$ procedures. In *Microbeam Analysis-1988* (D.E. Newbury ed.) pp. 239-246. San Francisco Press.

Basso, R., S. Carbonin, and A. Della Giusta (1991) Cation and vacancy distribution in a synthetic defect spinel. Zeitschrift für Kristallographie, 194, 111-119.

Beckett, J.R. (1986) The origin of calcium-,aluminum-rich inclusions from carbonaceous chondrites: an experimental study. Ph.D. thesis, University of Chicago.

Beckett, J.R. and L. Grossman (1988) The origin of type C inclusions from carbonaceous chondrites. Earth and Planetary Science Letters, 89, 1-14.

Beckett, J.R., A.J. Spivack, I.D. Hutcheon, G.J. Wasserburg, and E.M. Stolper (1990) Crystal chemical effects on the partitioning of trace elements between mineral and melt: An experimental study of melilite with applications to refractory inclusions from carbonaceous chondrites. Geochimica et Cosmochimica Acta, 54, 1755-1774.

Berman, R.G. (1983) A thermodynamic model for multicomponent melts with applica-

tion to the system CaO-MgO-Al_2O_3-SiO_2. Ph.D. thesis, University of British Columbia.

Berman, R.G. (1988) Internally-consistent thermodynamic data for minerals in the system Na_2O-K_2O-CaO-FeO-Fe_2O_3-Al_2O_3-SiO_2-TiO_2-H_2O-CO_2. Journal of Petrology, 29, 445-522.

Berman, R.G. and T.H. Brown (1985) Heat capacity of minerals in the system Na_2O-K_2O-CaO-MgO-FeO-Fe_2O_3-Al_2O_3-SiO_2-TiO_2-H_2O-CO_2: representation, estimation, and high temperature extrapolation. Contributions to Mineralogy and Petrology, 89, 168-183.

Biggar, G.M. and M.J. O'Hara (1969) Monticellite and forsterite crystalline solutions. Journal of the American Ceramic Society, 52, 249-252.

Blander, M., and L.M. Fuchs (1975) Calcium-aluminum-rich inclusions in the Allende meteorite: Evidence for a liquid origin. Geochimica et Cosmochimica Acta, 39, 1605-1619.

Bonnickson, K.R. (1955) High temperature heat contents of aluminates of calcium and magnesium. Journal of Physical Chemistry, 59, 220-221.

Boyd, F.R., J.L. England, and B.T.C. Davis (1964) Effects of pressure on the melting and polymorphism of enstatite, $MgSiO_3$. Journal of Geophysical Research, 69, 2101-2109.

Brearley, A.J., I. Casanova, M.L. Miller, and K. Keil (1991) Mineralogy and possible origin of an unusual Cr-rich inclusion in the Los Martinez (L6) chondrite.

Meteoritics, 26, 287-300.

Brigham, C.A. (1990) Isotopic heterogeneity in calcium-aluminum rich meteoritic inclusions. Ph.D. thesis, California Institute of Technology.

Brodowsky, H. and H. Husemann (1966) Wasserstoff in Palladiumlegierungen. Berichte der Bunsengesellschaft für Physikalische Chemie, 70, 626-630.

Brodowsky, H.A. and H.J. Schaller (1969) Thermodynamics of nonstoichiometric interstitial alloys. I. Boron in palladium. Transactions of the Metallurgical Society of AIME, 245, 1015-1020.

Brodowsky, H., Y.S. Oei, and H.J. Schaller (1980) Thermodynamische Eigenschaften von Palladium-Cadmium-Legierungen. Zeitschrift für Metallkunde, 71, 593-598.

Buddington, A.F. and D.H. Lindsley (1964) Iron-titanium oxide minerals and their synthetic equivalents. Journal of Petrology, 5, 310-357.

Carpenter, M.A., R. Powell, and E.K.H. Salje (1993a) Thermodynamics of non-convergent cation ordering in minerals, I: an alternative approach. In preparation.

Carpenter, M.A., R. Powell, and E.K.H. Salje (1993b) Thermodynamics of non-convergent cation ordering in minerals, II: spinels and the orthopyroxene solid solution. In preparation.

Chamberlin, L., J.R. Beckett, and E.M. Stolper (1993a) A new experimental method for the direct determination of oxide activities in melts and minerals. Accepted to Contributions to Mineralogy and Petrology.

Chamberlin, L., J.R. Beckett, and E.M. Stolper (1993b) Pd-oxide equilibration and the thermodynamic properties of $MgAl_2O_4$ spinel. In preparation.

Chamberlin, L., J.R. Beckett, and E.M. Stolper (1992c) Experimental measurement of oxide activities in melts in the system CaO-MgO-Al_2O_3-SiO_2-TiO_2 relevant to the origin of inclusions in carbonaceous chondrites. In preparation.

Chamberlin, L., J.R. Beckett, and E.M. Stolper (1993d) Experimental measurement of oxide activities across the join $MgAl_2O_4$-$Al_{8/3}O_4$ at 1400°C. In preparation.

Chamberlin, L., J.R. Beckett, and E.M. Stolper (1993e) Pd-oxide equilibration and the thermodynamics of forsterite and protoenstatite. In preparation.

Charlu, T.V., R.C. Newton, and O.J. Kleppa (1975) Enthalpies of formation at 970 K of compounds in the system MgO-Al_3O_3-SiO_2 from high temperature solution calorimetry. Geochimica et Cosmochimica Acta, 39, 1487-1497.

Chase, Jr., M.W., C.A. Davies, J.R. Downey Jr., D.J. Frurip, R.A. McDonald, and A.N. Syverud (1985) The JANAF Thermochemical Tables, third edition. Journal of Physical Chemistry Reference Data, 14, Supplement 1.

Cima, M., and L. Brewer (1988) The generalized Lewis acid-base titration of palladium and niobium. Metallurgical Transactions B, 19, 893-917.

Clayton, R.N., G.J. MacPherson, I.D. Hutcheon, A.M. Davis, L. Grossman, T.K. Mayeda, C. Molini-Velsko, J.M. Allen (1984) Two forsterite-bearing FUN inclusions in the Allende meteorite. Geochimica et Cosmochimica Acta, 48, 535-548.

Colin, F. (1968) Des phases formées au cours de la réduction de certains oxydes mixtes $n Al_2O_3.MO$. Revue Internationale des Hautes Températures et des Réfractaires, 5, 269.

Davidson, P.M. and D.K. Mukhopadhyay (1984) Ca-Fe-Mg olivines: phase relations and a solution model. Contributions to Mineralogy and Petrology, 86, 256-263.

Davis, A.M., G.J. MacPherson, R.N. Clayton, T.K. Mayeda, P.J. Sylvester, L. Grossman, R.W. Hinton, and J.R. Laughlin (1991) Melt solidification and late-stage evaporation in the evolution of a FUN inclusion from the Vigarano C3V chondrite. Geochimica et Cosmochimica Acta, 55, 621-637.

Deer, W.A., R.A. Howie, and J. Zussman (1978) *Rock-forming Minerals, Vol 2A: Single-chain silicates*, 2nd edition. Longman Group Ltd.

Dominik, B., E.K. Jessberger, T. Staudacher, K. Nagel, and A. El Goresy (1978) A new type of white inclusion in Allende: Petrography, mineral chemistry, ^{40}Ar–^{39}Ar ages, and genetic implications. Proceedings of the Lunar and Planetary Science Conference, 9, 1249-1266.

Dudson, P.J. and D.G. Fraser (1980) Nickel oxide activities in silicate melts in the system CaO-MgO-Al_2O_3-SiO_2-NiO. Progress in Experimental Petrology, 5, 247-251.

El Goresy, A., H. Palme, H. Yabuki, K. Nagel, I. Herrwerth, and P. Ramdohr (1984) A calcium-aluminum-rich inclusion from the Essebi (CM2) chondrite: Evidence for captured spinel-hibonite spherules and for an ultra-refractory rimming sequence. Geochimica et Cosmochimica Acta, 48, 2283-2298.

Eriksson, G., P. Wu, and A.D. Pelton (1993) Critical evaluation and optimization of the thermodynamic properties and phase diagrams of the MgO-Al_2O_3, MnO-Al_2O_3, FeO-Al_2O_3, Na_2O-Al_2O_3, and K_2O-Al_2O_3 systems. CALPHAD, 17, 189-205.

Evans, B. and G. Dresen (1991) Deformation of earth materials: six easy pieces. Reviews of Geophysics, 91, 823-843.

Fegley, B. and H. Palme (1985) Evidence for oxidizing conditions in the solar nebula from Mo and W depletions in refractory inclusions in carbonaceous chondrites. Earth and Planetary Science Letters, 72, 311-326.

Fischer, P. (1967) Neutronenbeugungsuntersuchung der Strukturen von $MgAl_2O_4$- und $ZnAl_2O_4$-Spinellen, in Abhängigkeit von der Vorgeschichte. Zeitschrift für Kristallographie, 124, 275-302.

Fiske, P.S. and J.F. Stebbins (1989) Evidence for multiple mechanisms of disorder in $MgAl_2O_4$ spinel: an ^{27}Al NMR study. Eos, Transactions of the American Geophysical Union, 70, 1375.

Frölich, H. (1936) *Elektronentheorie der metalle*. Julius Springer, Berlin.

Fulton, J.C. and J. Chipman (1954) Slag-metal-graphite reactions and the activity of silica in lime-alumina-silica slags. Journal of Metals, 200, 1136-1146.

Ghiorso, M.S., I.S.E. Carmichael, and R.O. Sack (1983) The Gibbs free energy of mixing of natural silicate liquids; An expanded regular solution approximation for the calculation of magmatic intensive variables. Contributions to Mineralogy and

Petrology, 84, 107-145.

Gillet, P., P. Richet, F. Guyot, and G. Fiquet (1991) High-temperature thermodynamic properties of forsterite. Journal of Geophysical Research, 96, 11805-11816.

Green, H.W. (1988) Rheological implications of the dissolution of volatiles in mantle olivines. Physics of the Earth and Planetary Interiors, 51, 123-124.

Grimsey, E.J. (1988) The effect of temperature on nickel solubility in silica saturated fayalite slags from 1523 to 1623 K. Metallurgical Transactions B, 19B, 243-247.

Grossman, L. (1972) Condensation in the primitive solar nebula. Geochimica et Cosmochimica Acta, 36, 597-619.

Grossman, L. (1973) Refractory trace elements in Ca-Al-rich inclusions in the Allende meteorite. Geochimica et Cosmochimica Acta, 37, 1119-1140.

Grossman, L. and S.P. Clark (1973) High-temperature condensates in chondrites and the environment in which they formed. Geochimica et Cosmochimica Acta, 37, 635-649.

Grossman, L. and R. Ganapathy (1976) Trace elements in the Allende meteorite-I. Coarse-grained, Ca-rich inclusions. Geochimica et Cosmochimica Acta, 40, 331-344.

Grossman, J.N., A.E. Rubin, and G.J. MacPherson (1988) ALH85085: a unique volatile-poor carbonaceous chondrite with possible implications for nebular fractionation processes. Earth and Planetary Science Letters, 91, 33-54.

Grove, T.L. (1981) Use of Fe-Pt alloys to eliminate iron loss problem in 1 atmosphere gas mixing experiments: Theoretical and practical considerations. Contributions to Mineralogy and Petrology, 78, 298-304.

Guse, W. and H. Saalfeld (1990) X-ray characterization and structure refinement of a new cubic alumina phase (σ-Al_2O_3) with spinel-type structure. Neues Jahrbuch für Mineralogie Monatshefte, 1990, 217-226.

Hallstedt, B. (1992) Thermodynamic assessment of the system MgO-Al_2O_3. Journal of the American Ceramic Society, 75, 1497-1507.

Haselton Jr., H.T. (1979) Calorimetry of synthetic pyrope-grossular garnets and calculated stability relations. Ph.D. thesis, University of Chicago.

Hashimoto, A. (1983) Evaporation metamorphism in the early solar nebula — evaporation experiments on the melt FeO-MgO-SiO_2-CaO-Al_2O_3 and chemical fractionations of primitive materials. Geochemical Journal, 17, 111-145.

Hashimoto, A., M. Kumazawa, and N. Onuma (1979) Evaporation metamorphism of primitive dust material in the early solar nebula. Earth and Planetary Science Letters, 43, 13-21.

Helgeson, H.C., J.M. Delany, H.W. Nesbitt, and D.K. Bird (1978) Summary and critique of the thermodynamic properties of rock-forming minerals. American Journal of Science, 278A, 229 p.

Holland, T.B.J. and R. Powell (1990) An enlarged and updated internally consistent thermodynamic dataset with uncertainties and correlations: the system K_2O-

Na_2O-CaO-MgO-MnO-FeO-Fe_2O_3-Al_2O_3-TiO_2-SiO_2-C-H_2-O_2. Journal of Metamorphic Geology, 8, 89-124.

Ireland, T.R., A.J. Fahey, and E.K. Zinner (1991) Hibonite-bearing microspherules: A new type of refractory inclusions with large isotopic anomalies. Geochimica et Cosmochimica Acta, 55, 367-379.

Jagodzinski, H. and H. Saalfeld (1958) Kationenverteilung und Strukturbeziehungen in Mg-Al-Spinellen. Zeitschrift für Kristallographie, 110, 197-218.

Jayaram, V. and C.G. Levi (1989) The structure of δ-alumina evolved from the melt and the $\gamma \rightarrow \delta$ transformation. Acta Metallurgica, 37, 569-578.

Jurewicz, A.J.G. and E.B. Watson (1988) Cations in olivine, Part 1: Calcium partitioning and calcium-magnesium distribution between olivines and coexisting melts, with petrologic applications. Contributions to Mineralogy and Petrology, 99, 176-185.

Kay, D.A.R. and J. Taylor (1960) Activities of silica in the lime+alumina+silica system. Transactions of the Faraday Society, 56, 1372-1386.

King, E.G. (1955) Heat capacities at low temperatures and entropies at 298.16°K of crystalline calcium and magnesium aluminates. Journal of Physical Chemistry, 59, 218-219.

King, E.G., R. Barany, W.W. Weller, and L.B. Pankratz (1967) Thermodynamic properties of forsterite and serpentine. U.S. Bureau of Mines Report of Investigations, 6962, 19 p.

Kleykamp, H. and S.-G. Kang (1991) The constitution of the uranium-palladium and uranium-rhodium-palladium systems. Zeitschrift für Metallkunde, 82, 544-552.

Krupka, K.M., D.M. Kerrick, and J. Ito (1985a) Low-temperature heat capacities and derived thermodynamic properties of anthophyllite, diopside, enstatite, bronzite, and wollastonite. American Mineralogist, 70, 249-260.

Krupka, K.M., D.M. Kerrick, and J. Ito (1985b) High-temperature heat capacities and derived thermodynamic properties of anthophyllite, diopside, dolomite, enstatite, bronzite, talc, tremolite, and wollastonite. American Mineralogist, 70, 261-27.

Kurat, G. (1975) The Lancé carbonaceous chondrite: a petrological analysis of the complex genesis of a chondrite. TMPM Tschermaks Mineralogische und Petrographische Mitteilungen, 22, 38-78.

Landa, Ya.A. and I.A. Naumova (1979) Determination of enthalpies and heat capacities of magnesian spinels in the interval 1400-2200 K (in Rus.). Ogneupory, 9, 9-11.

Landron, C., B. Cote, D. Massiot, J.P. Coutures, and A.M. Flank (1992) Aluminium XAS and NMR spectroscopic studies of calcium aluminosilicate glasses. Physica Status Solidi B, 171, 9-20.

Lange, R.A., J.J. DeYoreo, A. Navrotsky (1991) Scanning calorimetric measurement of heat capacity during incongruent melting of diopside. American Mineralogist, 76, 904-912.

Langenberg, F.C. and J. Chipman (1959) Activity of silica in CaO-Al_2O_3-SiO_2 slags at

1600° and 1700°C. Transactions of the Metallurgical Society of AIME, 215, 958-962.

Langenberg, F.C., H. Kaplan, J. Chipman (1958) The activity of silica in lime-alumina-silica slags at 1600°C. In *Physical Chemistry of Steelmaking*, pp. 65-67. John Wiley, New York.

Lejus, A. (1964) Sur la formation a haute température de spinelles non stœichiométriques et de phases dérivées; dans plusieurs systèmes d'oxydes a base d'alumine et dans le système alumine-nitrure d'aluminium. Revue des Hautes Températures et des Réfractaires, 1, 53-95.

Longhi, J. and J.F. Hays (1979) Phase equilibria and solid solution along the join $CaAl_2Si_2O_8$–SiO_2. American Journal of Science, 279, 876-890.

Mackwell, S.J., D.L. Kohlstedt, and M.S. Paterson (1985) The role of water in the deformation of olivine single crystals. Journal of Geophysical Research, 90, 11319-11333.

MacPherson, G.J. and A.M. Davis (1993) A petrologic and ion microprobe study of a Vigarano Type B refractory inclusion; evolution by multiple stages of alteration and melting. Geochimica et Cosmochimica Acta, 57, 231-243.

MacPherson, G.J. and L. Grossman (1981) A once-molten, coarse-grained Ca-rich inclusion in Allende. Earth and Planetary Science Letters, 52, 16-24.

MacPherson. G.J. and L. Grossman (1984) "Fluffy" type A Ca-,Al-rich inclusions in the Allende meteorite. Geochimica et Cosmochimica Acta, 48, 29-46.

MacPherson, G.J., J.M. Paque, E. Stolper, and L. Grossman (1984) The origin and significance of reverse zoning in melilite from Allende Type B inclusions. Journal of Geology, 92, 289-305.

MacPherson, G.J., D.A. Wark, and J.T. Armstrong (1988) Primitive material surviving in chondrites: refractory inclusions. In *Meteorites and the Early Solar System* (J.F. Kerridge and M.S. Matthews eds.). University of Arizona Press, Tucson.

Marvin U.B., J.A. Wood, and J.S. Dickey Jr. (1970) Ca-Al rich phases in the Allende meteorite. Earth and Planetary Science Letters, 7, 346-350.

Mattioli, G.S., B.J. Wood, and I.S.E. Carmichael (1987) Ternary-spinel volumes in the system $MgAl_2O_4$-Fe_3O_4-γ $Fe_{8/3}O_4$: Implications for the effect of P on intrinsic f_{O_2} measurements of mantle-xenolith spinels. American Mineralogist, 72, 468-480.

Mattioli, G.S., M.B. Baker, M.J. Rutter, and E.M. Stolper (1989) Upper mantle oxygen fugacity and its relationship to metasomatism. Journal of Geology, 97, 521-536.

McAlister, A.J. (1986) The Al-Pd (aluminum-palladium) system. Bulletin of Alloy Phase Diagrams, 7, 368-374.

Merzbacher, C.I. and W.B. White (1991) The structure of alkaline earth aluminosilicate glasses as determined by vibrational spectroscopy. Journal of Non-Crystalline Solids, 130, 18-34.

Millard, R.L., R.C. Peterson, and B.K. Hunter (1992) Temperature dependence of cation disorder in $MgAl_2O_4$ spinel using ^{27}Al and ^{17}O magic-angle spinning nuclear magnetic resonance spectroscopy. American Mineralogist, 77, 44-52.

Moffatt W.G. (1982) *Handbook of Binary Phase Diagrams*. General Electric Company, Schnectady, New York.

Mohanan, K., S. Sharma, and F.C. Bishop (1993) A Raman spectral study of forsterite-monticellite solid solutions. American Mineralogist, 78, 42-48.

Murdoch, J.B., J.F. Stebbins, and I.S.E. Carmichael (1985) High-resolution ^{29}Si NMR study of silicate and aluminosilicate glasses: the effect of network-modifying cations. American Mineralogist, 70, 332-343.

Nagahara, H. and I. Kushiro (1982) Calcium-aluminum-rich chondrules in the unequilibrated ordinary chondrites. Meteoritics, 17, 55-63.

Navrotsky, A. (1986) Cation-distribution energetics and heats of mixing in $MgFe_2O_4$-$MgAl_2O_4$, $ZnFe_2O_4$-$ZnAl_2O_4$, and $NiAl_2O_4$-$ZnAl_2O_4$ spinels: Study by high-temperature calorimetry. American Mineralogist, 71, 1160-1169.

Navrotsky, A. and O.J. Kleppa (1967) The thermodynamics of cation distribution in simple spinels. Journal of Inorganic and Nuclear Chemistry, 29, 2701-2714.

Navrotsky, A., B.A. Wechsler, K. Geisinger, and F. Seifert (1986) Thermochemistry of $MgAl_2O_4$-$Al_{8/3}O_4$ defect spinels. Journal of the American Ceramic Society, 69, 418-422.

Navrotsky A., D. Ziegler, R. Oestrike, and P. Maniar (1989) Calorimetry of silicate melts at 1773 K: measurement of enthalpies of fusion and of mixing in the systems diopside-anorthite-albite and anorthite-forsterite. Contributions to Mineralogy and Petrology, 101, 122-130.

Nayeb-Hashemi, A.A. and J.B. Clark (1985) The Mg-Pd (magnesium-palladium) system. Bulletin of Alloy Phase Diagrams, 6, 164-167.

O'Neill, H. St. C. and A. Navrotsky (1983) Simple spinels: crystallographic parameters, cation radii, lattice energies, and cation distribution. American Mineralogist, 68, 181-194.

Ozturk, B. and R.J. Fruehan (1987) Activity of silica in calcium-aluminate based slags. Metallurgical Transactions B, 18B, 746-749.

Paque, J.M. and E.M. Stolper (1984) Crystallization experiments on a range of Ca-Al-rich inclusion compositions. Lunar and Planetary Science, XV, 631-632.

Peterson, R.C., G.A. Lager, and R. Hitterman (1991) A time-of-flight neutron diffraction study of $MgAl_2O_4$ at temperatures up to 1273°K. American Mineralogist, 76, 1455-1458.

Pluschkell, W. and H.J. Engell (1968) Ionen- und Elektronenleitung im Magnesiumorthosilikat. Berichte der Deutschen Keramischen Gesellschaft, 45, 388-394.

Reid A.M., R.J. Williams, E.K. Gibson Jr., and K. Fredriksson (1974) A refractory glass chondrule in the Vigarano chondrite. Meteoritics, 9, 35-46.

Rein, R.H. and J. Chipman (1963) The distribution of silicon between Fe-Si-C alloys and SiO_2-CaO-MgO-Al_2O_3 slags. Transactions of the Metallurgical Society of AIME, 227, 1193-1203.

Rein, R.H. and J. Chipman (1965) Activities in the liquid solution SiO_2-CaO-MgO-Al_2O_3 at 1600 C. Transactions of the Metallurgical Society of AIME, 233, 415-

425.

Ricoult, D.L. and D.L. Kohlstedt (1986) Creep behavior of single crystals of vanadium-doped forsterite. Journal of the American Ceramic Society, 69, 770-774.

Robie, R.A., B.R. Hemingway, and J.R. Fisher (1978) Thermodynamic properties of minerals and related substances at 298.15 K and 1 bar (10^5 Pascals) pressure and at higher temperatures. USGS Bulletin, 1452, 1-456.

Robie, R.A., B.S. Hemingway, and H. Takei (1982) Heat capacities and entropies of Mg_2SiO_4, Mn_2SiO_4, and Co_2SiO_4 between 5 and 380 K. American Mineralogist, 67, 470-482.

Róg, G., B. Langanke, G. Borchardt, and H. Schmalzried (1974) Determination of the standard Gibbs free energies of formation of the silicates of cobalt, magnesium, and strontium by e.m.f. measurements. Journal of Chemical Thermodynamics, 6, 1113-1119.

Roy, D.M., R. Roy, and E.F. Osborn (1953) The system MgO-Al_2O_3-H_2O and influences of carbonate and nitrate ions on the phase equilibria. American Journal of Science, 251, 337-361.

Sack, R. (1980) Spinels as petrogenetic indicators: Activity-composition relations at low pressure. Contributions to Mineralogy and Petrology, 78, 169-186.

Sack, R.O. and M.S. Ghiorso (1991) Chromian spinels as petrogenetic indicators: Thermodynamics and petrological applications. American Mineralogist, 76, 827-

847.

Sahoo, P. and R.G. Reddy (1984) Activity coefficient of nickel oxide in FeO-NiO-$FeO_{1.5}$-$AlO_{1.5}$-SiO_2 at 1573K. In *Second International Symposium on Metallurgical Slags and Fluxes* (H.A. Fine and D.R. Gaskell eds.), pp. 533-545. Metallurgical Society of AIME, Warrendale, Pennsylvania.

Sato, M. (1971) Electrochemical measurements and control of oxygen fugacity and other gaseous species with solid electrolyte sensors. In *Research Techniques for High Pressure and High Temperature* (G.C. Ulmer ed.), pp. 43-100. Springer-Verlag, New York.

Schaller, H.J. (1976) Aktivitätskoeffizienten von Zirkon in Palladium und Platin. Berichte der Bunsengesellschaft für Physikalische Chemie, 80, 999-1002.

Schaller, H.J. (1978) Der Einfluβ der Lage der Fermi-Energie auf das Mischungsverhalten von Palladium/Aluminum-Legierungen. Berichte der Bunsengesellschaft für Physikalische Chemie, 82, 365-371.

Schaller, H.J. (1979) Über die extrem hohe thermodynamische Stabilität von Pd-Th-Legierungen. Zeitschrift für Naturforschung, 34a, 464-468.

Schaller, H.J. and H. Brodowsky (1978a) Thermodynamische Eigenschaften von Palladium/Zinn-Legierungen. Zeitschrift für Metallkunde, 69, 87-93.

Schaller, H.J. and H. Brodowsky (1978b) Thermodynamic properties of palladium-indium alloys. Berichte der Bunsengesellschaft für Physikalische Chemie, 82, 773-338.

Schaller, H.J., R.S. Craig, W.E. Wallace (1972) Magnetic and crystallographic characteristics of solid solutions of Gd in Pd and Pd-Ag alloys. Journal of Solid State Chemistry, 5, 338-341.

Seifert, F., B.O. Mysen, and D. Virgo (1982) Three-dimensional network structure of quenched melts (glass) in the systems SiO_2–$NaAlO_2$, SiO_2–$CaAl_2O_4$ and SiO_2–$MgAl_2O_4$. American Mineralogist, 67, 696-717.

Sharma, R.A. and F.D. Richardson (1965) Activities of manganese oxide, sulfide capacities, and activity coefficients in aluminate and silicate melts. Transactions of the Metallurgical Society of AIME, 233, 1586-1592.

Sharma, S.K., B. Simons, and H.S. Yoder (1983) Raman study of anorthite, calcium Tschermak's pyroxene, and gehlenite in crystalline and glassy states. American Mineralogist, 68, 1113-1125.

Sharma, S.K., H.S. Yoder, and D.W. Matson (1988) Raman study of some melilites in crystalline and glassy states. Geochimica et Cosmochimica Acta, 52, 1961-1967.

Sheng, Y.J. (1992) Origin of plagioclase-olivine inclusions. Ph.D. thesis, California Institute of Technology.

Sheng Y.J., I.D. Hutcheon, and G.J. Wasserburg (1991) Origin of plagioclase-olivine inclusions in carbonaceous chondrites. Geochimica et Cosmochimica Acta, 55, 581-599.

Shirasuka, K. and G. Yamaguchi (1974) Precise measurement of the crystal data and the solid solution range of the defective spinel MgO-n Al_2O_3. Yogyo Kyokaishi,

82, 650-653.

Simon, S.B., L. Grossman, A.M. Davis, J.R. Beckett, and L. Chamberlin (1993) Evidence for extremely high-temperature melting in the solar nebula from a $CaAl_4O_7$-bearing spherule from Murchison. Meteoritics, 28.

Smith, J.V. (1959) The crystal structure of proto-enstatite, $MgSiO_3$. Acta Crystallographica, 12, 515-519.

Snyder, D.A. and I.S.E. Carmichael (1992) Olivine-liquid equilibria and the chemical activities of FeO, NiO, Fe_2O_3, and MgO in natural basic melts. Geochimica et Cosmochimica Acta, 56, 303-318.

Stephenson, D.A., C.B. Sclar, and J.V. Smith (1966) Unit cell volumes of synthetic orthoenstatite and low clinoenstatite. Mineral Magazine, 35, 839-846.

Stolper, E.M. (1982) Crystallization sequences of Ca,Al-rich inclusions from Allende: An experimental study. Geochimica et Cosmochimica Acta, 46, 2159-2180.

Stolper, E. and J.M. Paque (1986) Crystallization sequences of Ca-Al-rich inclusions from Allende: The effects of cooling rate and maximum temperature. Geochimica et Cosmochimica Acta, 50, 1785-1806.

Téqui, C., R.A. Robie, B.S. Hemingway, D.R. de Neuville, and P. Richet (1991) Melting and thermodynamic properties of pyrope ($Mg_3Al_2Si_3O_{12}$). Geochimica et Cosmochimica Acta, 55, 1005-1010.

Torgeson, D.R. and Th.G. Sahama (1948) A hydrofluoric acid solution calorimeter and the determination of the heats of formation of Mg_2SiO_4, $MgSiO_3$, and $CaSiO_3$.

Journal of the American Chemical Society, 70, 2156-2160.

Tsukihashi, F., A. Werme, F. Matsumoto, A. Kasahara, M. Yukinobu, T. Hyodo, S. Shiomi, and N. Sano (1984) Thermodynamics of the soda slag system for hot metal treatment. In *Second International Symposium on Metallurgical Slags and Fluxes* (H.A. Fine and D.R. Gaskell eds.), pp. 89-106. American Institute of Mining, Metallurgical, and Petroleum Engineers Inc., New York.

Wagner, V.H. (1932) Zur Thermochemie der Metasilikate des Calciums und Magnesiums und des Diopsids. Zeitschrift für Anorganische Allgemeine Chemie, 208, 1-22.

Wagner, R.D. and J.W. Larimer (1978) Condensation and stability of oxide/silicate melts. Meteoritics, 13, 651.

Wark, D.A. (1979) Birth of the presolar nebula: the sequence of condensation revealed in the Allende meteorite. Astrophysics and Space Science, 65, 275-295.

Wark, D.A. (1987) Plagioclase-rich inclusions in carbonaceous meteorites: Liquid condensates? Geochimica et Cosmochimica Acta, 51, 221-242.

Wark, D.A., W.V. Boynton, R.R. Keays, H. Palme (1987) Trace element and petrologic clues to the formation of forsterite-bearing Ca-Al-rich inclusions in the Allende meteorite. Geochimica et Cosmochimica Acta, 51, 607-622.

Warner, R.D. and W.C. Luth (1973) Two-phase data for the join monticellite ($CaMgSiO_4$)-forsterite (Mg_2SiO_4): experimental results and numerical analysis. American Mineralogist, 58, 998-1008.

Weill, D.F., R. Hon, and A. Navrotsky (1980) The igneous system $CaMgSi_2O_6$-$CaAl_2Si_2O_8$-$NaAlSi_3O_8$: variations on a classic theme by Bowen. In *Physics of Magmatic Processes* (R.B. Hargraves ed.), pp. 49-92. Princeton University Press, Princeton, New Jersey.

Wood, B.J., R.J. Kirkpatrick, and B. Montez (1986) Order-disorder phenomena in $MgAl_2O_4$ spinel. American Mineralogist, 71, 999-1006.

Wood, J.A. and G.E. Morfill (1988) A review of solar nebula models. In *Meteorites and the Early Solar System* (J.F. Kerridge and M.S. Matthews eds.), pp. 329-347. University of Arizona Press, Tucson.

Ziman, J.M. (1969) *The physics of metals*. Cambridge University Press, London.